THE TWENTY-ONE CENTIMETER HYDROGEN LINE IN ABSORPTION

Thesis by

Barry Gillespie Clark

In Partial Fulfillment of the Requirements

For the Degree of

Doctor of Philosophy

California Institute of Technology

Pasadena, California

1964

(Submitted April 16, 1964)

ACKNOWLEDGEMENTS

I owe a debt of gratitude to almost all of the Professors, Fellows, and graduate students in the Astronomy and Radio Astronomy Departments during the period of this research. I especially mention Professor M. Schmidt and Mr. V. Radhakrishnan, who have been very helpful in many discussions, and G. J. Stanley, the Director of the Owens Valley Radio Observatory, for providing the necessary observing time. I wish to express my appreciation to K. I. Kellermann, G. A. Seielstad, and J. F. Bartlett for assistance with the observations. Parts of the receivers with which these observations were made were designed and constructed by G. J. Stanley, R. W. Wilson, D. Morris, R. B. Read, and J. F. Bartlett. The problem was originally suggested to me by J. G. Bolton, former Director of the Radio Observatory, and V. Radhakrishnan. I acknowledge the tenure of the van Maanen Fellowship and of a National Science Foundation scholarship during part of this research, and also financial support from the California Institute of Technology. I wish to thank my wife Betty for typing the final manuscript of this thesis.

This work was supported by the Office of Naval Research under contract NONR 220 (19).

ABSTRACT

The brightness distributions across five intense radio sources have been investigated in the hydrogen line absorption features. In some cases there has been found a variation of the absorption across the face of a source, which, with the kinematical distance to the cloud in question, allowed a typical length to be estimated, which in turn allows estimations of densities and masses. Densities range from a few atoms per cubic centimeter, to, in the case of a small cloud in front of Orion A, as much as 700 atoms per cubic centimeter. Masses range from a few solar masses up to perhaps a thousand solar masses in the cloud causing the deep line in Cas A.

The absorption profiles of the bright sources were analysed into Gaussian components, allowing parameters to be quoted for individual clouds, and, in a few cases, allowing an interesting upper limit to the temperature to be set from the dispersions of the separated components.

The absorption features in several other sources were briefly investigated, including three absorption spectra never before published, and new upper limits for the absorption of apparently unabsorbed sources were set in six cases. This material is briefly analysed statistically, from which it is concluded that the distribution law for central optical depths is approximately $e^{-\tau_o}$, and that

a line of sight, on the average, intersects 4.1 clouds per kiloparsec in the galactic plane. There is some evidence that the density is about twice this in the local spiral arm.

Some evidence is presented in favor of a "raisin pudding" model of the interstellar medium, in which clouds with temperatures of less than a hundred degrees supply all absorption, and most of the hydrogen line emission, while an appreciable part of the emission profiles is due to a hot intercloud medium of neutral hydrogen, at a temperature of several thousand degrees, and a density of about one half atom per cubic centimeter.

TABLE OF CONTENTS

I

INTRODUCTION

The history of astronomy has been greatly influenced by the early beginnings of the science in the study of the clearly visible stars, and only recently has it become apparent that many of the larger features of our galaxy and of the universe are shaped by forces too subtle to act on such dense objects as stars. Even the general existence of interstellar matter was doubted until the work of Shapley, Hubble, Trumpler and Oort in the early 1930's demonstrated the importance of interstellar absorption, and this was not clearly systematized until the work of Schalén and many others in the decade following 1936 succeeded in deriving considerable information about the nature and numbers of the particles causing the absorption. However, prior to the advent of radio astronomy, most of the effort directed to the understanding of interstellar matter was expended on the more readily visible emission nebulae, and to a lesser degree, the reflection nebulae, than on the general or average conditions between the stars.

Radio astronomy meant two things for the study of interstellar matter. Firstly, ionized hydrogen could be detected to distances that the absorption bound optical astronomy could not reach, and really peculiar nebulae could be isolated by the presence of synchrotron radiation

detectable in their spectra. But the more important contribution was the study of the 21 cm line of neutral hydrogen. This was first detected by Ewen and Purcell after a suggestion by van de Hulst, and their lead was quickly followed in Leiden and in Sydney. The double nature of the emission line in some directions was quickly found and attributed to the spiral structure of the galaxy. By following the change of brightness with projected path length in a spiral arm, van de Hulst, Muller, and Oort[1] found that the brightness temperature extrapolated to infinite path length is 125° K, which, under certain assumptions, is the harmonic mean temperature. This value is two and a half times the estimate given by Spitzer and Savedoff[2] of the temperature of the interstellar medium, which is quite close considering the uncertainties of the calculation. Both Leiden[3] and Sidney[4] soon published maps of the hydrogen distribu-

---

[1] van de Hulst, H. I.; Muller, C. A. and Oort, J. H. BAN, 12, 117, (1954)

[2] Spitzer, L. and Savedoff, M. P. ApJ; 111, 593, (1950)

[3] van de Hulst, H. I.; Muller, C. A. and Oort, J. H. BAN, 12, 117, (1954)
Kwee, K. K.; Muller, C. A. and Westerhout, G. BAN, 12, 211, (1954)
Westerhout, G. BAN, 13, 201, (1957)
Schmidt, M. BAN, 13, 247, (1957)

[4] Kerr, F. J.; Hindman, J. V.; and Gum, C. S. Aust J Phys 12, 270, (1959)

tion over the face of the galaxy, using a model of galactic rotation to convert velocity into distance.

The hydrogen line in absorption was first observed by Hagen and McClain[5] and it was quickly noticed that although the absorption spectra were clearly related to the emission spectra, there was not the simple relation

$$\tau = -\log(1 - T_b/125^\circ)$$

to be expected from a homogeneous medium at 125° K. The absorption spectra have rather narrower peaks than the emission profiles, and in some cases these lines are not much broader than the thermal Doppler profile of hydrogen at 125° K. This discrepancy was explained in terms of the cloud model of the interstellar medium, the general emission in the vicinity of the source to be due to the aggregate emission of many clouds like the few directly in front of the source, which cause the absorption.

The observation of absorption was taken up by several observers. It was used by Davies[6] to estimate the distance to galactic objects from the total absorption in front of them (in view of the chance of entirely missing clouds for great distances inherent in the cloud model, and the known spotty distribution of hydrogen, this is a somewhat risky

---

5 Hagen, J. P. and McClain, E. F. ApJ, 120, 368, (1954)

6 Davies, R. D. M. N., 116, 443, (1956)

procedure), and an excellent collection of profiles was published by Muller[7]. Clark, Radhakrishnan, and Wilson[8] (henceforth referred to as CRW) proposed that the examination of the brightness distribution over the faces of the sources would be of interest, and although the observations which prompted this have now proved to be in error, there was yet other information available in the interferometer investigations of the sources, and this thesis is an extension of the investigation reported there.

After that paper was published, absorption profiles, uncorrected for the expected profile, have appeared in various discussions of the Zeeman effect in the 21 cm line[9]. A most useful collection of the deeper profiles has been produced by Slater and Verschuur, which presents profiles obtained with the Manchester 250 foot telescope with a receiver of 3 kc/s bandwidth and a resolution of the spectra into Gaussian components. The features presented are the Orion Arm profile in Cas A, and the spectra of Taurus A and Cygnus A. There has also been one attempt to directly measure the brightness distribution at the bottom of an

---

7 Muller, C. A. ApJ, 125, 830, (1957)
Paris Symposium (Ed. R. Bracewell), S. U. Press, (1958)

8 Clark, B. G.; Radhankrishnan, V.; and Wilson, R. W. ApJ, 135, 151, (1962)

9 Davies, R. D.; Verschuur, G. L.; and Wild, P. A. T. Nature, 196, 563, (1962)

Davies, R. D.; Shuter, W. L. H., Slater, C. H.; Verschuur, G. L.; and Wild, P. A. T. MN, 126, 353, (1963)
Weinreb, S. ApJ 136, 1149, (1962)

absorption line, with a 80 kc/s bandwidth and the 8!5 x 5° beam of the Pulkova telescope[10]. This investigation noted that the absorption at zero velocity in Sagittarius A was uniformly distributed over the face of the source, but that the scan taken at the center frequency of the 3 kpc expanding arm indicated that one of the components of the source, at a distance 16' from the center source, was not covered by the absorbing matter and thus viewed between clouds, or alternatively, was not associated with the galactic center at all.

That an investigation of the brightness distributions would be valuable is indicated by the fact that the clouds observed with an effective beam the size of the source, about 5', are still very different from what is seen with the moderate beam of a twenty-five meter parabola, 36'. If there are to be many clouds in one beam area, there is a rather good chance to catch the edge of a cloud, or at least a tapering off, in a fiftieth of this area. The leverage may be further decreased by observing individual clouds in emission close by at intermediate latitudes where one obtains much the same sort of spatial resolution as by observing clouds in front of a source at several kiloparsecs distance.

---

10 Ryzhkova, N. F.; Egorova, T. M.; Gasachinskii, I. V.; and Bystrova, N. V. Soviet Astronomy--AJ (translation) 7, 12, (1963)

Egorova, T. M. Soviet Astronomy--AJ (translation)7, 290, (1963)

Various estimates of cloud diameters have been made. For instance, van de Hulst[11] estimated an average cloud diameter of 18-35 pc by the method of noting the correlation distance of hydrogen emission, as observed with a 25 meter paraboloid, in the Perseus and Orion arms of the galaxy. These numbers are suspiciously near his beam width, and may therefore have large selection effects against smaller clouds. Blaauw, Takakubo, and van Woerden[12] found a cloud diameter of about 2-1/2 - 6 pc, which, however, appears somewhat sensitive to the model adopted. Narrow features in emission can often be traced for two or three degrees in the intermediate latitude catalogue of van Woerden et al.[13], which, if the typical distance is three or four hundred parsecs, corresponds to about 15 pc. Optical data tend to give a similar range of cloud sizes.

---

11 van de Hulst, H. C. (1958) RMP, 30, 913, (1958)

12 Blaauw, A. Interstellar Matter in Galaxies, (Ed. L. Woltjer) Benjamin Press (1962)

13 van Woerden, H.; Takakubo, K.; and Braes, L. L. E. BAN, 16, 321, (1962)

II

THE OBSERVING TECHNIQUE

2.1 The Receivers and telescopes

The observations to be discussed in this thesis were all made with the variable spacing interferometer of the Owens Valley Radio Observatory, which consists of two ninety-foot equatorially mounted paraboloids. The spacings employed were 200 feet north-south, 100 feet, 200 feet, and 400 feet east-west, and a short run at 280 feet at azimuth 135°. The dates of these observations are given in Table I.

Table I. The Observations

Dates, inclusive	Spacing	Receiver	Zenith Fringe Spacing
Nov.22 -- Dec. 4 1961	200' N-S	A	12'
Dec. 6 -- Dec.10 1961	283' NW-SE	A	8:5
Mar. 1 -- Mar.11 1962	100' E-W	B	24'
May 27 -- June 7 1962	200' E-W	B	12'
Jan. 8 -- Jan.14 1963	400' E-W	B	6'

Two different receivers were used in this observing program. They are denoted in Table I as receivers A and B. A block diagram of receiver A is presented in Figure 1.[14] The variable frequency local oscillator is shown in Figure 3.

[14] See also Read, R. B. ApJ, 138, 1 (1963)

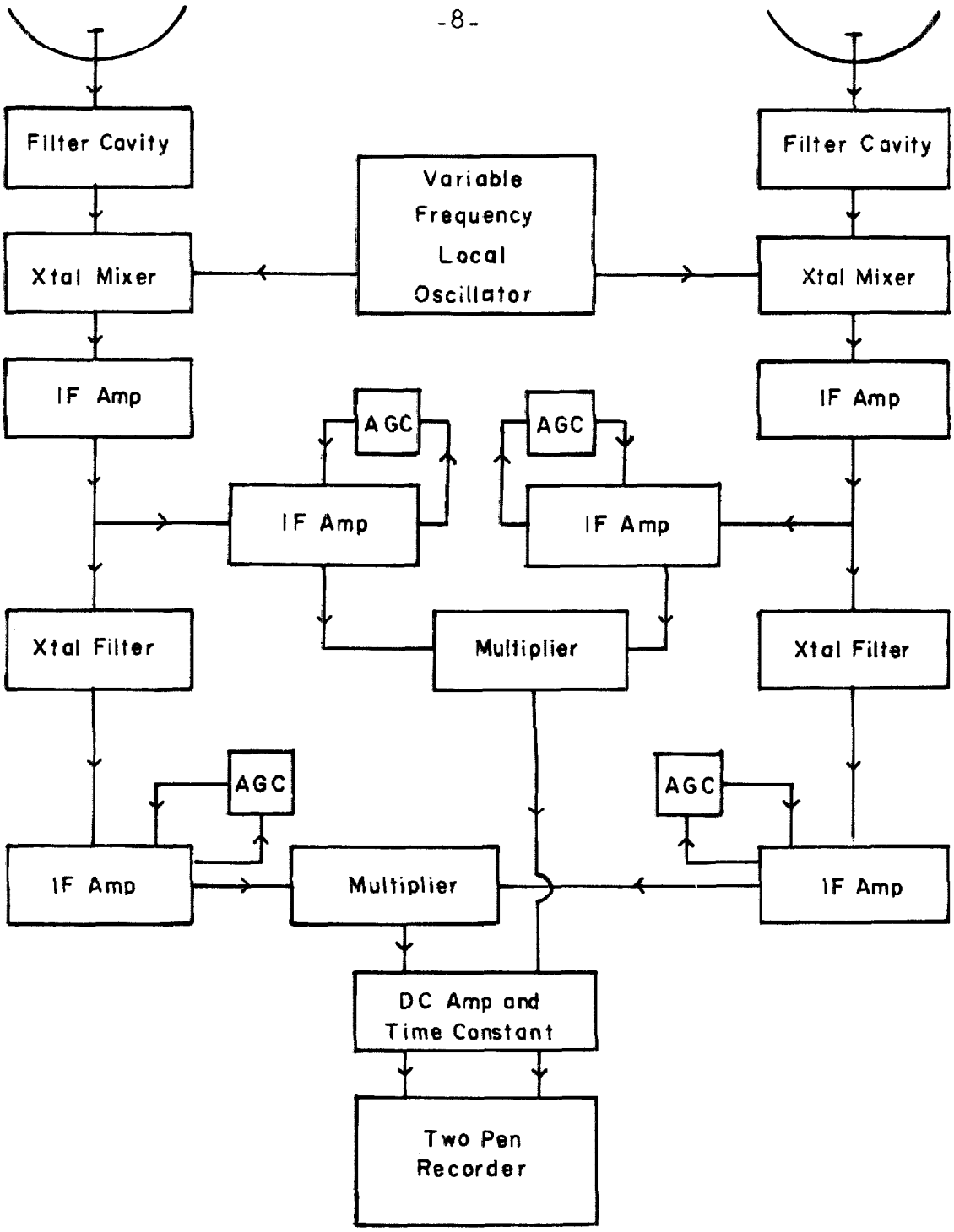

Figure 1. Receiver A Block Diagram.

The input noise from the antenna was first run through a filter cavity to reject the image. These cavities had a loss of less than one decibel, but, because the signal and image were so closely spaced, the image was rejected by only about 16 db. The noise output from the cavity was then mixed with the local oscillator in a crystal mixer and the resultant signal was amplified at 10 megacycles. After the initial amplification, the power was divided into two channels, one of which was a conventional multiplying interferometer receiver with a bandwidth of about 4 Mc/s, and the other was a narrow band line interferometer, with the bandwidth restricted to 6 kc/s by means of crystal filters. Both channels were stabilized with their own AGC. This receiver had a single sideband system noise temperature of about 1100° K. Its prime disadvantage was the incomplete rejection of the 1440 Mc/s image, which could not be more thoroughly rejected without a large sacrifice in loss in the filter cavity, and hence in the system noise of the receiver.

Receiver B eliminates this problem. The image is actually rejected at IF frequencies. A block diagram of the receiver is shown in Figure 2. The local oscillators are run at frequencies differing by two megacycles, and hence the IF frequencies differ by 2 Mc/s. The image of the receiver with the 10.7 Mc/s IF lies at 1441.8 Mc/s, which

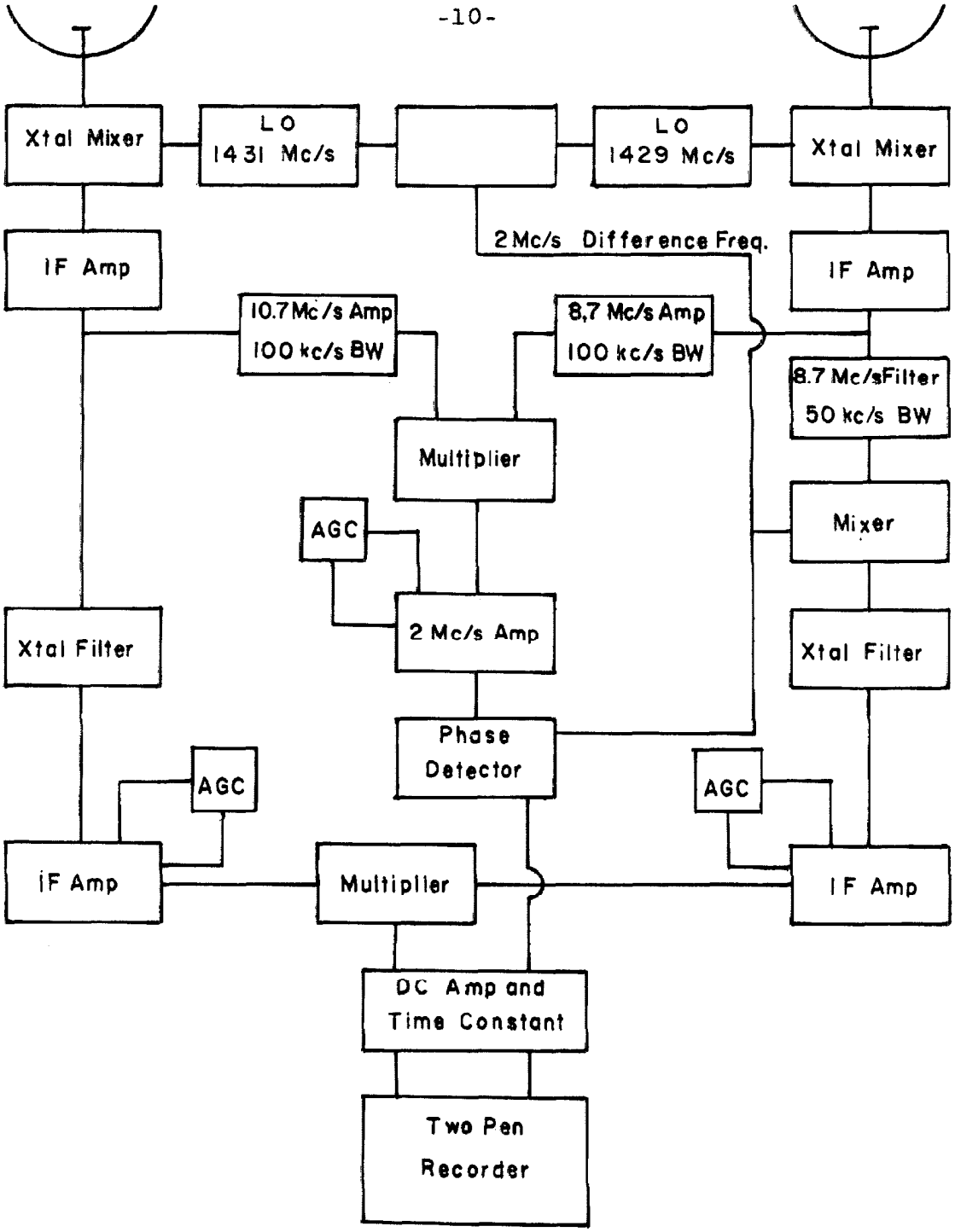

Figure 2. Receiver B Block Diagram.

enters the IF of the other antenna at 12.7 Mc/s, and is thus well rejected by an 8.7 Mc/s image rejection filter. In the line receiver, the frequency is changed after the initial amplification, by mixing with the two megacycle difference signal of the local oscillators. Thereafter, the line channel is as in receiver A. The broadband receiver is handled somewhat differently. The 8.7 and 10.7 Mc/s IF's are multiplied directly in order to produce two megacycle fringes. These fringes are then amplified and phase detected against the two megacycle difference signal to produce fringes at the natural fringe rate.

Without the need for a cavity in front of the crystal receiver, the noise figure was slightly better than that of receiver A, about 1000° system temperature, and the image rejection was vastly better, being in excess of 27 db. The broadband receiver was an unimproved experimental design, built to see if the system would work at all, and several features in it decreased signal to noise ratio (improper tuning of the 8.7 and 10.7 Mc/s filters, use of a detector rather than a true multiplier to produce the 2 Mc/s fringes, phase detecting against a clipped difference signal at 2 Mc/s instead of multiplying by a sine wave), and this form of receiver is intrinsically $\sqrt{2}$ less sensitive than that used for the line receiver. However, it still retained a sensitivity several times that of the narrow band receiver,

and hence was entirely adequate for the observations reported here, where it served only as an interference monitor and a guide to receiver sensitivity.

The method of measuring the image rejection was as follows: the receiver frequency was set to a frequency near the bottom of the deep line in the spectrum of Cas A. The fringes at this point are due to roughly equal contributions from the highly absorbed source and from the highly rejected image. However, the signal and image have different fringe periods, causing beats in the fringe system. The average fringe amplitude is one contribution, and half the difference between maximum amplitude and minimum amplitude is the other. If the fringes at minimum amplitude are in phase or in antiphase with the broad band fringes, the larger component is respectively residual signal or image.

The local oscillator train is shown in Figure 3. The first element in the train is a 53.602 Mc/s crystal controlled oscillator with a stability of about 10^{-7} per hour. The frequency was adjusted by means of a Collins permeability tuned oscillator, which has a frequency stability of about 10^{-5} per hour and a center frequency of 700 kc/s. The two oscillators were combined in a single sideband mixer, whose output was sampled for frequency display on a Hewett Packard scaler whose frequency standard was, in the June 1962 and January 1963 observations, derived from a

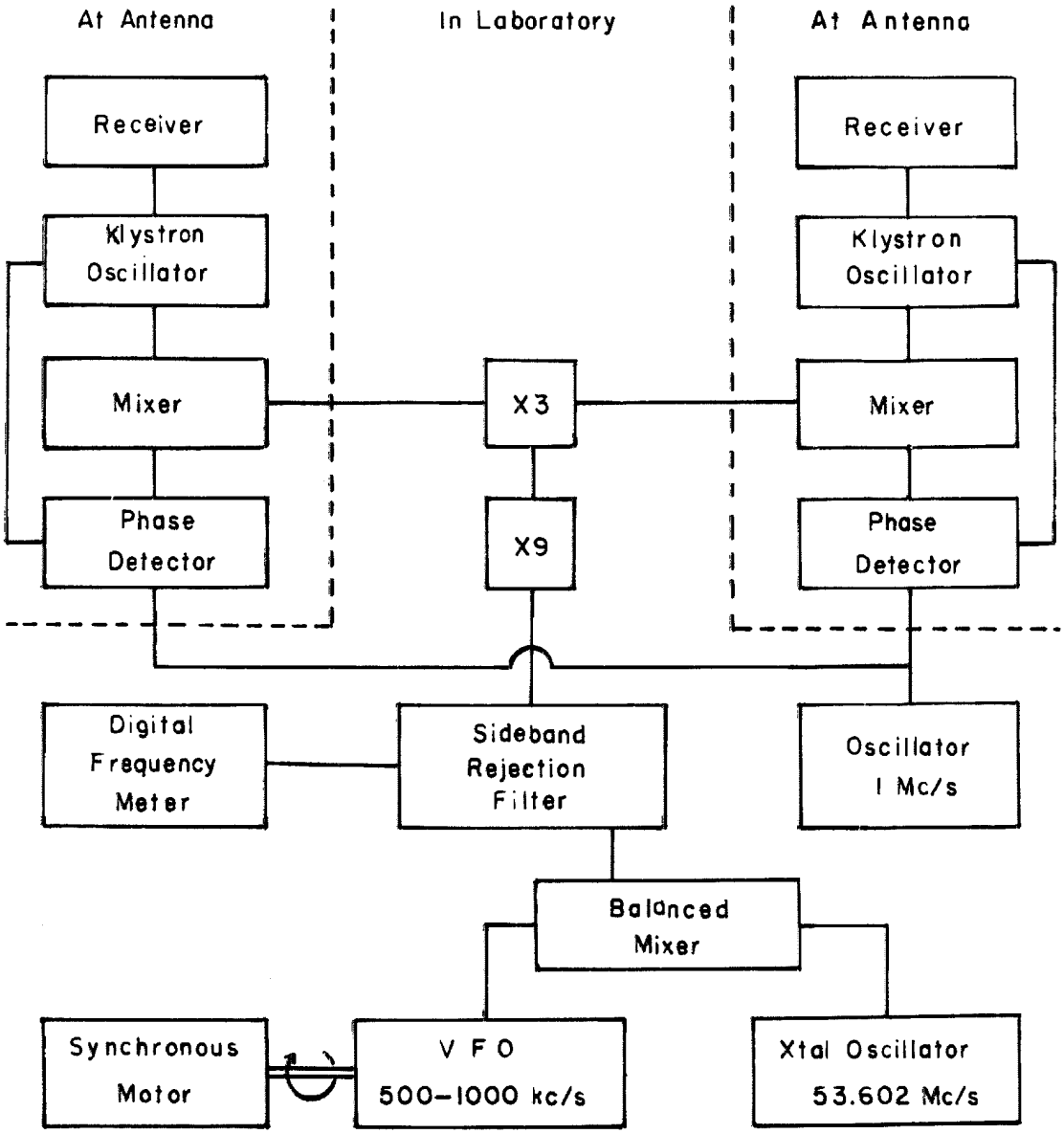

Figure 3. Local Oscillator Block Diagram.

standard oscillator of stability greater than 10^{-9} per day, and otherwise whose standard was checked against the frequency of WWV twice daily to an accuracy exceeding 5×10^{-8}. From the single sideband mixer the oscillator went to a chain of frequency multipliers and thence to the antennas. The local oscillator power at the antenna is supplied by a klystron oscillator phase locked to the sum or difference of the high frequency reference and a one megacycle low frequency reference (Read, 1963). An appreciable response at harmonics of 700 kc was found in the final output of the multiplier chain, but the time constant of the phase lock system should prevent them from appearing in the local oscillator power supplied to the receivers. For receiver A, both klystrons were locked on the difference of 1432 Mc/s and 1 megacycle, and for receiver B one klystron was locked on the sum and one of the difference of the two frequencies, and the 1 Mc/s oscillator output was doubled in frequency to supply the 2 Mc/s local oscillator difference frequency.

Observations could be made by setting the local oscillator to a fixed frequency and observing the resulting fringe amplitude, or the Collins variable oscillator could be driven by a synchronous motor, to provide frequency scanning at rates of 75 kc/s/hr or 150 kc/s/hr at 1420 Mc/s. On those observations taken by frequency scanning an additional uncertainty occurs in the frequency, in that the Collins

oscillator had an appreciable nonlinearity of frequency output with shaft position, and this function was replaced with a linear interpolation at intervals of about 2 kc/s, which introduced errors of up to 10 cps at 700 kc/s or 270 cps at 1420 Mc/s.

The crystal filters at 10.7 Mc/s appear quite stable, there being no detectable shift in mean frequency (to within 200 cps) from December 1961 to January 1963. However, in receiver B the image rejection filter, of 50 kc/s bandwidth, could change the mean frequency if it were not precisely centered on the frequency of the crystal filter. Estimates of this effect indicate that it should be less than 200 cps. The pass band of the crystal filters is nearly square, though with a ripple of about one db, and has a median frequency of 10699.93 ± 0.10 kc/s. It is displayed in Figure 4a.

From the figures on oscillator and filter stabilities it was estimated that the final frequency uncertainty of the receiver was about 350 cps at 1420 Mc/s. An attempt to measure the stability by observing the steep slopes in the spectrum of Cas A indicated that there were no scans with frequency errors as large as 1 kc/s, and that the average frequency stability is better than ± 0.5 kc/s, confirming the extremely high frequency stability calculated for the receiver.

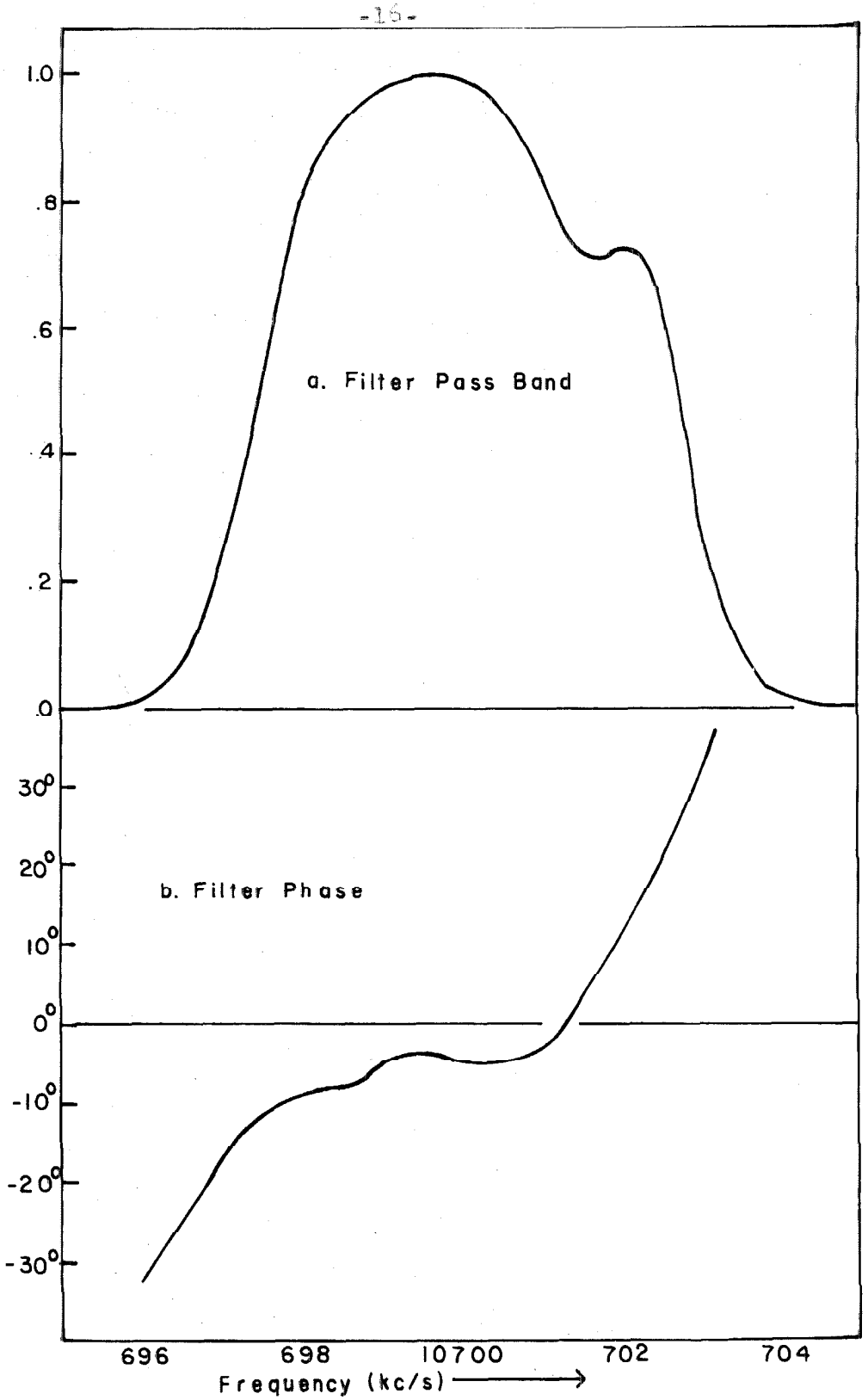

Figure 4. Crystal Filter Characteristics.

AGC is applied to the receiver at the stage immediately before the multiplier. This removes gain fluctuations of the amplifiers and lends a great deal of stability to the receiver. However, it makes the gain dependent on hour angle as varying amounts of stray radiation strike the ground. This effect is the same in the broad and narrow channels. Also, the gain in the narrow channel varies with the frequency in the absorption spectrum as the source power may make up an appreciable part of the total noise power in the receiver, which is being held constant by the AGC. This effect must be corrected for.

In the 6 kc/s channels, the varying delay to different parts of the sky is unimportant, as the longest baseline was only 400 nanoseconds, whereas one would expect a delay difference of several microseconds would be necessary to produce an appreciable effect in such a narrow bandwidth. However, in the broad band monitor channel the effects of delay can be very important. In receiver A this had a bandwidth of about 4 Mc/s, and in receiver B it had a bandwidth of about 100 kc/s. For this reason, the delay was tracked with a lumped constant variable delay line. Before each set of observations, the center delay (white light fringe) of the interferometer was determined and also the functional form of the loss of correlation with change of delay.

2.2 The Observations and Reductions

For the observations the antennas were pointed at the source with an accuracy greater than about 2', and tracked it across the sky while observations were made of fringes at various fixed frequencies, or, more commonly, while the receiver frequency was scanned through the absorption feature under study. The frequency of the local oscillator was read from the digital scaler and recorded on the chart once every twenty minutes or oftener. Sidereal time markers were automatically put on the record once per sidereal minute. The delay was adjusted back to delay center every 25 nanoseconds of delay for receiver A, and every 50 or 100 nanoseconds for receiver B.

The amplitudes were read from the records by drawing in the appropriate fringe maxima and minima smoothly with a pencil, connecting the adjacent minima with straight lines, and measuring the amplitude of this smooth curve at fringe maxima. Fringe times were measured about every twenty fringes, and interpolation sufficed to give accurate times, and hence frequencies. For convenience in this interpolation, a computer program was written which calculated the fringe times for various spacings and lobe rotator conditions. It provided for each fringe such auxiliary data as time constant corrections, frequency correction for the rotation of the earth, and the frequency at either of two

scan rates. Frequencies were corrected for the earth's motion about the sun and the sun's motion toward the apex by the tables of McRae and Westerhout[15]. Corrections were also applied for the component of the earth's rotational velocity in the direction of the source (up to 1600 cps), but not for the motion of the earth about the earth-moon barycenter (up to 60 cps). The time constant correction to frequency is shown to be

$$C_\tau \frac{1}{1+\omega_f^2\tau^2}$$

in Appendix I. (C is the rate of frequency scan, τ the time constant, and ω_f the fringe frequency.) With the 10 second time constant employed for these observations and a scan rate of 75 kc/s/hr this correction is less than 200 cps, and was neglected except in the case of the deep and narrow lines in the spectrum of Cas A, which are extremely sensitive to frequency.

The amplitudes read from the records were corrected for time constant, $10^{s}3$, and then plotted against frequency. These plots of individual scans werethen examined for unusual features, such as a change in profile with hour angle, or any other gross deviation from the other profiles taken at that spacing. If such was found, the record was con-

---

[15] MacRae, D. A. and Westerhout, G., Lund Observatory, (1956)

sidered separately and not added into the general mean.

The quantity of interest is the fraction of unabsorbed source intensity remaining, which I shall call R, as this varies only because of distributional effects over the face of the source. In order to derive this percentage, one must know what fringe amplitude the unabsorbed source would produce at any instant. Most frequency scans went well beyond the absorbed area, so that a good sample of the unabsorbed source was found at either end of the scan. If these amplitudes agreed to within four or five percent, a straight line (linear in frequency and hence time) was drawn connecting the ends of the scan. The residual, R, was taken to be the ratio of the observed fringe height to the height of this line. If the amplitudes at the ends of the scan did not agree (more likely due to changing resolution with hour angle than actual change in gain of the receiver), or if, for some reason or other, the amplitude were determined at only one end of the scan, then the observations with the broad band receiver were used to determine the amplitude of the unabsorbed source. The broad band amplitudes were read from the record, corrected for time constant and delay, and plotted on the same graphs as the narrow channel points, after multiplication by a constant to make the broad band points coincide with the average of the narrowband points at some frequency where the source was unabsorbed. The

broad band channel was not corrected for image, which was quite appreciable in both receiver A and receiver B. However, at 200 and 400 feet east-west, most scans covered a sufficient range of delay that the sinusoidal beat between signal and image could be observed clearly and the effect of image diminished by choosing the points where the signal and image were in quadrature. With receiver A the delay was tracked sufficiently often that variation due to this cause was somewhat reduced. If the scan had unabsorbed source recorded at both ends, any differences between the curve derived from the broad band observations and the two observations of the unabsorbed source (these were always small) were interpolated linearly.

The fixed frequency observations were made using an electromechanical integrator to phase detect and integrate the fringes output from the receiver (Morris, Clark, and Wilson, 1963). This device consists of an analogue computer which produces a sine wave of the same frequency as the source fringes. The fringes are multiplied by this sine wave in a resolver and then are integrated in a mechanical integrator. The mechanical integrator was read every ten to twenty minutes. If the source was not clearly detected in twenty minutes, the phase of the analogue computer was measured relative to that of the broadband record, in order that several such integrations may be combined

coherently even if there is a small error in the mechanical analogue computer. The numbers thus obtained were then corrected for time constant and divided by the unabsorbed source amplitude in the same manner as the frequency scans.

A plot was then made at very large scale containing the values of $\underline{R}$ as computed above for all frequency scans and fixed frequency observations at a given spacing. If the scatter was large enough to confuse the general picture, the individual scans were first smoothed by averaging of adjacent points, or else all points from all scans within a given frequency range, usually 2-1/2 kc/s, were averaged and plotted. In either case, a smoothed mean line was drawn on the large scale plot and taken to be the observed absorption spectrum.

This observed spectrum was then corrected for the AGC effect. Before each series of observations, the response of Cas A as a fraction of noise was measured with a square law detector for each antenna. The AGC controls the receiver gain to keep the total noise constant. The power gain is thus proportional to

$$1/(T_r + T_s)$$

where T_r and T_s are the geometric mean of the receiver temperature and the source antenna temperature respectively. The AGC correction, after returning to a percentage basis,

is thus a factor of

$$(T_r + T_s R)/(T_r + T_s)$$

for receiver A and

$$(T_r + \frac{1+R}{2} T_s)/(T_r + T_s)$$

for receiver B.

A crude bandwidth correction was applied to the data by the method of Bolton and Westfold[16], in those cases where the curvature of the spectrum and the accuracy of the data seemed to warrant it. It is interesting to note the effects of bandwidth on a single Gaussian. The reciprocal of the exact center frequency bandwidth correction is plotted against dispersion or halfwidth in Figure 5. We see that the Gaussian is virtually unaffected by the bandpass filter until it becomes as narrow as 3 kc/s dispersion, 7.5 kc/s halfwidth. It becomes quite impossible to recover from the presence of noise something as narrow as 1-1/2 kc/s dispersion or 3 kc halfwidth. 7.5 kc/s halfwidth corresponds to about 55° K. In the case of large optical depth, the bandwidth correction becomes more difficult after the exponentiation.

Of possibly equal importance is the broadening of the profiles themselves causing them to lose detail. As a general rule, it is very difficult to separate two lines of

---

[16] Bolton, J. G. and Westfold, K. C. Aust J Sci Res, 3, 19 (1950)

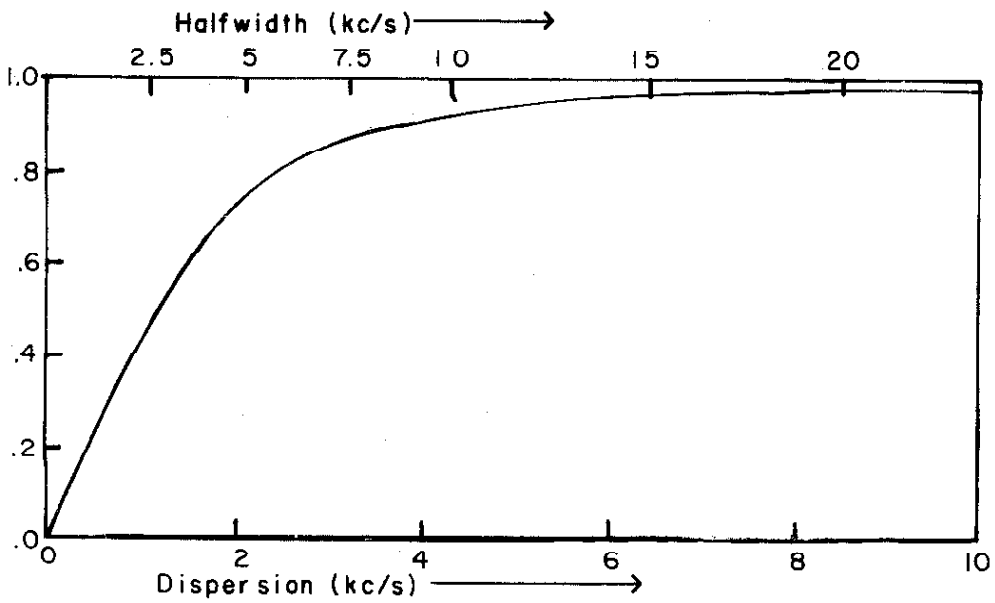

Figure 5. Inverse bandwidth correction for Unsaturated Gaussian.

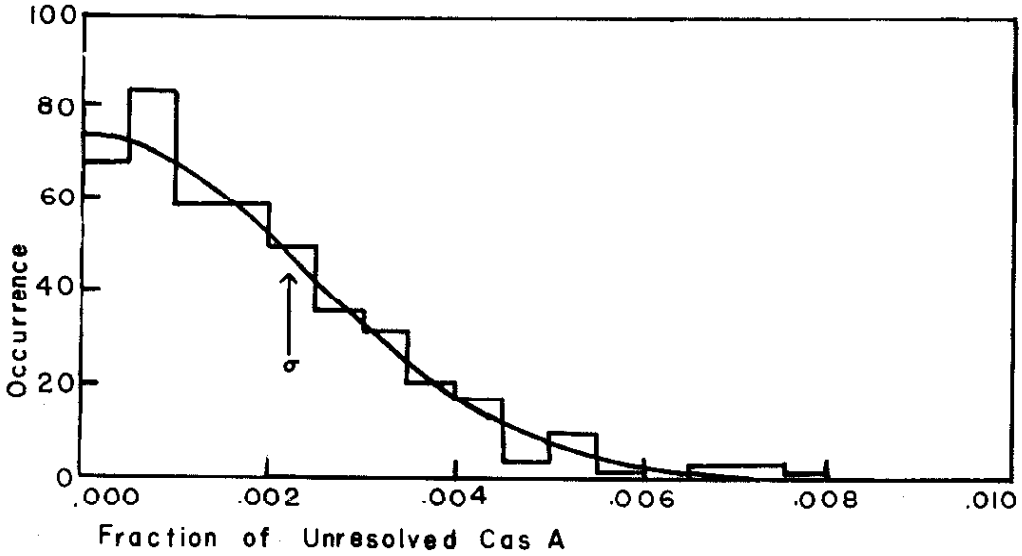

Figure 6. Distribution of noise records. 20 Minute Integrations.

like depth and dispersion if they are separated by less than the sum of their dispersions. This is especially true if the lines are deep, and thus the center region is quite noisy and uncertain. Many of the lines listed here as single may actually be blends of two or more components. There is some question about the physical significance of such close pairs, as the apparent division may actually be some small variation in the turbulent velocity within one region, rather than two spacially separated regions. There is really no physical reason for the cloud profiles to have a neat Gaussian shape, and indeed in the case of Cas A there is excellent evidence to the contrary.

Some of the profiles were provided with a least squares resolution into Gaussians by computer. The program was a modification of the Los Alamos general curve fitting program written by Moore, Zeigler and McWilliams[17]. The program iterates small changes in the parameters by Gauss' method to eventually produce a least squares fit. The principle modification was a device to insure convergence. This was done by taking the calculated parameter change vector, $\underline{\Delta P}$, and searching briefly for a factor α such that $\underline{P} + \alpha \underline{\Delta P}$ minimizes the mean square error. This guaranteed convergence, but, due to oscillations, the convergence was sometimes very

---

[17] Moore, R. H. and Zeigler, R. K. Los Alamos Scientific Report LA2367 (1960)

slow, especially if two components were well blended. The parameters generally converged to less than 0.1% change per iteration after about 25 iterations.

Errors arise in the amplitudes from two basic causes. These are the thermal noise in the receiver, and the gain instabilities and related uncertainties involved in estimating the fringe amplitude of the unabsorbed source at any time. In the strong sources the first is chiefly important near the bottoms of the lines, and the second does not enter for the weak sources. In the course of an attempt to detect the Zeeman splitting of the hydrogen line, a large number of twenty minute integrator records were taken, mostly with receiver A, on what is essentially noise. A histogram of the frequency of occurrence of a given integrator output plotted against the absolute value of the output is shown in Figure 6, along with a Gaussian of the same second moment. It is seen that the noise is, indeed, essentially random, and that in twenty minutes it amounts to about 0.003 of the unresolved Cas A. In a single fringe it amounts to about 1% of the unabsorbed, unresolved Cas A.

The gain and other instabilities associated with drawing the baseline are always of the order of 3% of the source, on a single record. Averaging helps somewhat, but probably not as much as on random noise, since some of the difficulties keep the same form from day to day (for instance,

crystal current may depend on LO frequency, and noise figure depends somewhat on crystal current). I take the following form to be a reasonable representation of the error in a profile at three kc/s intervals, and consisting of the average of three scans:

$$\Delta R = 0.02R + 0.01/S \qquad (1)$$

where S is the unabsorbed source strength as a fraction of unresolved Cas A. This may be locally reduced by the integrator records.

In addition to the above effects there may be systematic errors due to the method of reading the frequency scans. It is well known that the fringe height read from the record tends to be overestimated at small signal levels, even to the extent of reading a finite fringe height when no signal is present. In an attempt to minimize this effect, fringes in phase with the broad band record were sought, and both positive and negative fringe heights were preserved for averaging. However, this personal effect is probably still present to some extent, and thus at the bottoms of lines when the signal to noise ratio approaches one, the mechanical integrator records are much to be preferred, as they are reasonably impartial.

These errors in the profile are related in a very complicated way to the errors in the parameters describing the components of the profile. In those cases where there

was computer fitting of the profiles, the computer supplied an error based on the assumption that the errors for the various points are random and uncorrelated. In some cases this was increased to allow for the correlation introduced by drawing a smooth curve through the points and taken to be the actual error. Otherwise, the errors quoted for the parameters are estimates of the amount of deviation allowable without having the model exceed the given limits on the observed profile by a significant amount. The mean square error as a function of the parameters of the Gaussian components will in general have several local minima, so that it is entirely possible that the true resolution is quite different from the one quoted here.

Phases were read from most of the high quality records taken with receiver B and from some of the records taken with receiver A. The method of reading the phases was to approximate the linear parts of the two fringe sides with straight lines where they cross the zero line. The center of the fringe was found from these lines as described in Read (1963), except that, in this case, each fringe was read individually rather than the mean about the meridian. A similar procedure was applied to the continuum, and the quantity read was the difference between the continuum phase and the line phase, expressed in seconds. This quantity, even for a fixed frequency observation, may change with

time for the following reasons:

1) Part of the phase lag in an unabsorbed source is due to an intrinsic displacement of one pen relative to the other on the chart record--this part will remain constant in seconds--and part is due to differing line lengths in the line and broadband receivers--this part will remain a constant number of degrees of phase shift. As the finge period varies with the hour angle, the sum of the two is constant in neither seconds nor degrees.

2) A slight difference in average frequency in the line and broad band channels results in a relative phase shift at large distances from the central fringe of the interferometer. For receiver B this was a small effect--the effective frequencies were the same to within 100 kc/s, which meant that the effect was very small in the distance from the interferometer central fringe that these observations were taken. In receiver A, however, the broad channel had a mean frequency of 9.2 Mc/s at IF, 1.5 Mc/s from the narrow channel, though with this receiver delay was tracked sufficiently often to greatly reduce the effect of this difference.

3) An intrinsic change in the receiver phase with time may occur only in the latter part of the receiver as the two channels shared the same mixers and IF preamplifiers. There were many fairly narrow tuned circuits in both channels of

receiver B, and if any of these had been slightly detuned, the phase could be somewhat temperature sensitive. However, all the circuits not shared by the two channels were located in a temperature stabilized laboratory, which should minimize the effect. This effect was thought to be small because the day to day stability of the relative phase was rather good, varying no more than two seconds from average through a single observing period, and this could have been due to so prosaic a cause as bending of the recorder pens during servicing.

Because these effects are somewhat cumbersome to separate and correct for, the phase observations, like the amplitude observations, were reduced by interpolating a baseline between unabsorbed frequencies in the source. Observations far from the meridian, where the fringe period changes rapidly, were for the most part, not reduced for phase, so the difference in relative phase from one end of the scan to another usually amounted to only one or two seconds of time. The difference between a straightline interpolation between the ends of a scan and the measured relative phase is taken to be the true relative phase.

Phase measurements are subject to two types of bandwidth correction. The first is the usual sort, similar to that applied to amplitudes, and is due to an intrinsic variation of phase over the bandpass in the radiation as it

arrives at the antenna, resulting in a smearing of detail. For the most part this is a correction smaller than noise, and has not been taken into account in this investigation. The other type of bandwidth correction is due to variation of instrumental phase as a function of frequency within the bandpass. This effect was measured by feeding a signal generator into the two crystal filter channels with phases differing by ninety degrees, and correlating the signals output from the filters. The resulting curve of phase versus frequency is displayed in Figure 4b. All important phase deviations occur at very small signal levels, so they make little change in the relative phases measured unless the center of the filter is well blanked out by very heavy absorption. The only place where this correction becomes significantly large is the deep line in the Perseus arm feature in Cas A, where it is estimated that it might amount to about 15°, rather smaller than the observed phase, but this quantity is dependent on the exact shape of the amplitude spectrum at this point, which in turn is rather poorly determined because of its own bandwidth corrections and the generally poor signal to noise ratio at the bottom of the deep line. Because of this uncertainty, the effect was not corrected for, but arguments presented when the source is discussed will indicate that the effect is not very important.

Measurements of phase with receiver A are extremely unreliable because of the large residual image encountered, which is difficult to correct for. With receiver B and a 200 foot east-west baseline, a long record containing several sections of unabsorbed Cas A at the same frequency was analyzed to find the scatter in phase observations on a strong source. The observations were found to agree to within about half a second. From the known amplitude uncertainty at small signal levels, the following form is suggested for the phase error:

$$\Delta\phi = 1^{\circ}.2 + 0^{\circ}.5/SR \quad , \tag{2}$$

where S is the unabsorbed source strength as a fraction of Cas A.

2.3 The Theory of the Observations.

Following the discussion of van de Hulst, Muller, and Oort[18], we see that the absorption coefficient of neutral hydrogen is inversely proportional to the temperature,

$$K = \frac{d\tau}{dr} = \frac{dN_n(V)}{dr} \quad \frac{g_m c^3 h\nu}{g_n 8\pi\nu^2 kT}$$

Converting to frequency units and calculating the numerical value

$$k(\nu) = \frac{\beta\, n(\vec{r},\nu)}{T} \tag{3}$$

---

[18] van de Hulst, H. I.; Muller, C. A., and Oort, J. H. BAN, 12, 117, (1954)

where $n(\vec{r},v)$ is the local density of atoms centered on frequency v, at point $\vec{r}$, and,

$$1/\beta = 3.88 \times 10^{17} \text{ /kc/s} .$$

The local emissivity per unit volume is

$$n(\vec{r},v)\beta$$

independent of temperature. The solution of the equation of transfer for an antenna of finite beamwidth, observing HI in emission, is thus

$$T_a(v) = \int_{\text{beam}} \int_{\substack{0 \\ \text{on line of sight}}}^{\infty} \beta\, n(\vec{r},v)\, e^{-\tau(\vec{r})}\, d\vec{r}\, d\Omega\, /\Omega_{\text{beam}} \qquad (4)$$

where $\vec{r}$ is in the direction associated with the element of solid angle $d\Omega$, and

$$\tau(r,v) = \int_{\substack{0 \\ \text{on line of sight}}}^{\vec{r}} \frac{\beta\, n(\vec{r},v)}{T(\vec{r})}\, dr \qquad (5)$$

When $T_a(v)$ is interpolated to the region of the source, it is called the expected profile. The interferometer strongly discriminates against this quantity because of resolution. A series of records were taken of positions containing no continuum source with the interferometer at a spacing of 100 feet east-west. For 18 regions on the galactic ridge within 30° of the anticenter the frequency was scanned over about 75 kc/s near the peak of the profile in the Leiden catalogue. In no case was the emission detectable. The upper limit to the back ground radiation in the antenna beam is about 0.02 of Cas A.

The quantity observed in ordinary absorption measurements is

$$\int_{\text{source}} e^{-\tau(\vec{r}_o)} \, d\Omega / \Omega_{\text{source}}$$

where $\vec{r}_o$ is the vector to a given part of the source. By using the resolving power of the interferometer, one can seek to unfold the integral and obtain $e^{-\tau(\vec{r}_o)}$

If we make certain assumptions:

1) The structure in the hydrogen in the plane of the sky is larger than the antenna beam.

2) Variations in $n(\vec{r},v)$ are uncorrelated with variations in $T(\vec{r})$, and occur in an optical distance much shorter than one,

then we can directly solve the equation of transfer in a layer of thickness r.

$$\tau = \beta \bar{n} r \left\langle \frac{1}{T} \right\rangle$$

$$T_a = \frac{1}{\left\langle \frac{1}{T} \right\rangle} (1 - e^{-\tau}) = \frac{1}{\left\langle \frac{1}{T} \right\rangle} (1 - R) \qquad (6)$$

$$R = e^{-\tau}$$

Actually, the absorption profile does not bear a proportional relationship to the emission profile, so at least one of those two assumptions breaks down.

The model advanced by Hagen, Lilley, and McClain involved the breakdown of 1). In this picture, there are few clouds in front of the source, so the expected profile

directly in front of the source is different from that seen by the finite beamwidth of the antenna, which is made up of many contributions like that from in front of the source. In this model, we should expect that at very large distances the absorption lines will become shallower as the clouds no longer cover the whole source, and at very small distances the clouds will fill the beam of the antenna, and the emission profile will resemble more closely the absorption profile. The most distant absorbing cloud studied here is that in front of Cygnus A at a kinematical distance of 12 kpc. It would be interesting to learn if this cloud covers both of the components of the double Cygnus source, but the present observations were not executed with sufficient care to determine this. On the other hand, the emission profiles in the Orion arm bear no more resemblance to the absorption profiles than in other cases, though in this case the clouds certainly lie within a kiloparsec, and some other cases lie several times farther away.

Assumption 2) can be violated in several ways. Perhaps the simplest is a model in which the velocity dispersion is a strong function of the temperature, and there are not many clouds in front of most sources. The absorption spectrum will have a profile with peak width characteristic of the cold hydrogen, whereas the emission profile will tend to reflect the dispersion of the hot material.

The distribution of $\underline{r}$ on the plane of the sky is chiefly important in that it supplies a typical dimension of the cloud if a distance to the cloud can be estimated. For this limited purpose one may obtain a great deal of information without performing a full synthesis of the absorbed source brightness distribution and dividing it by the unabsorbed source distribution. Any variation of profile with baseline, or any variation of relative phase with frequency indicates a change in optical depth across the source, and hence that a typical angular length in the cloud is about the angular diameter of the source. From the specific nature of the change in question, a reasonable model with one or two free parameters should supply almost as good an estimate of typical length as would a complete brightness distribution on the plane of the sky, since variations in the line of sight cannot be determined in any case.

Thus, these measurements contain almost all the available information about typical lengths.

I shall close this section by noting three questions which should be kept in mind in the ensuing discussions, though one is unable to answer them with any degree of certainty at the present time.

1) What is the temperature in the hydrogen? Is it all at about the same temperature, or is it necessary to invoke a two component model? This question will be dis-

cussed in Section 4.2, but must wait for a complete answer on an antenna with a beamwidth small enough to directly investigate the question whether the expected profiles of the sources are indeed the sum of many profiles with peaks as sharp as those of the absorption spectra.

2) In the gap between peaks in the profiles, the absorption is often many times less than in the peaks. If, indeed, this corresponds to physical separation of the clouds, what force keeps the clouds stable, and effectively prevents them from expanding into this open space?

3) What relation do these clouds bear to objects seen optically, such as dark nebulae, Bok globules, the gas forming the interstellar lines, or the dust producing the interstellar polarization?

III

DESCRIPTION OF THE OBSERVATIONS

Five sources were observed at all baselines in an attempt to determine details of the surface brightness distribution across the face of the source: Casseopeia A, Taurus A, Sagittarius A, Orion A, and the Omega Nebula. The characteristics of these sources are listed in Table II for convenient reference. Table IIA gives the intensity, size, and distance. Table IIB gives the fringe visibilities at the various spacings employed in this investigation. The fluxes and east-west visibilities have been taken from Lequeux[19], and the north-south visibilities are approximate measures from the broad band records of the present investigation. These are rather inaccurate as inadequate calibration sources were taken near the time of observation; however, they serve as the rough guide to fringe visibility needed here. Each of these sources will be discussed in detail below. In addition to the five sources which have been studied intensively, sixteen others, of which ten show absorption spectra, were observed at one baseline only, with widely varying limits of sensitivity. These weaker sources will be discussed briefly at the end of this section.

---

[19] Lequeux, J. Ann d'Ap, 25, 221, 1962

Table II The Five Intense Sources

A.

Source	Distance kpc	Intensity $I/I_{Cyg\ A}$	Size
Cas A	3.4	1.62	4!4
Tau A	1.1	0.59	4'
Sgr A	10.0	0.68	3!5*
Ori A	0.5	0.27	7'
Omega Neb		0.40	6!5

B. Fringe Visibilities. Below are given the meridian fringe visibilities and effective baselines in wavelengths for the various sources.

Baseline / Source	100' E-W	200' E-W	400' E-W	200' N-S	283' NW-SE
Cas A	143 .97	287 .75	576 .40	267 .77	396 .63
Tau A	143 .94	287 .77	576 .36	275 .78	403 .65
Sgr A	143 .27	287 .20	576 .08	158** .20	313 .16
Ori A	143 .63	287 .44	576 .28	212 .55	360 .42
Omega Neb	143 .67	287 .34	576 .15	171 .41	337 .21

* The source consists of two components. The 3!5 given here is an inner core in a halo of diameter about 1^{o}. If the large source is subtracted out, the fringe visibilities in the table below should be multiplied by 3.4.

** On the meridian, the north dish is shaded by the south one at the declination of Sgr A. Observations were therefore made east and west of the meridian at hour angles centered about $2^{h}20^{m}$, approximately. The two different figures for fringe visibility are for the east and west hour angles respectively.

3.1 The Perseus Arm Feature in Casseopeia A.

The absorption profile of Cas A is distinguished by having two separate regions of absorption arising in different spiral arms and well separated in frequency. The optical depth between the two regions falls to less than 0.01. We may therefore consider each feature separately, with no difficulty of separating the two components. The feature arising in the Perseus arm again has two minima, both quite deep, with an absorption of 50% in the maximum of the profile between the two minima. In the following discussion, these two minima will be referred to as the "broad line" at 176 kc/s, and the "deep line" at 228 kc/s (see Figure 7). There are in addition several sudden changes of slope or inflection points which may indicate the presence of other components. Two of these were pointed out by Muller (1958). The most obvious one is an inflection point located on the low frequency shoulder of the line at about 157 kc/s, indicating the presence of a component in the profile at about 155 kc/s with an optical depth in the neighborhood of 0.3.

The broad feature is at least double in nature. There is a very well marked inflection point near the bottom of the line, and a faint change of slope suggestive of another component on the high frequency side of the line. However, one wishes to be a bit cautious about the interpretation of

such features. The thermal broadening, for any reasonable temperature, is sufficient to produce a line width of at least 5 kc/s between half optical depth points. Thus, the entire Perseus arm feature covers only about twenty-five of these typical widths. Since it takes three parameters to describe a cloud (maximum optical depth, center frequency, and dispersion) one would expect that any distribution of velocity over the matter in the region in question could be reasonably well represented as about eight Gaussian components. As we shall see, we approach this limit rather closely, without even attempting to fit all the small, barely significant deviations in the profile, but instead keeping a generally reasonable choice of parameters.

In interpreting blends, there is a tendency on the part of the observer to consider that a spectrum line is localized near the point where it produces its maximum effect in the observed spectrum. For instance, if a shallow, broad component is concentric with a deep, narrower component, one may be tempted to interpret this as three lines, a deep narrow one in the center and two shallow narrow ones on its wings. In marginal cases, this sort of interpretation is extremely difficult. In this thesis the broad, Perseus arm feature in the spectrum of Cas A is interpreted as a narrow feature added to a broad, deep line which produces most of the integrated absorption in the area. This interpretation

is preferred because the phase measurements indicate that the absorption on either side of the extreme minimum of the profile is located at about the same right ascension, whereas the radiation appearing at the bottom of the profile comes from quite a different location.

If one fits reasonable Gaussians to the two peaks in the optical depth profile, one quickly finds that there is a considerable area above the sum of the Gaussians between the two lines. It is fairly clear that there is some hydrogen with central frequencies within this range, but the resolution into separate components is very difficult if not impossible. At present it appears impossible to fit this residue with but a single Gaussian; however, a small change in the parameters used to describe the two main peaks might allow one to do this because the differences from a single Gaussian are rather small compared with the depths of the two main components.

It is clear that the deep line in this feature is very deep. The optical depth was given as 2.0 by Hagen, Lilley, and McClain[20], 4 by Muller (1958), and greater than 4.5 by Shuter and Verschuur. The values given in CRW were > 4.3 single dish, and 3.6 with the interferometer. This last

---

[20] Hagen, J. P.; Lilley, A. E. and McClain, E. F. ApJ, 122, 361

measurement now appears to be erroneous. The present series of measurements, taken with essentially the same interferometer, and a receiver improved by the use of crystal rather than L-C filters, indicate that the optical depth at the bottom of the deep line is indeed very high. Let us consider, for instance, the 200 foot east-west observations, which is the same spacing reported in CRW. The fringes at the bottom of the line were integrated for a total of about eight hours. The residual intensity observed in this time was about 0.007 ± 0.0015. Correction for the effect of bandwidth is very difficult because in the region of interest, the profile is very noisy, and the bandwidth correction is rather dependent on the exact profile. However, a bandwidth correction was estimated on the basis of a Gaussian in optical depth fitted in the frequencies of the $\tau = 2$ points and in the height of the peak. After an iteration one finds from this model that the residual, corrected for bandwidth, is 0.004. The further correction for the effect of AGC brings this figure down to 0.0033. With the estimated error for the uncertainty in the bandwidth correction added to that for the noise, this figure is a marginally significant 0.0033 ± 0.0020. In any case, this averaged optical depth is certainly greater than 5.0. The data for 100 feet east-west agree with this to within the observational error of about 0.002. There was insufficient integration time taken with

the 400 foot east-west baseline to detect the residual with any certainty, but it was certainly not much greater than this quantity.

The observations taken at 100 feet and 200 feet east-west agree very well with each other. Therefore, to improve signal to noise ratio the two sets of observations were averaged with appropriate weights. The 200 foot observations have the greatest weight in this average as there were more scans of higher quality. This profile was taken to be the basic, short spacing profile, to which all other spacings may be referred, and which was the basic data in the attempts to fit the line profile with a set of model clouds.

The absorption profiles for this source are presented in Figure 7. Figure 7a is the expected profile, taken from CRW, which was derived from observations with a small antenna, in which the source contributes very little to the antenna temperature. These profiles average over a much larger region than necessary, but they are adequate for this investigation as they are useful only to indicate from the emission what hydrogen is available to absorb the radiation from the source, and do not play any integral part in the analysis. Figure 7b is the short spacing east-west profile as described above.

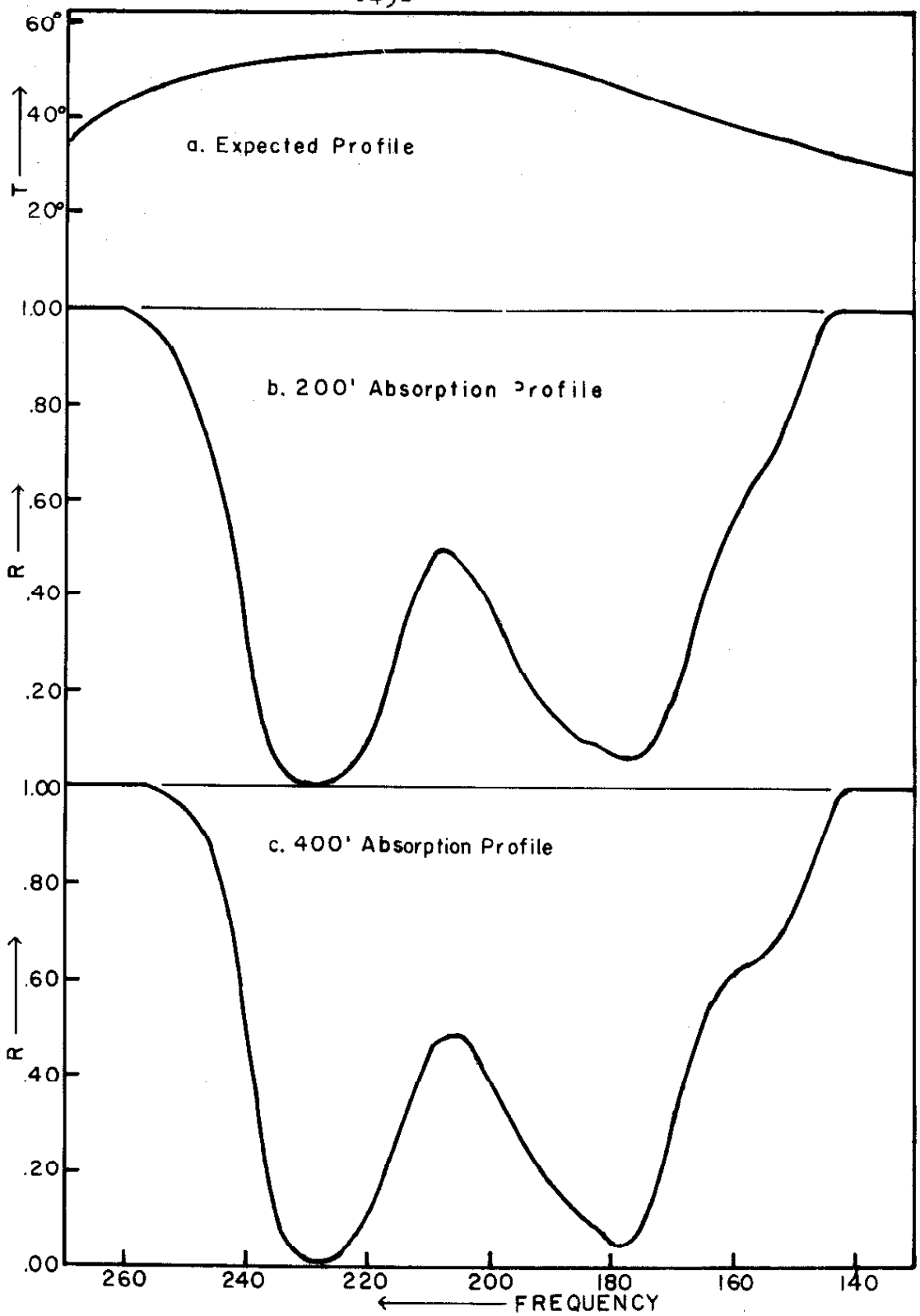

Figure 7. Cas A Profiles

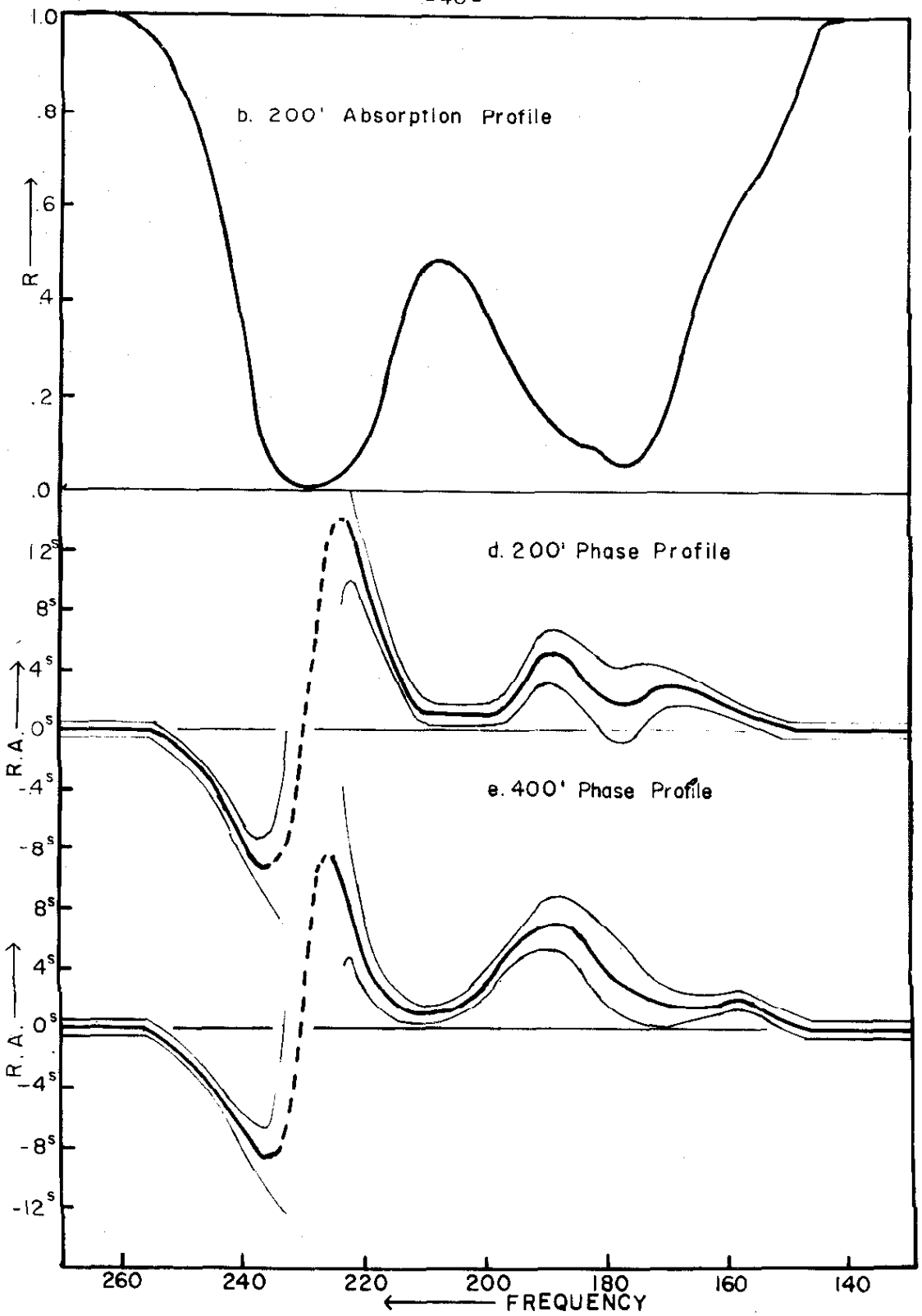

Figure 7 (continued). Cas A Profiles.

Figure 7c is the profile observed with the 400 foot east-west spacing. It is clear that there is a large difference between this and the small spacing profile in the vicinity of the feature at 155 kc/s. This is mostly due to the fact that the broad, deep line is somewhat narrower at this spacing, allowing the weak component to stand out more clearly, although the weak component itself is actually slightly deeper. The narrowing of the broad component implies that in the wings of the line the source appears smaller than the unabsorbed source, while remaining about the same size at the center.

The 200 foot north-south observations were taken with receiver A and thus suffered from a large amount of image in the receiver, and so the line bottoms cannot be compared in detail with the east-west observations. However, when one allows for the error possibly introduced by the image, the observed profile nowhere differs significantly from the short spacing profile. The diagonal NW-SE baseline was also used with receiver A, and in addition suffers from the disadvantage that the resolution is changing rapidly near the meridian where most of the observations were made. Within the limitations set by these considerations, the profile taken with this separation also agrees with the short spacing profile.

The phase, or rather the right ascension, measured along the profile at the 200 foot east-west spacing is presented in Figure 7d. The ordinate of the figure is in seconds of time. The dotted portion of the curve is the part which is completely uncertain because the source is essentially totally absorbed and hence the signal to noise ratio is too small to determine the phase at all. The two lighter lines surrounding the dark phase curves are the limits of error according to equation (2) Section 2.2. Inasmuch as there are real effects of differential phase lags between the two crystal filters, perhaps some argument is needed that the exceedingly gross features in this diagram are not merely observational errors. All frequency dependent phase effects introduced in the receiver and not found in the radiation coming from the sky must introduce a phase shift, and hence a right ascension shift inversely proportional to baseline. However, all effects present in the sky will correspond to a frequency dependent right ascension shift, roughly independent of baseline. The phase measured at 400 feet east-west is shown in Figure 7e. It is seen that the right ascension shifts are about the same in the two cases, while the phase shifts are about twice as large in the case of the 400 foot observations. As a further check, the 100 foot east-west observations were reduced for phase. At this spacing, the natural period of the fringes of Cas A

is 183 seconds, which was considerably longer than that of most other fringes in the observing program, so a phase rotation introduced by a one RPM synchronous motor was added to the natural fringe rate to produce a fringe rate of 45 seconds, about the same as the natural fringe period at 400 feet east-west, 46-1/2 seconds. The phase shifts were much smaller than those found on the 400 foot records. When the phase shifts were translated into right ascension, they were again found to give about the same curve as the 200 foot measurements give, though with considerably worse accuracy, since a given displacement of the fringe now corresponds to a much larger shift in right ascension.

It is informative to plot the phase against R. This is done for the 200 foot east-west spacing in Figure 8. The tick marks are placed on the curve every two kc/s frequency change. The inner curve gives the phase behavior at the bottom of the broad component, and the large outer loop describes the behavior in the deep component. The two straight lines bounding the curve are approximately the curves which would result if an opaque blind were being drawn across the source, and hence, for this spacing, represent the maximum possible phase shifts obtainable. It is seen that the observed curve occupies a large fraction of this maximum. Therefore, a very efficient mechanism for obtaining phase shifts must be at work, and these necessarily

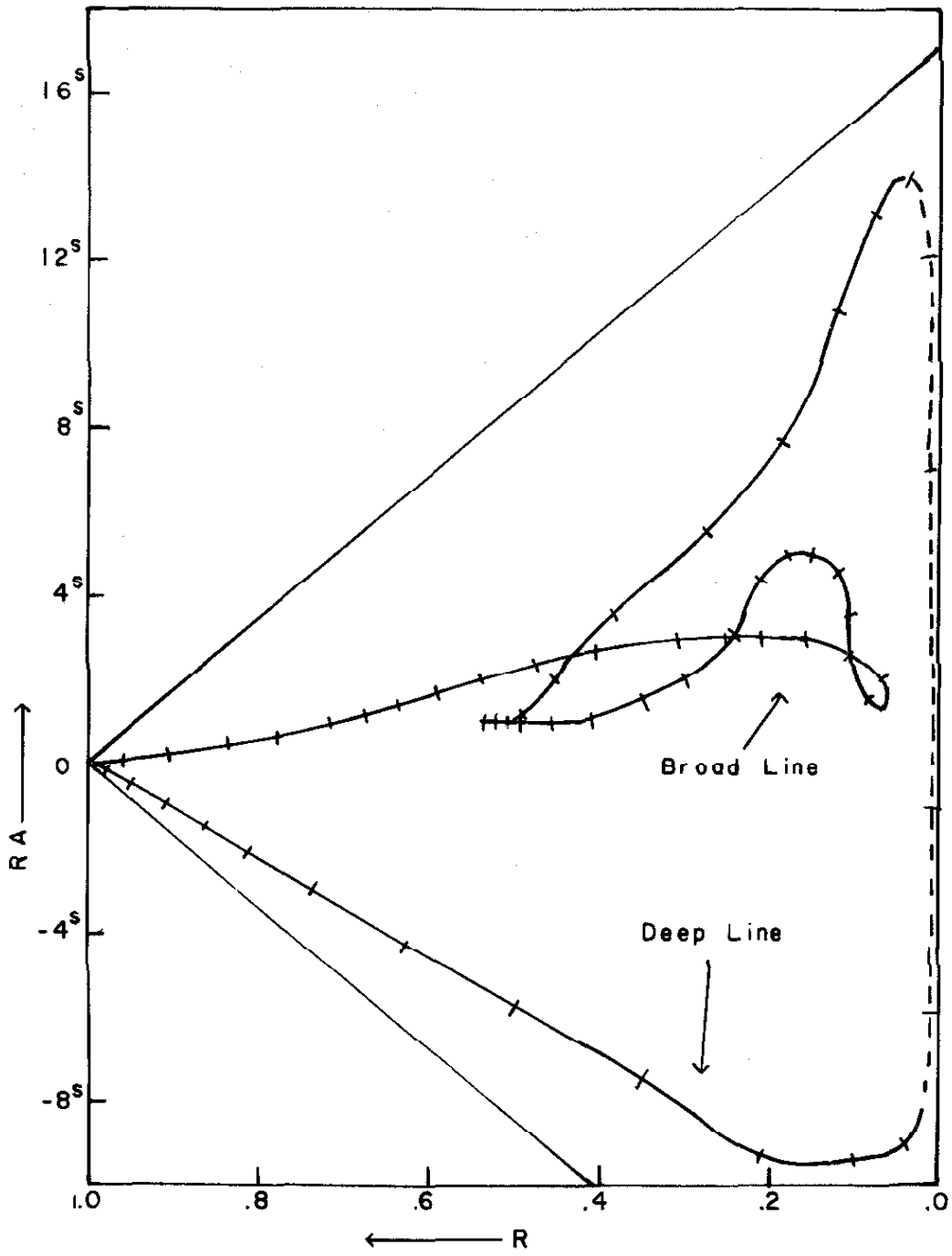

Figure 8. Phase plotted against amplitude for the Perseus arm feature in Cas A. Frequency is the running parameter.

involve fairly large optical depths.

The phase shifts from the north-south and NW-SE baselines were used only with great caution because of the extreme sensitivity of the phase to the correction for the image. The error in phase may be as great as

$$\Delta\phi = \text{Image/Signal}$$

In the region of interest the observed fringes may consist of about three quarters signal and one quarter image, which could correspond to a phase shift of nearly a minute of arc, a quite considerable part of the source.

In order to achieve some sort of understanding of the effects present in this profile, I shall present a model, which, though it does not precisely reproduce the observed profile in both amplitude and phase, at least demonstrates qualitatively the effects present, and, in most cases, can be modified in a number of different ways to produce the exact observed profile. The model consists of six clouds, several of which are resolved by the interferometer in ways described below. In calculating the models, only the simplest clouds sufficient to qualitatively produce the observed effects were used. The reason for this is the previously mentioned difficulty in the number of parameters in the model being nearly as large as the number of independent pieces of information.

For the purpose of calculating the model, the brightness temperature across Cas A was taken to be a simple rectangular distribution in one dimension[21]. In the frequency dependencies quoted below, a parameter $\underline{x}$ is defined on the face of the source, with x being positive to the east and $\underline{x} = \pm 1$ corresponding to the edges of the source, which was taken to be a rectangle of length 4.4' so that a unit of $\underline{x}$ corresponds to 2!2.

The error in the assumed brightness distribution should not affect the parameters of the fitted model too much. The small extension on one side may appreciably change the phase in the neighborhood of the bottom of the deep line, but not too much. Any detail of sufficiently high angular frequency to escape Lequeux's observations would be smoothed out unless the interstellar clouds show structure of the same order of size, which appears unlikely in view of the smoothness of clouds several times nearer than these in front of this and other sources.

In the following discussion, kinematical distances to the various clouds have been quoted. These were computed from the rotation curves of Schmidt[22] with the abscissa multiplied by 10.0/8.2 to reflect subsequent improvement in

---

21 see Lequeux, J. Ann d'Ap, 25, 221, 1962

22 Schmidt, M. BAN, 13, 15, (1956)

the value of the distance to the galactic center. The masses, $\underline{M}$, and escape velocities, $\underline{v_e}$, given below are computed on the basis of a spherical cloud model with the line of sight through the center. That is, if the typical length is L, the mass has been taken to be

$$M = 1.3 \frac{\pi}{6} M_P N_H L^2 = 0.0021 \int \tau \, d\nu \; L_{pc}^2 \; T \; M_\odot \qquad (7)$$

where the factor of 1.3 allows for 30% helium by weight in the interstellar medium, and $\underline{M_p}$ and $\underline{N_H}$ are the mass of the hydrogen atom and the surface density of hydrogen, respectively.

$$v_e = \sqrt{\frac{2MG}{L}} \qquad (8)$$

A computer program was written which supplied the residual $\underline{R}$ and the phase given the following parameters for each component: depth, dispersion, center frequency, linear variation of central optical depth across the source, and linear variation of velocity across the source. Because of the limited amount of information available, a more elaborate set of parameters was not made available. A set of models was produced by this program, and the one best fitting the 200 foot east-west amplitudes and phases is presented below.

I shall now consider each of the clouds in turn.

1) In the model profiles to be presented in Figure 9 this cloud was taken to have the following profile:

$$\tau(f,x) = (0.25 - 0.10\,x)\exp\left[-(f-155)^2 / 2\cdot(5.9)^2\right]$$

From noting the change in fit with the observed profile it is possible to estimate the errors in these parameters. They are as follows: central optical depth $\tau_o = 0.25 \pm 0.15$. Variation in optical depth 0.10 ± 0.15. This small variation in optical depth was inserted because of the tendency of the phase measurements to tail out from the broad band line somewhat more slowly than one would expect from the model for the broad line. Actually, the situation is somewhat more complicated. This is indicated by the difference between the 200 foot and 400 foot profiles in this area. It is seen from a casual inspection that the step in the profile at this point is much more noticeable on the 400 foot spacing profile. This arises from two causes: firstly, the profile for the broad deep feature is somewhat narrower, which will be discussed with that feature, and also, the 155 kc/s feature is actually deeper. This more separated profile suggests that a more appropriate optical depth for this component is 0.4. The second aspect, that the 155 kc/s feature is deeper, is slightly variable with hour angle. Most observations were relatively near the meridian, and produced a curve falling well below that obtained at 200 feet. However, a single observation at 3^h30^m hour angle falls well above the 200 foot curve, and an observation at

1^h hour angle seems to be to some degree intermediate. Since the curve can actually go both below and above the 200 foot curve, it is easier to explain the effect by the rotation of the effective baseline than by the change of its length with hour angle. If, for instance, the absorption is a bar, lying across the source in a position angle near 140°, the source near the meridian and earlier than the meridian would appear double with a transform which drops faster than that of the unabsorbed source, and hence the line would appear deeper than at zero baseline. At large positive hour angles, the fringes would run perpendicular to the absorbing band, so the strip scan would appear slightly smaller than the unabsorbed source. This interpretation is rather uncertain, as the effect can be explained in several other ways as well. Even granting the basic explanation, the uncertainty in the position angle of the absorbing bar is at least 20°, and no estimate can be made of the optical depth of the bar, or of its extent, save noting that it must cover more than a quarter of the source. Within this description, any reasonable distribution of density is capable of giving the observed result.

The center frequency is 155 ± 2 kc/s, and the dispersion is 5.9 ± 1.5 kc/s. This dispersion corresponds to thermal broadening at a temperature of 190° K, but the uncertainty in this figure is about 80°. The integrated

optical depth is 2.6 ± 1 kc/s. If we take the temperature to be 100° K, this corresponds to 1.0×10^{20} atoms per square centimeter in the line of sight. The kinematical distance of the feature is 2.6 kpc. If the bar picture of the absorption is approximately correct, a typical distance in the cloud is slightly less than the diameter of the source, say 3'. At a distance of 2.6 kpc, this is 2.3 psc = 7.3×10^{18} cm. The density is thus in the neighborhood of 12 atoms/cc, with an uncertainty of a factor of two. The mass of the cloud is 3.5 $M_\odot$. The velocity of escape from the surface is 0.15 km/s, whereas the speed of sound is about 1 km/s; therefore, the cloud is unstable against expansion, unless there is another source of pressure. For reference, the above parameters are computed also for a 10 parsec cloud. The density becomes 3 atoms/cc, the mass is 55 solar masses, and the escape velocity is .31 km/s.

2) The second cloud in the model has the following frequency profile:

$$\tau(f,x) = (2.4 - .80x) \exp\left[-(f - 180)^2 / 2\,(11.3)^2\right]$$

With estimated errors, the parameters are as follows: central optical depth, 2.4 ± 0.2. Variation of optical depth 0.8 ± 0.2. Center frequency 180 ± 1.0. Dispersion 11.3 ± 1.0 kc/s. In this case there definitely appears to be a variation of optical depth over the source indicated by

the considerable phase shifts as one scans through this line in frequency. Since the phase shifts go in the same direction on either side of the very bottom of this broad feature, it has been interpreted as a broad feature with a narrow feature superimposed near the peak absorption. Any other interpretation would involve at least three components instead of two. It is of some interest to know the direction of the gradient in optical depth; the right ascension component of the gradient is given by this observation with an east-west baseline. The equivalent quantity for a north-south baseline would give the absolute direction of the gradient, but the observations are somewhat unreliable due to the presence of large amounts of image. Making appropriate corrections for image one finds that the shift is rather small--about 0!2 $\pm$ 0!2, whereas the shift at 200 feet east-west is 0!65 near 189 kc/s. Thus the gradient is nearly due east-west, with the greatest optical thickness to the west.

Because of this gradient in the optical depth, the absorbed source appears smaller than the unabsorbed source, and hence the line bottom should not appear to be as deep at large spacings as at small ones. Near the bottom, the gradient in the third component roughly cancels this tendency, but the line sides should rise, making the line narrower at large spacings.

The kinematical distance is 2.9 kpc. If, as the phase measurements suggest, the scale of length in the cloud is slightly greater than the source size, say 8', the cloud is about 7 pc in size. The integrated optical depth is 68 ± 10 kc/s, which at a temperature of 100° K is 2.6×10^{21} atoms/ sq cm in the line of sight. This corresponds to the rather high density of 120 atoms/cc. The total mass of the cloud is 1.4×10^{36} grams, or 680 M_0. The escape velocity at the surface is thus 1.3 km/s, which is comparable with the velocity of sound, but is still rather smaller than the 2.4 km/s observed velocity dispersion. The cloud is at best temporarily stable without an external source of pressure. If the density is uniform, the potential energy is 1.3×10^{46} ergs and the kinetic energy is 7.8×10^{46} ergs.

3) The third cloud in the model has frequency profile:

$$\tau(f,x) = (0.7 + 0.525x) \exp\left[-(f-177)^2/2\cdot(3.6)^2\right]$$

The errors on the parameters are as follows: central optical depth, 0.7 ± 0.3. Variation of optical depth 0.525 ± 0.2. The variation of optical depth is necessary to produce the observed local minimum in the phase plot at the frequency at which the amplitude plot has its minimum. Center frequency 177 ± 2 kc/s. Dispersion 3.6 ± 1.0 kc/s. This dispersion corresponds to a thermal doppler broadening from hydrogen at 70° K. The large uncertainty quoted on the

dispersion comes from the fact that the dispersion is rather critically dependent on the shape of the profile in the region of the plateau near the bottom of the line, and this portion of the profile is quite dependent on the bandwidth correction. However, we see from Figure 5 that a 3.6 kc/s Gaussian is only 10% reduced in the present bandpass. If one chooses to interpret the profile as two neighboring lines which produce the strong inflection point rather than narrow and broad components at about the same frequency, the depth and dispersion of the line centered near this frequency go up considerably. The phase curves observed with the north-south interferometer do not appear to be double peaked, which perhaps indicates that the gradient of this component also lies roughly east-west.

The kinematical distance of this cloud is 2.9 kpc. The rather small integrated optical depth, 6.3 kc/s, corresponds to 2.4×10^{20} atoms/sq cm at 100° K, or 1.7×10^{20} atoms/sq cm at 70° K. If we again take a cloud size of 7 pc, we obtain a density of about 11 atoms/cc, and a total mass of about 64 $M_{\odot}$. The escape velocity at the surface is only 0.39 km/s, much less than the velocity of sound.

4) This cloud and the next are more or less chosen to fill in the gap in the optical depth profile which would be left by the other features making the deep peaks on

either side. Because of the deep features, these components are more or less completely swamped. It is especially difficult to estimate the dispersion of the component in these circumstances. For this component, there is a small change in slope which may mark it out, but the deviation from a smooth slope in the side of the broad deep component is only about 4% of the unabsorbed source. This may be the same component noted by Muller at 200 kc/s. I find the optical depth to be given by

$$\tau(f,x) = 0.40 \quad \exp\left[-(f-198)^2 / 2\cdot(8.5)^2\right]$$

The errors are as follows: central optical depth 0.40 ± 0.15. Center frequency 198 ± 4 kc/s. Dispersion 8.5 ± 3 kc/s. In addition to these errors it appears likely that there is another arrangement of the components which would produce a mean square error comparable with the present one, but which has these two center components in drastically different positions or strengths.

The kinematical distance is 3.2 kpc. The integrated optical depth is 8.5 kc/s, which at 100° K. is 3.3×10^{20} atoms/sq cm in the line of sight. There is no information available about the scale of length, but if we take 10 psc, this produces densities of about 11 atoms/cc and a total mass of about 180 M_0, though this mass could be wildly wrong because of lack of knowledge about the scale length.

5) It is entirely possible that changing the parameters associated with the neighboring components could make this one vanish entirely. However, it seems simplest to use this weak component to make up an excess of optical depth left over when all others are subtracted. Very little can be said about the parameters of the cloud. Those used in the present model are

$$\tau(f,x) = 0.35 \exp\left[-(f-213)^2 / 2\cdot(6.2)^2\right]$$

The errors given below are those which can be associated with this interpretation; a grossly different interpretation might change any one by 100%. Central optical depth 0.35 ± 0.15. Center frequency 213 ± 6 kc/s. Dispersion 6.2 ± 3 kc/s. The integrated optical depth is 5.4 ± 3 kc/s, corresponding to 2.1×10^{20} atoms/sq cm in the line of sight, at 100° K. With a 10 pc typical length, this becomes 7 atoms/cc and a total mass of 115 $M_{\odot}$. The kinematical distance is 3.6 kpc, although the distance to the source is given by Minkowski to be 3.4 kpc.

6) This cloud is the most remarkable one studied. The fact that the phase is radically different on the high frequency side of the line from that on the low frequency side indicates that the absorbing material is in systematic motion across the face of the source. The extremely high optical depth in the center of the line indicates that the cloud is a particularly thick and massive one, and also

considerably restricts the range of models, since any model must cover all of the source to rather high optical depths at the center frequency of the line. The parameters adopted for this model are given below, the adopted optical depth being:

$$\tau(f,x) = 6.7 \exp\left[-(f-227.5+6.0\cdot x)^2 / 2\cdot(7.0)^2\right]$$

The value of the central optical depth and the gradient in average velocity are determined by the residual radiation at center frequency and the shape of the phase curve. Given a velocity gradient, the central optical depth is well determined by the center frequency residual; however, a large range of gradients, each with its own central optical depth, gives much the same curve of phase versus frequency. Thus the uncertainty in both of these parameters is large, although there are fairly tight restrictions on one given the other. It is clear that the optical depth is certainly greater than the negative logarithm of the central frequency residual, which guarantees it to be greater than 5.5. It is entirely possible that there might be "lumps" in the absorption where the optical depth is much higher than the 6.7 given above.

The amplitude curve given by this model differs considerably from a simple Gaussian with an appropriately broadened dispersion, and indeed fits the observed profile

rather better than the simple Gaussian. The simple Gaussian model tends to require a weak component on the high frequency side of the profile, at about 248 kc/s, which is rather less necessary with the non-Gaussian model. It is to be noted that, although the phase curve of the model resembles that observed, it is far from an exact fit. The asymmetry might be due to either a change in density distribution across the source or a deviation of the velocity change from a simple linear law. The latter explanation is probably correct, as the observed phase curve apparently cannot be produced by a linear or step change in optical depth across the face of the source. The effect of a nonlinear velocity distribution on the curves has not been investigated.

The north-south observations have been reduced for phase in this case, though the corrections for the image were made only approximately. The range of hour angles is rather restricted, usually to within an hour of the meridian, though one scan was taken at an hour angle of $+ 3^h$. The asymmetric part of the phase change appears to vanish and change sign at about -1^h. This corresponds to a position angle of the perpendicular to the dispersive motion of about 10^o. The symmetrical part of the phase is not very large, at least less than 1', the large uncertainty being due to the presence of image, incompletely corrected for. This indicates that the total absorption is

more or less uniform across the face of the source. Thus, at the moment we have no direct information bearing on the size of this cloud.

The uncertainty in the various parameters of this line are about as follows: Central optical depth $6.7\ ^{+\infty}_{-1.2}$. The central optical depth could be quite high, depending on the law assumed for the variation of the velocity with position. Center frequency 227.5 ± 0.7 kc/s. Dispersion 7.0 ± 1.0 kc/s. The error in the dispersion is somewhat correlated with those in the change in velocity with position and in central optical depth. The velocity gradient is 6.0 ± 2 kc/ 2!2. The kinematical distance to the feature is 3.8 kpc, which is greater than the 3.4 kpc given by Minkowsky for the distance of the source determined by its expansion velocity and proper motion. This difference in velocity would correspond to a peculiar motion of only 4-1/2 km/s. Taking a distance of 3.4 kpc, the velocity gradient of the model, 0.57 km/s/min, is 0.57 km/s/pc, which is an angular velocity corresponding to a period of revolution of 11 million years, comparable with the likely period of existence of the cloud. With this sort of period it seems unlikely that the cloud is in a true, stable rotation. An alternate explanation might be the passage of a shock wave through the cloud at an angle with the line of sight, so that part of the cloud

has been accelerated to a new velocity, preferentially on one side of the source. Since the phase deviations are more extreme on the low frequency side of the line, going east, and it is more natural to associate this more extreme deviation with a narrower line, one could even suggest the direction of the shock wave as going away from us and westward rather than towards us and eastward.

The integrated optical depth is about 117 kc/s, which is somewhat uncertain because of the uncertainty in the central optical depth. It should be noted that the integrated optical depth in this case is not obtainable simply by taking the logarithm of the observed curve and integrating with frequency, because the optical depth varies across the source. The cloud has a diameter of at least 5 pc, in order to cover the entire source. Table III below lists some of the parameters for clouds with diameters 5, 10, and 15 pc. This cloud may be stable against disruption by internal pressure, but is probably unstable with respect to centrifugal forces. Thus, in this model we have met no clouds which are unqualifiedly stable.

The observed curve for 200 feet east-west is compared with that given by the model in Figure 9. Figure 9a is the curve given by the model, and Figure 9b is the difference between the observed curve and the model curve. The fit is to an error of better than 2% in most places. The remaining

Table III

The Deep Line in the Perseus Arm Feature in Cas A

Cloud Diameter (pc)	5	10	15
$\int \tau \, d\nu$ (kc/s)	117	117	117
N_H at 100° K (10^{20} atoms/sq cm)	45	45	45
n_H (atoms/cc)	290	145	97
$M / M_\odot$	610	2500	5500
Velocity of escape (km/s)	1.4	2.0	2.5
Surface gravity (10^{-9} cm/s^2)	1.3	1.3	1.3
Centrifugal Acceleration (10^{-9} cm/s^2)	2.5	5.0	7.5

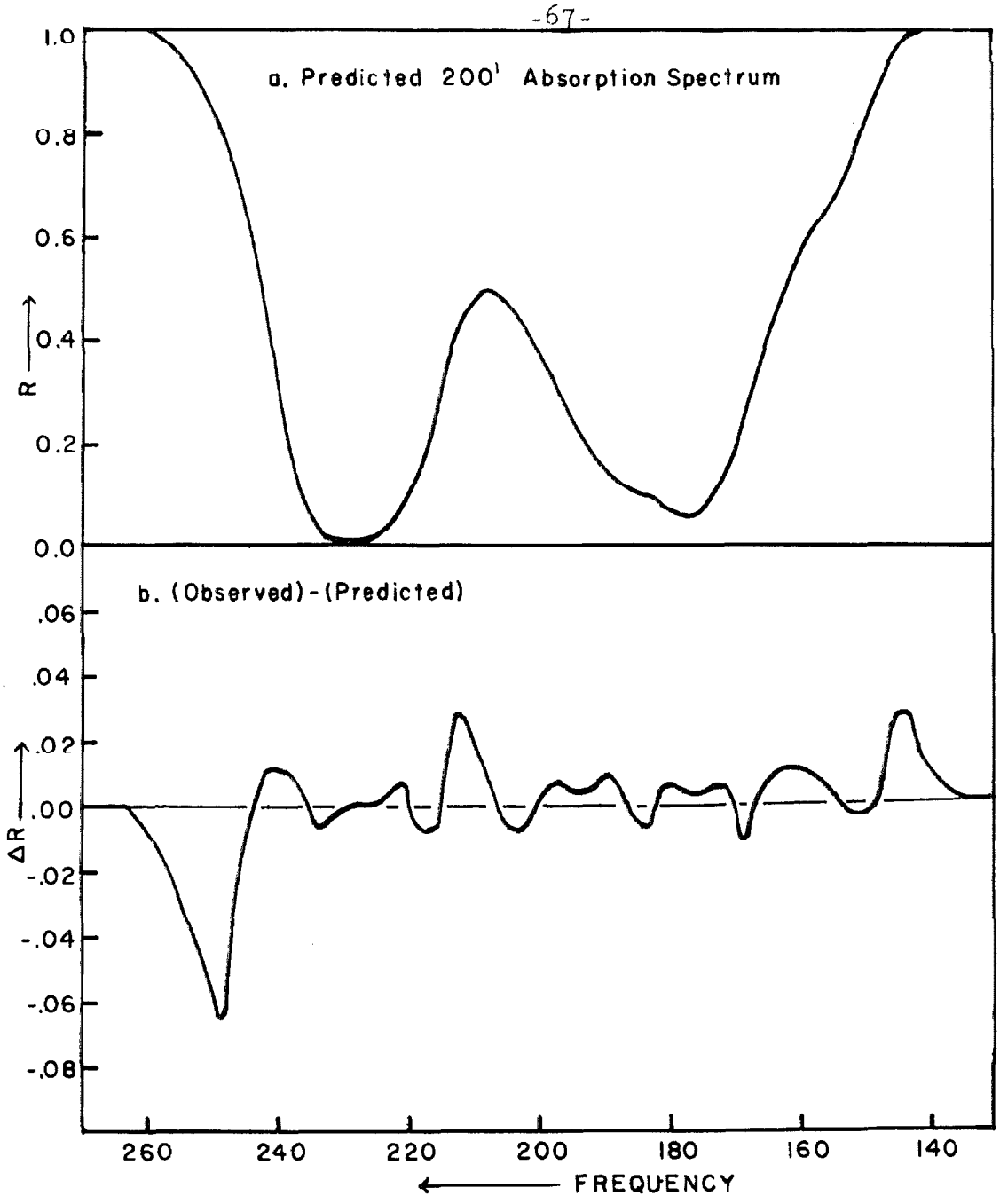

Figure 9. Cas A
Model Profile for 200 feet east-west.

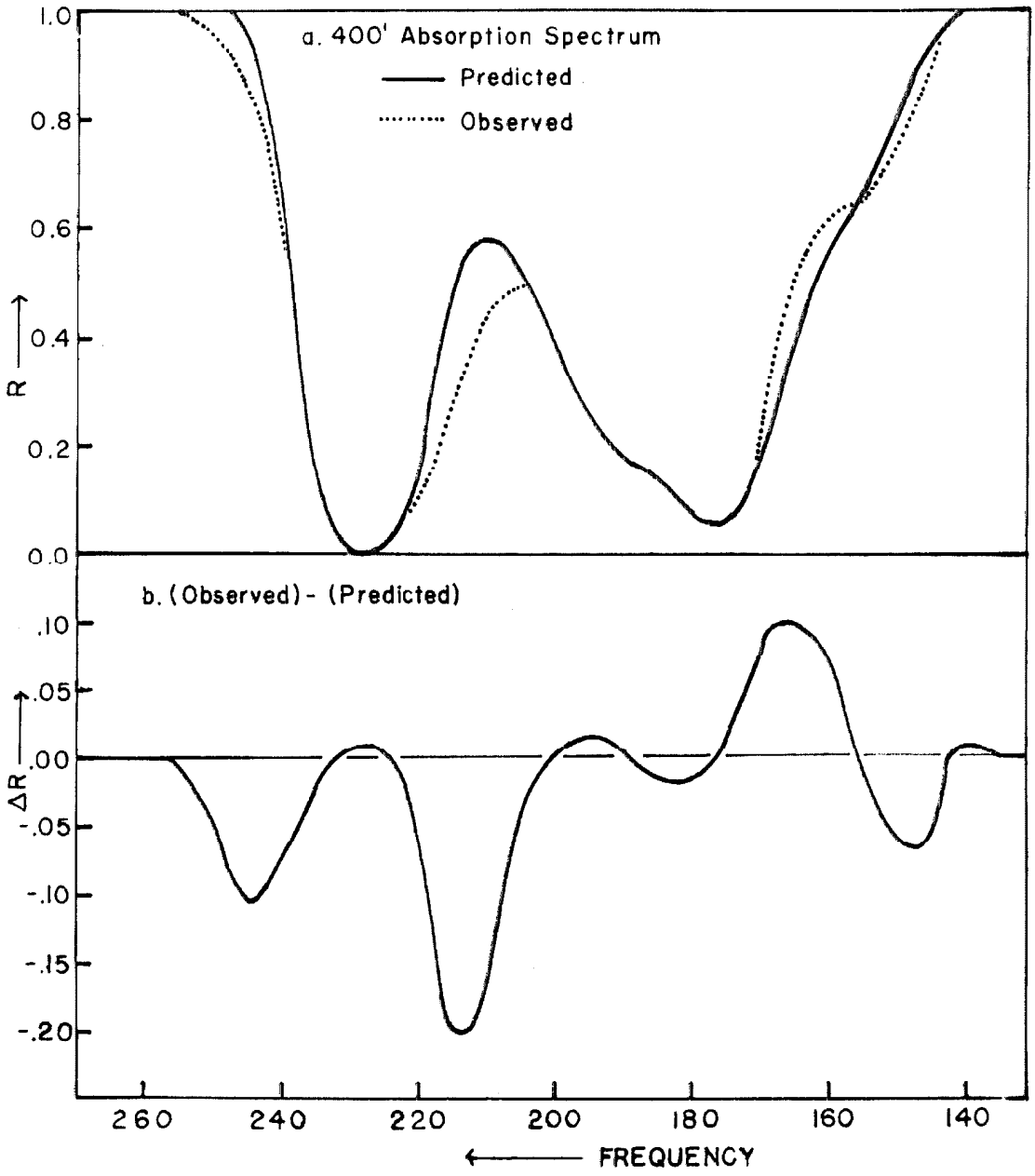

Figure 10. Cas A.
Model Profile for 400 feet east-west.

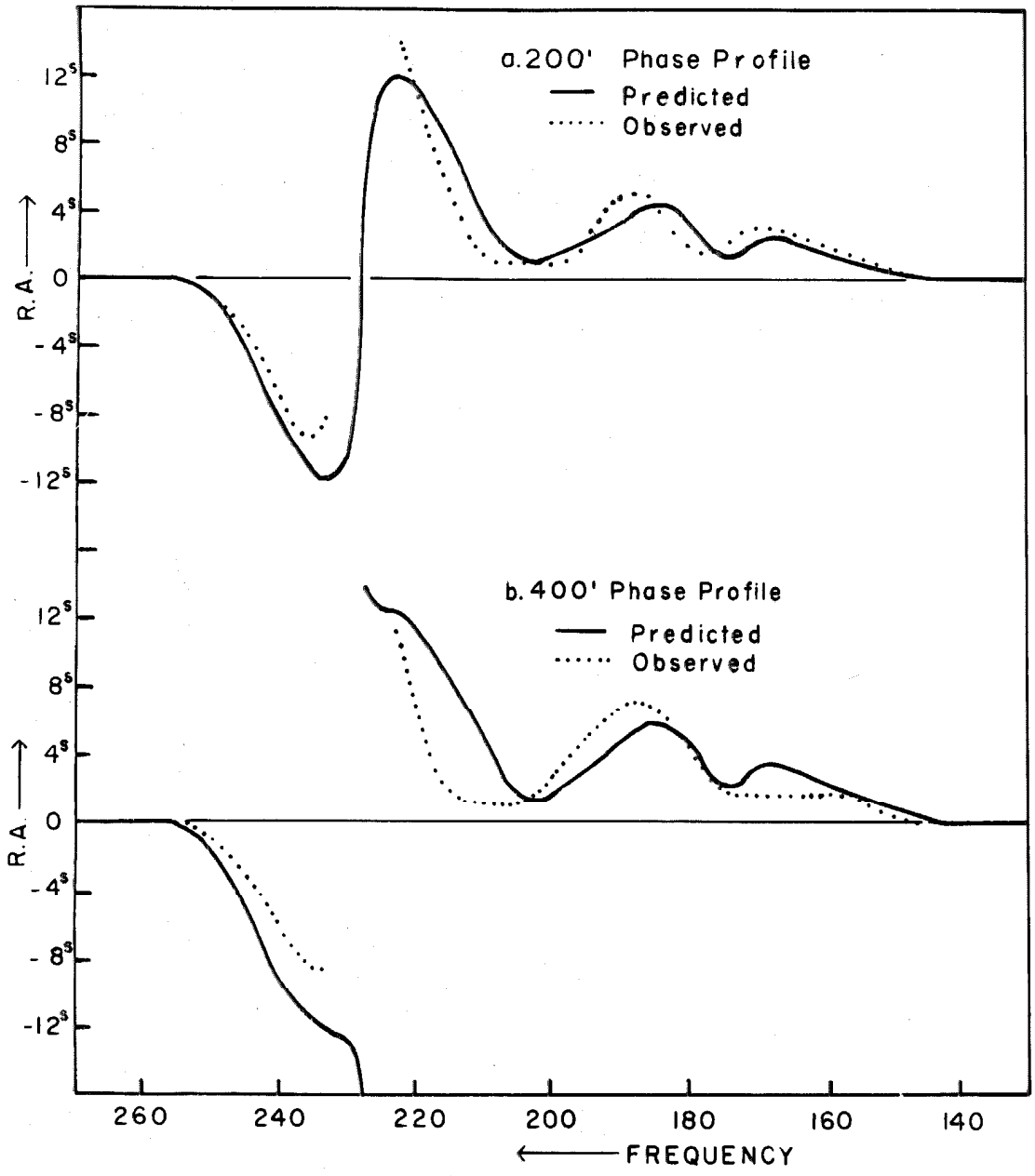

Figure 11. Cas A.
Model phase profiles.

large deviation is at 249 kc/s, and could be mostly explained by adding another component, though this should show up on the 400 foot profile if it were really there.

A similar comparison is presented in Figure 10 for the 400 foot amplitudes. Figure 10a contains the curve given by the model, with the observed curve given as a light line when it deviates noticeably from the model curve. Figure 10b is the difference curve. Since the parameters of the model were chosen to explain the amplitude and phase of the 200 foot observations, the 400 foot observations disagree somewhat with the predicted curve. The narrowing of the deep line on the high frequency side is fitted fairly well, but the line does not rise as predicted on the low frequency side. An insertion of an optical depth gradient in the weak line in the center of the profile might remedy this defect. The broad line is predicted to be somewhat narrower than the width at 200 foot spacing, but not so much as the observed curve, so the 155 kc/s component is not so obvious.

Figure 11 shows the comparison between the observed and predicted phases. Figure 11a is for 200 feet east-west, and Figure 11b is for 400 feet. The heavy line is the model phase and the light line is the observed phase. The main deviation of the phases from the expected is the asymmetry of the curve about 227-1/2 kc/s, which is presumably a

reflection of some asymmetry of the velocity variation across the face of the source, and the narrower width of the phase peak at 223 kc/s. This is probably related to the fact that the height of the maximum between the components does not change as predicted.

It is of interest to at least note the results obtained by Weinreb and Barrett[23] in their observations of the OH line in absorption in this source. This is interesting for two reasons. Firstly, it should enable us to separate the microturbulent velocities from the thermal velocities, since the thermal velocities of OH are a factor of four smaller than for H. Secondly, the variation of the ratio τ_{OH}/τ_H should convey some information about the state and history of the cloud. If the OH concentration is uniform in all space, then the τ_{OH}/τ_H ratio would indicate merely the kinetic temperature of the hydrogen since the τ_{OH} is roughly dependent only on radiation temperature and independent of the kinetic temperature, whereas the τ_H is inversely proportional to the kinetic temperature.

The width of the deep feature given by Weinreb and Barrett is 4.5 km/s, already somewhat broader than the corresponding feature in the hydrogen line profile, which, in my model, would have a width of 2.6 km/s. Indeed a

---

[23] Weinreb, S.; Barrett, A. H.; Meeks, M. L.; and Henry, J. C. Nature, 200, 829, (1964)

width of 4.5 km/s strikes the observed profile at about the $\tau = 1.7$ point, clearly much further down than half optical depth. If this measurement is correct, it is an indication of variation of temperature or abundance of OH within the cloud. The feature at 37 km/s is even more puzzling. Firstly it is not clear which of the clouds near the 181 kc/s this OH feature is associated with, and secondly, it is curious that the other OH feature is apparently associated with a relatively minor feature in the H spectrum. Clearly, more examples of OH lines are needed to examine the correspondence. If the situation is even more complex, as reported by Dieter and Ewen[24], then the meaning of the OH observations is not clear at all. One would expect OH to be more or less correlated with the H distribution even if the ratio did vary somewhat from area to area.

3.2 The Orion Arm Feature in Casseopeia A

The Orion arm profile is considerably simpler than the Perseus arm profile in several respects. Firstly, the optical depths are smaller, so that they can be measured accurately, and secondly, there is apparently no phase shift associated with the absorption, which one would expect since the clouds causing this feature are about three times nearer than those causing the Perseus arm feature.

---

[24] Dieter, N. H. and Ewen, H. I. Nature, 201, 279, (1964)

The situation is complicated by the presence of several weak lines of central optical depth about 0.1, which are either absent in the Perseus arm feature, or else are sufficiently centrally located that they are unrecoverable from the extremely deep features.

As in CRW, it is somewhat difficult here to properly fit the weak lines since the receiver gain instabilities enter in full force in this determination, as well as the resolution corrections, errors in time constant correction and similar terms. Even after summing several scans, the profile is undetermined to about two percent. The observed profile covers about 130 kc/s, which is about 25 bandwidths. I found it necessary to fit the profile with six Gaussian components, thus having 18 free parameters, very close to the number of bandwidths in the profile. In fact, this sort of behavior is fairly general, the more detail one looks for, the more one finds. After the computer fitting of the profile, the RMS error is about 1.4 times the theoretical error, but it would appear impossible to approach the theoretical error with only five components.

The values for the parameters of the six components fitted to this profile are listed in Table IV, along with the values reported in Muller, CRW, and Shuter and Verschuur, for comparison. Also listed are n_H and M which have been computed for $T_s = 100^o$ K and 10 parsec clouds. A plot of

Table IV. Orion Arm Features in the Spectrum of Cas A.

f_o kc/s	τ_o	σ kc/s	$\int \tau\, d\nu$ kc/s	N_H $10^{20}/cm^2$	n_H /cc	M $M_\odot$
-37.6 ± 3	0.09 ± .02	9.1 ± 3	2.0	0.78	2.5	42
-16.0 ± 2.2	0.10 ± .02	6.3 ± 2	1.6	0.62	2.0	34
- 1.9 ± 2.2	1.41 ± .3	5.8 ± 0.7	20.4	7.9	25	430
7.1 ± 1.2	0.73 ± .4	3.7 ± 1.2	6.8	2.6	8.2	200
22.8 ± 1.5	0.14 ± .02	8.0 ± 1.3	2.8	1.1	3.5	59
54.5 ± 4	0.07 ± .02	12.9 ± 4.2	2.3	0.9	2.8	48

f_o				τ_o					σ				
M	CRW	SV	C	M	CRW SD	CRW Int.	SV	C	M	CRW SD	CRW Int.	SV	C
-36	-36		-37.6	0.08	0.08	0.13		0.09	9.5	6.4	10.2		9.1
			-16.0					0.10					6.3
		-1	- 1.9				1.5	1.41				4.0	5.8
4	4			1.85	1.98	2.00			7.1	6.4	7.2		
		5.5					1.4					2.3	
			7.1					0.73					3.7
		9.5					0.63					2.2	
			22.8					0.14					8.0
59	64		54.5	0.07	0.05	0.09		0.07	12.3	12.7	5.1		12.9

Investigators: M--Muller,
CRW--Clark, Radhakrishnan, and Wilson SD--Single Dish Int.--Interferometer
SV--Shuter and Verschuur
C--Present investigation

the absorption spectrum is shown in Figure 12. Figure 12a is the expected profile, taken from CRW, and Figure 12b the observed absorption profile. A small scale plot of the spectrum of Cas A showing both features is presented in Figure 13.

The phase observations indicate that there is no phase change across this profile in excess of 10" in an east-west direction. This implies that the deep lines do not vary linearly in optical depth across a diameter of the source by 20%. This smoother behavior would indeed be expected if the clouds in this feature are the same size as those in the Perseus arm feature. This lack of phase change, however, sets little restriction on the weak lines, and even the possibility that they are optically thick regions covering a small part of the source is not excluded by the observations.

The deep line is at least double in nature, with a very well marked inflection point at the bottom, and appreciably different slopes on the two sides. It is somewhat surprising that the only two components of appreciable optical depth are found within 6 kc/s of each other if the dispersion of cloud velocities is near the 8 km/s found by Kwee, Muller, and Westerhout[25]. Therefore, it may well be

---

[25] Kwee, K. K.; Muller, C. A. and Westerhout, G. BAN, 12, 211, (1954)

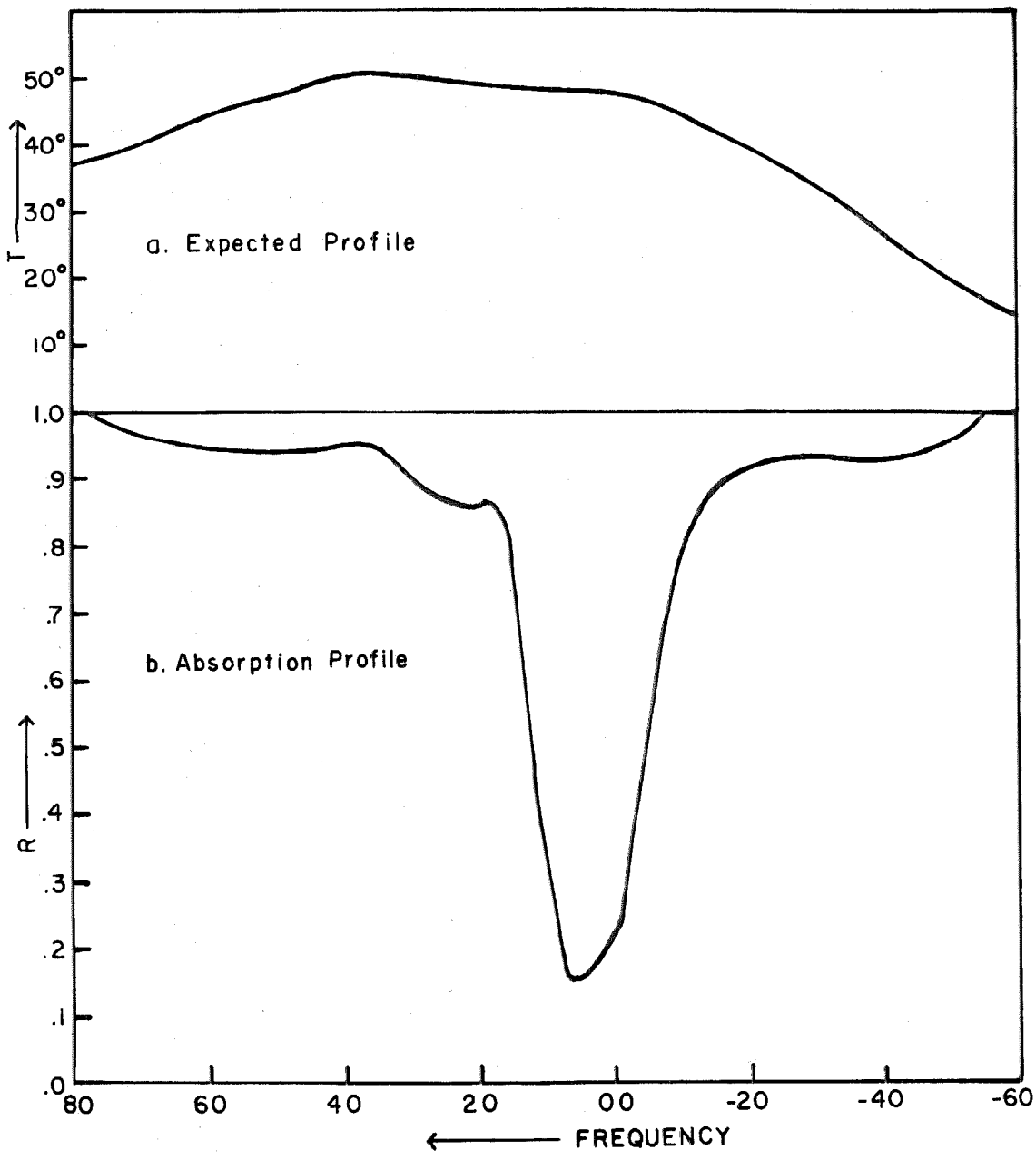

Figure 12. Cas A.
Orion arm feature.

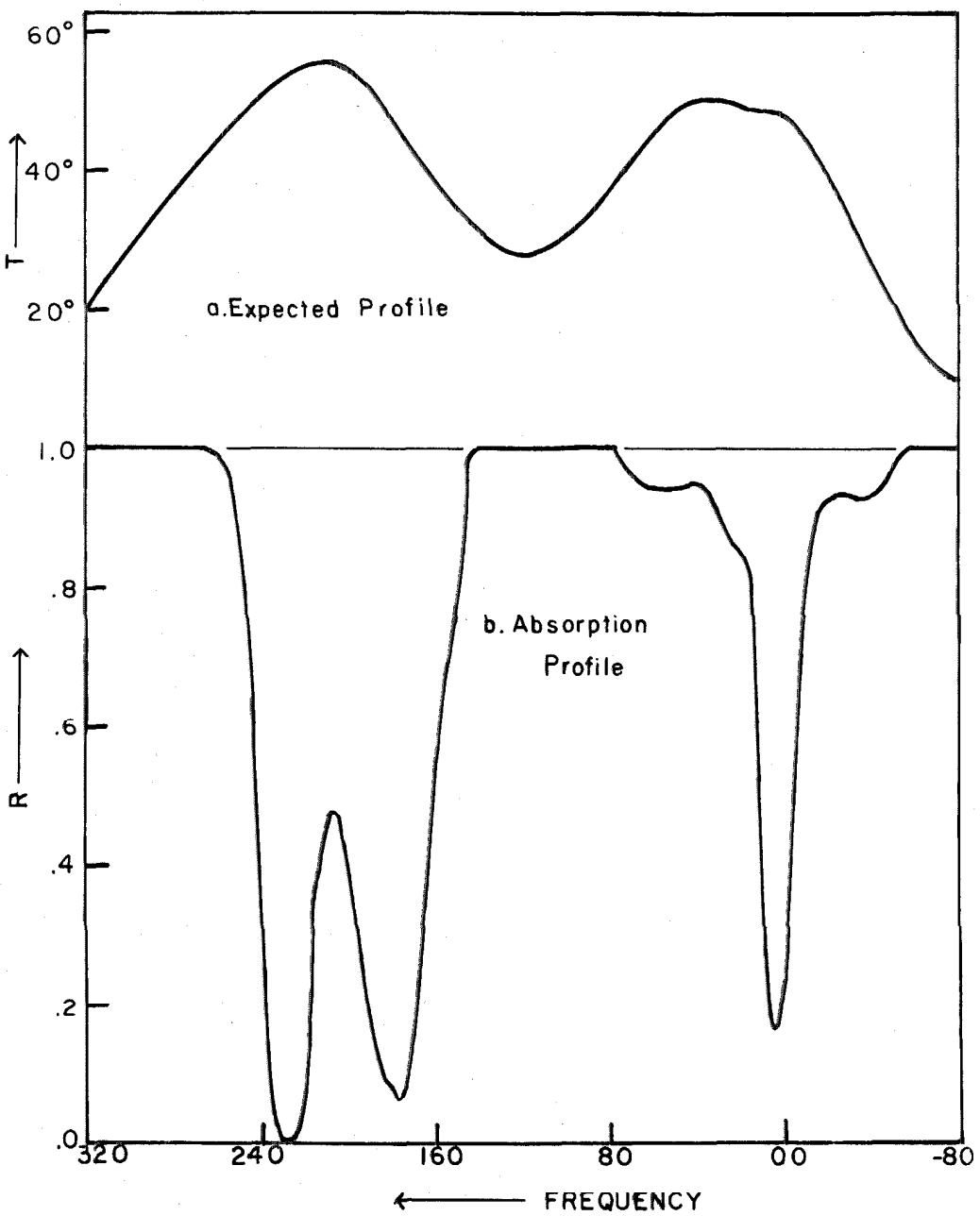

Figure 13. Small scale plot of Cas A absorption spectrum

that this splitting is a streaming motion within a single cloud rather than two or more spacially separated clouds. The parameters of the two lines are not very well determined because of their strong interaction. Shuter and Verschuur find three lines within the deep feature, and there is a very faint change of slope at the position of their third component in the present data. However, the maximum deviations from the fitted profile are less than 2%, so the present data alone would not suffice to claim the existence of the third component, especially with the reasonably small RMS error the present resolution into components provides.

We should note at this point that the deviations of this profile from the expected profile are in as great discordance as in the case of the Perseus arm feature, at least three times further away. If the spatially discontinuous character of the clouds give rise to the difference between the emission and absorption profiles, one would expect that either the emission in the Orion arm should be breaking up to resemble the absorption profiles more closely, or that the Perseus Arm profiles should not show deep absorptions because of the failure of the clouds to cover the source. This is a qualitative indication that the hydrogen seen in emission may indeed be at a different--higher--temperature than that seen in absorption.

It is interesting to note that with an assumed temperature of 100° K the total amount of hydrogen between here and Cas A is 9.4×10^{21} atoms/sq cm, mostly in the Perseus arm. This corresponds to an average density of 0.87 atoms/cc, which is somewhat greater than the average usually given from emission work, though not significantly so, considering the uncertainties.

3.3 Taurus A

Taurus A is identified with the Crab Nebula, the remnant of the supernova of 1054 AD, and is located at a distance of about 1100 parsecs. It lies very close to the anticenter, and therefore it is impossible to derive kinematical distances to features in its spectrum, but one knows that the hydrogen is certainly local, as the nebula itself is only a little more than a kiloparsec away. The absorption profile has two strong peaks, with the stronger and narrower being located at about +10 km/s, which must, of course, be a peculiar motion as the component due to differential rotation is essentially zero.

The profile does not vary significantly with baseline, so the various baselines have been averaged to improve signal to noise ratio. The 200 foot east-west observations were most heavily weighted. The average profile is given in Figure 14. There are no phase shifts greater than about 20 seconds of arc.

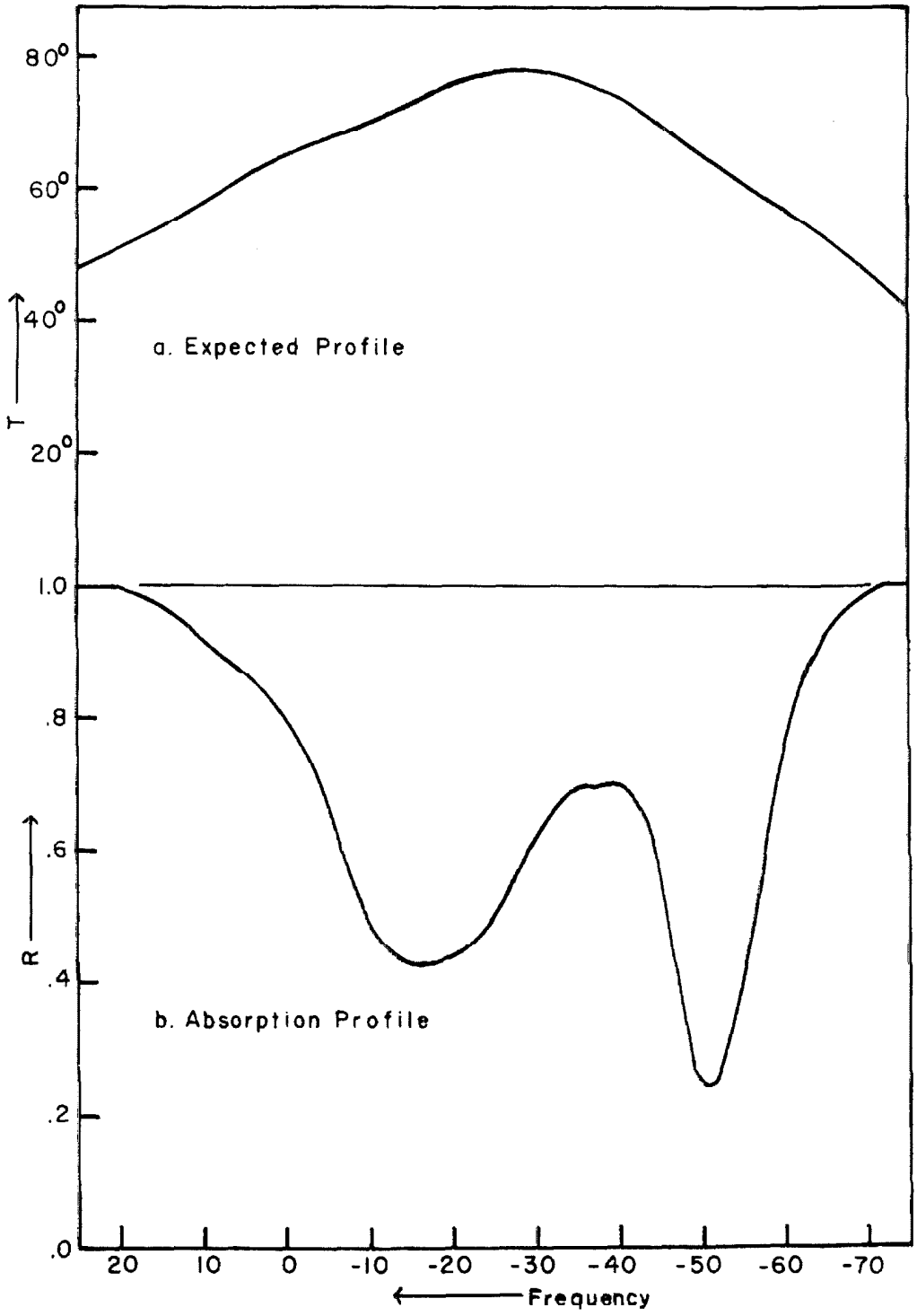

Figure 14. Taurus A Absorption Spectrum.

Table V. Components of the Spectrum of Taurus A.

f_o kc/s	τ_o	σ kc/s	$\int \tau\, d\nu$ kc/s	N_H $10^{20}/cm^2$	n_H /cc	M $M_\odot$
-51.6 ± 1.0	.86 ± .08	6.0 ± 0.3	12.9	5.0	16	270
-50.5 ± 0.8	.58 ± .08	2.72 ± 0.3	4.1	1.6	5	86
-37.9 ± 2	.14 ± .03	3.7 ± 1.4	1.2	0.5	1.5	25
-18.7 ± 1.1	.82 ± .10	10.7 ± 0.8	22.0	8.5	27	460
-10.7 ± 1.1	.12 ± .10	3.4 ± 1.1	1.0	0.4	1.2	21
5.9 ± 3.5	.07 ± .03	6.0 ± 2.5	1.0	0.4	1.2	21

f_o				τ_o					σ				
M	CRW	SV	C	M	CRW SD	CRW Int.	SV	C	M	CRW SD	CRW Int.	SV	C
		-51.0					1.05					3.2	
			-51.6					.86					6.0
-49	-48	-47.0		1.9	1.56	1.05	1.30		4.8	5.5	5.5	2.9	
			-50.5					.58					2.7
		-40.0					0.43					2.5	
		-34.0	-37.9				0.34	.14				3.4	3.7
	-28	-26.0				0.5	0.55					3.4	
-18.5	-20	-20.0	-18.7	.6	0.68		0.60	.82	6.6			3.5	10.7
						0.72				10.6	8.5		
-14	-10	-12.5	-10.7	.6	0.53		1.00	.12	6.6			4.2	3.4
		- 5.0					0.40					3.5	
	3	3.0	7.8		0.21	0.24	0.26	.07		6.4	5.5	4.0	6.0
19				.07					8.0				

The puzzling part of this spectrum is the maximum optical depth of the feature near -50 kc/s. This quantity as observed by the various observers is given below:

M	CRW SD	CRW Int.	SV	Present Investigation
1.9	1.56	1.05	1.90	1.31

There is thus some indication that the interferometer sees a shallower line than single dishes, but the explanation is not clear. The 250 foot telescope has more resolving power than the 100 foot spacing interferometer, yet there is no apparent change of profile with baseline in the present investigation. Perhaps the explanation lies in the bandwidth corrections. However, the bandwidth corrections to the present data would have to be quadrupled to account for the discrepancy.

There is considerable difficulty in resolving this profile into Gaussian components, as there appear to be several of them and they are very narrow. A beginning approximation of the profile of about the form shown below was arrived at after several attempts to fit the profile with Gaussians by hand computation:

f	τ_o	σ
-60	0.14	3.5
-50	1.43	4.1
-38	0.16	3.5
-23	0.60	9.2
-12	0.50	6.4
3	0.15	7.1

The component at -60 accounts for the wing on the red edge of the profile, and the two features in the -17 kc/s component are nearly equal in depth, and not too different in dispersion. When this initial guess was submitted to the computer for improvement, it converged to a solution resembling this for about ten iterations, when it became unstable and sought a new pattern, which is given in Table V, with errors and comparison with other observers. The feature to note in this analysis is that the negative frequency toe of the profile has been explained by a broad component with approximately the same frequency and optical depth of the much narrower component producing the peak of the -50 kc/s line. This solution seems to have a mean square error about half the theoretical value and about one third that of the solution based on the initial guess.

There are suggestions in several profiles that components of nearly equal optical depths tend to be located at the same frequency. This same solution of narrow component superimposed on a broad component was used for the broad line in the Perseus arm feature of Cas A. It may well be that these close doublings represent the passage of a shock wave through the cloud, or fairly large scale internal motions within the cloud rather than the accidental superposition of physically separate clouds.

Some of the dispersions of the Gaussian components for this profile seem to be excessively small. The 2.72 kc/s dispersion found for the narrow part of the deep line corresponds to a kinetic temperature of only 41° K, a third of the generally assumed value for the cloud temperatures. At this narrow width, the bandwidth corrections may not be properly made, and certainly many uncertainties are present in the process of interpreting the profile as Gaussian components, but a temperature as high as 125° K appears to be excluded by the observations.

The integrated optical depth in front of this source is 42.1 kc/s, corresponding to 1.64×10^{21} atoms/sq cm at 100° K. This number may be substantially reduced if the temperature is indeed very low. This surface density gives an average density of 0.47 atoms/cc between us and the source, which is quite reasonable, or even a bit low, for paths through this spiral arm.

3.4 Sagittarius A.

The source Sagittarius A is interesting on several grounds. Firstly, it is located at the center of the galaxy, and hence on the model of circular motion, all the hydrogen between the sun and the center will fall together at zero frequency, resulting in an extremely high optical depth. Secondly, the three kiloparsec expanding arm appears in absorption in front of the source, and hence the

absorption profile tells something about the parameters of this expansion. And thirdly, it is interesting because the interferometer contributes greatly to the study of its spectrum since the expected profile is so complicated that it is difficult and time consuming to produce it with a pencil beam instrument.

The source was observed with the usual baselines, with one exception. With the 200 feet north-south baseline, the south antenna casts a shadow on the north one when the source is viewed on the meridian. Therefore, the source was not observed on the meridian, but for a range of hour angles on either side of the meridian, centered on about 2^h20^m, and running about 40^m either way from this center. At the eastern apparition, the fringes lie approximately perpendicular to the galactic equator, and at the western apparition, they lie approximately along it.

The original report of the three kiloparsec expanding arm by Rougoor and Oort[26] gave an optical depth of about 0.5. Both CRW and the present investigation, although they disagree somewhat about the shape of the line, agree that the optical depth is slightly greater than 1. Furthermore, there seems to be no appreciable change of this depth

---

[26] Rougoor, G. W. and Oort, J. H. Paris Symposium (Ed. R. N. Bracewell) S. U. Press (1958)
--------- Proc Nat Ac Sci, 46, 1, (1960)

with baseline. It is certainly identical to within 5% for the 100 feet east-west, 200 foot east-west, and 200 foot north-south baselines, and these have been averaged to improve accuracy. With the 400 foot east-west baselines, the source is so resolved that noise reduces the accuracy to about 10%, but to within this error the line still has the same depth. The composite profile is presented in Figure 15b. The expected profile in Figure 15a is taken from Muller (1958). It is seen that the profile appears to consist of two components, one a weak wing on the previously reported single component. There is no evidence for the peculiar shape reported in CRW and the profile appears to agree rather well with a Gaussian.

The parameters of the two components are as follows:

f	τ_o	σ	$\int \tau \, d\nu$
254.8 ± 1.0	1.08 ± 0.06	13.7 ± 0.7	37
291.8 ± 3	0.10 ± 0.04	5.1 ± 3	1.3

The total integrated optical depth in this feature is 38 kc/s, which at a temperature of 100° corresponds to 1.5×10^{21} atoms/sq cm. If the arm is half a kiloparsec through, this is an average density of 0.94 atoms/cc.

The source does show a measured phase effect with frequency. The observed phase curves are shown in Figure 15c. At the longer east-west baselines, less phase effect is found than at 100 feet east-west. Thus the effect is

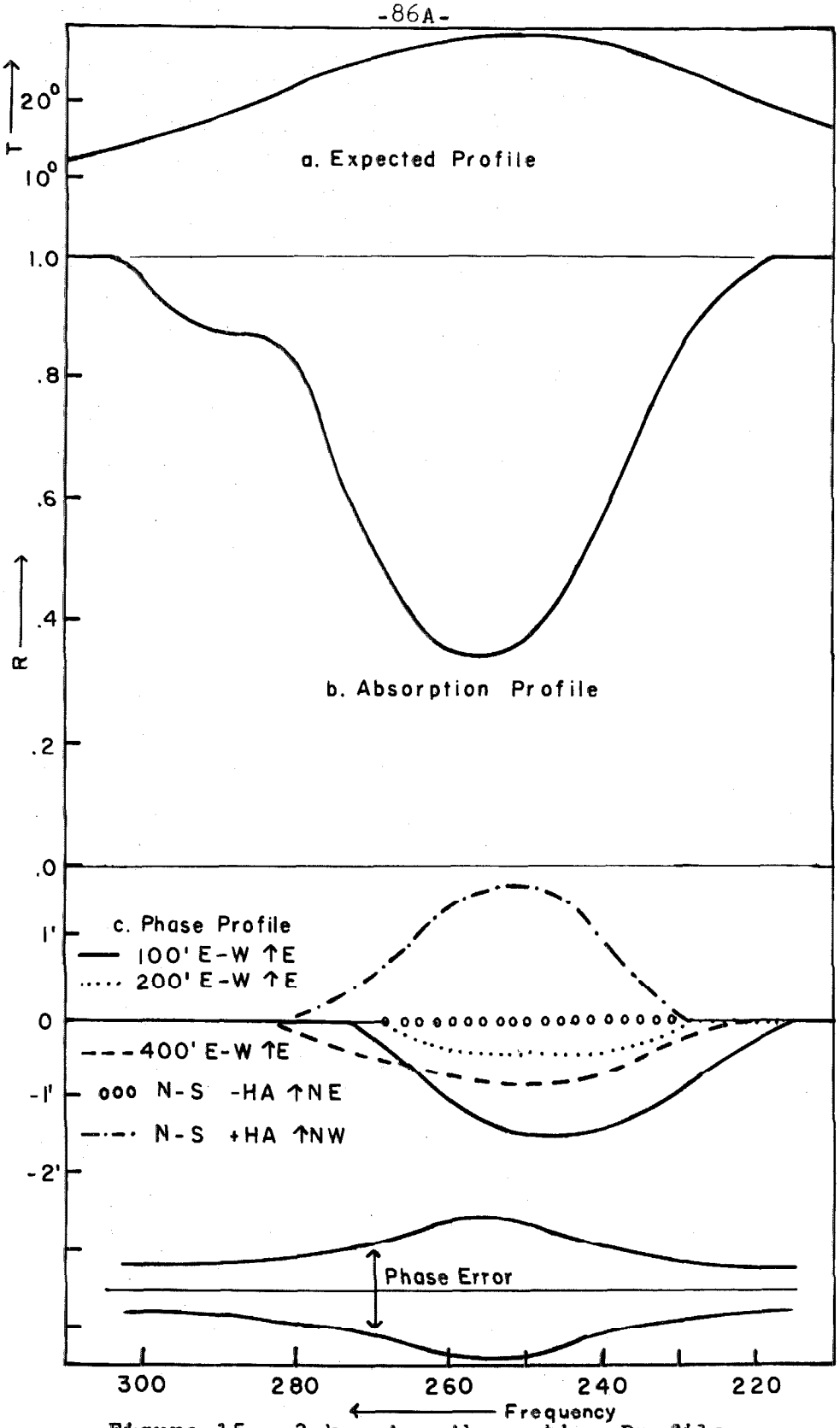

Figure 15. 3 kpc Arm Absorption Profile.

probably associated with the large component of the source, which is already well resolved at 100 feet. The observations taken with the north-south base-line at western hour angles also indicated the presence of a phase effect of about the same size as that at 100 feet east-west. Since this effect is changing with the resolution of the source, it may be premature to associate the lack of phase effect at the eastern apparition with the fringes being parallel to the displacement of the source, but if this is indeed the case, then the absorption appears heavier in position angle 135°, approximately perpendicular to the galactic equator. The maximum apparent displacement of the source is about 1!5. The degree of change in absorption that this calls for is highly uncertain because of the difficult resolution effects. If the lower optical depth reported by Muller is due to a hole in the absorption covering the extended part of the source, then this hole could also produce the observed phase shift, and be of large enough diameter that it would be resolved at the 200 foot baseline.

Egorova (1963) reports that the source coming about 1^m earlier than the center source does not appear to be absorbed at the center frequency of the 3 kpc arm. This should cause a position shift to the north-east, rather than to the north-west as observed.

The feature near zero velocity presumably results from the superposition of many clouds lying in the seven kiloparsecs between the sun and the three kiloparsec arm. One would thus expect the optical depth to be very high. It is indeed high, being greater than 3. After two hours of integration at zero frequency with the 200 foot east-west baseline, a non-significant result of R = 0.028 ± 0.016 was obtained. R ± 0.028 is an optical depth of 3.6. Observations at ± 20 kc/s indicated somewhat shallower optical depths, of about 2.5 to 3, depending on the exact frequency, also with marginal significance.

The profile is shown in Figure 16b. The expected profile in 16a is taken from Muller. The general picture is the single very deep feature with four little lines on the wings. The two clouds at negative frequencies were smeared into a simple wing in CRW, though upon re-examination of the records, the peak structure appears. Because of the fact that the deep feature is a close superposition of many clouds, it is impossible to attempt to separate it into Gaussian components. Since Blaauw[27] reported that a more appropriate law for the motions of individual clouds is a simple exponential, it might be worthwhile to attempt to fit the feature with $\underline{A} \exp \frac{f}{\eta}$. Figure 17 shows - log $\underline{R}$

---

[27] Blaauw, A. BAN, 11, 459, (1952)

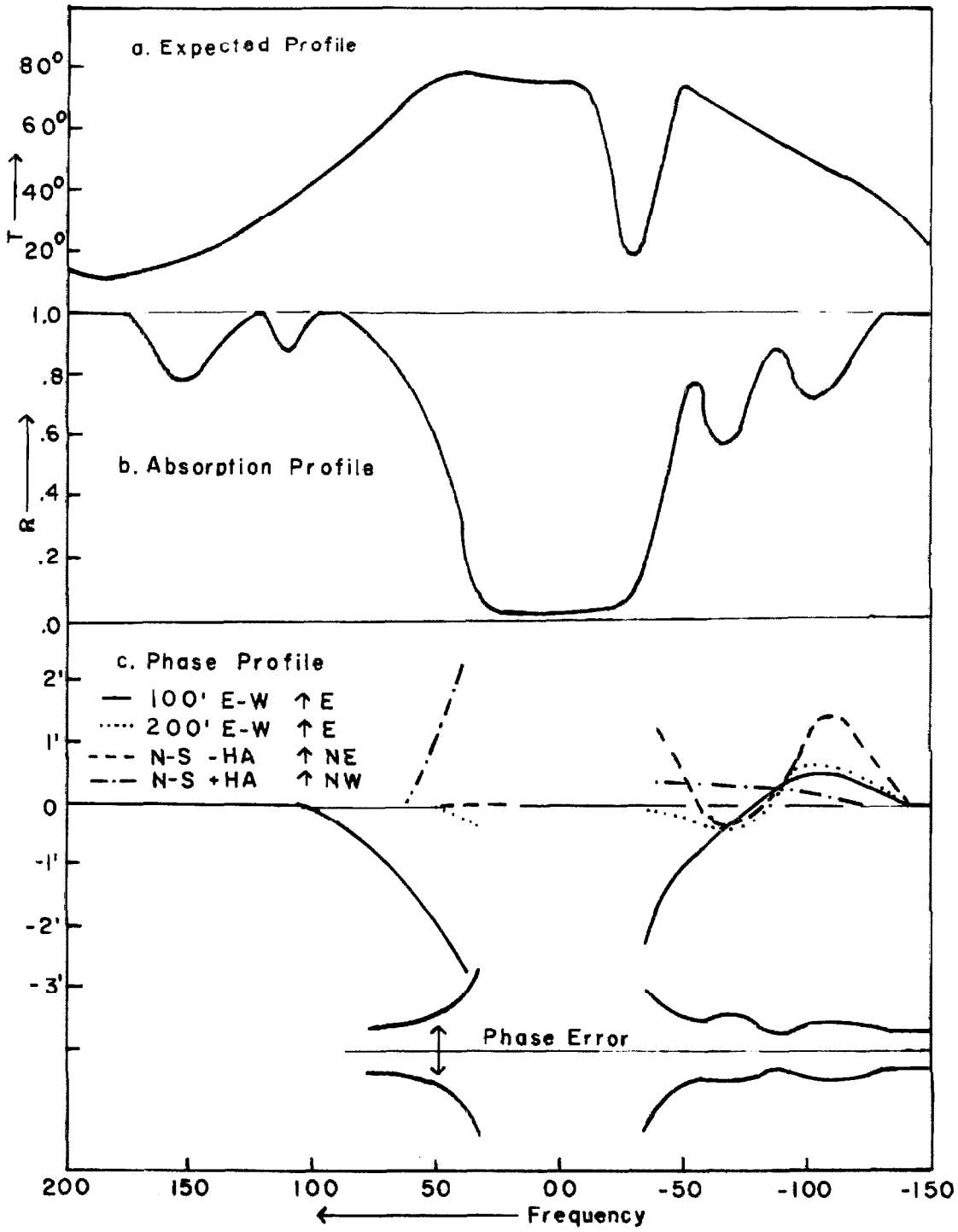

Figure 16. Sagittarius A Absorption Spectrum.

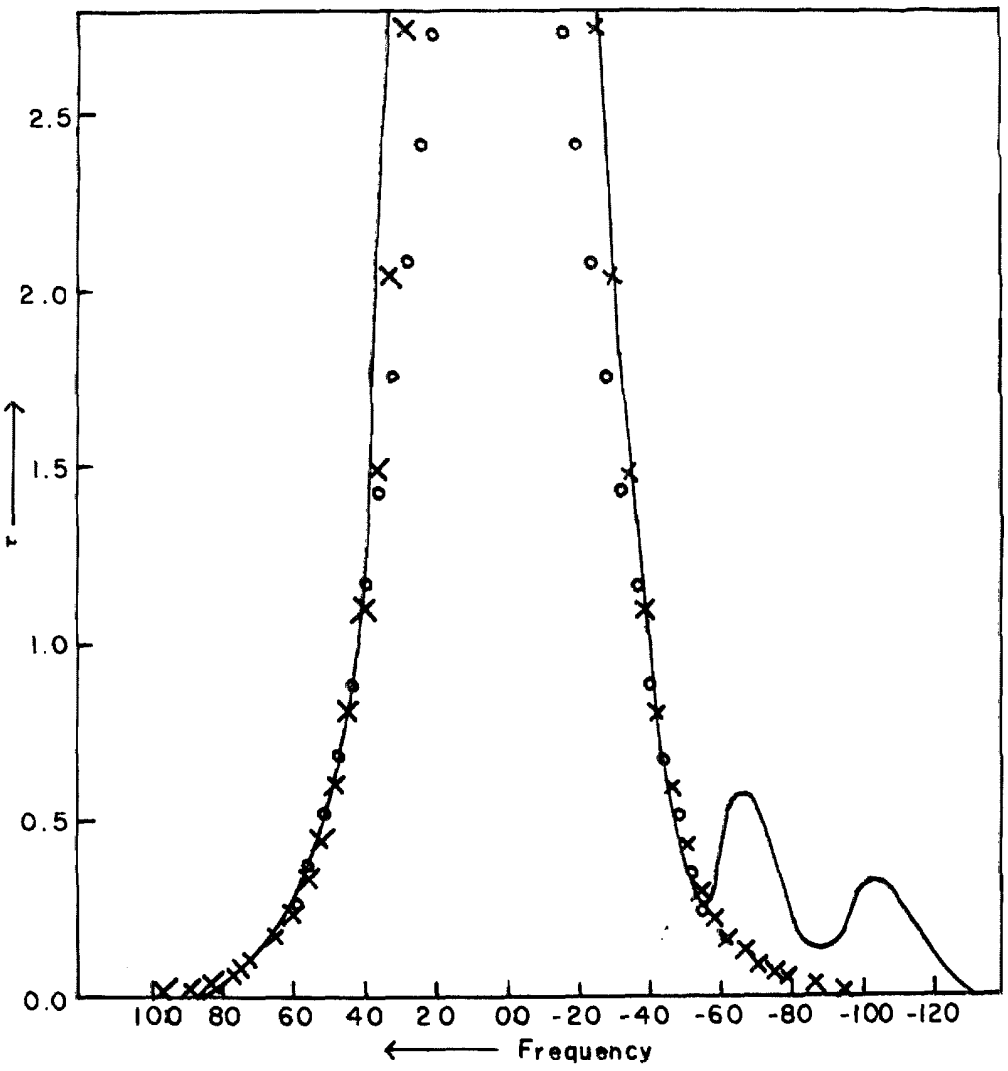

Figure 17. Sagittarius A Deep Line
fitted with exponential (x) and Gaussian (o).

plotted against frequency, with an exponential (x's) and a Gaussian (o's), both fitted in frequency and slope at τ = 1.0. The observed slopes appear to be too steep at high optical depths to fit a Gaussian, while the $\underline{A}$ exp $\frac{f}{\eta}$ formula produces reasonable agreement. The values of $\underline{A}$ and $\underline{\eta}$, $\underline{A}$ = 22, and $\underline{\eta}$ = 13 kc/s are, however, highly unreasonable. The optical data which suggested the exponential form gave an $\underline{\eta}$ of something like 5 - 8 km/s, two or three times this value. And if the optical depth follows this law on in to the center of the line, then Bolton, van Damme, Gardner, and Robinson[28], and Weaver and Williams[29], observing in the OH line, would probably have found a greater optical depth, and certainly a narrower line. If this law does obtain, then the integrated optical depth would be 570 kc/s, which, at 100° K, gives an average of 1.0 atoms/cc, assuming that all this hydrogen lies in the seven kiloparsecs between the sun and the 3 kpc arm. This figure is again somewhat high, indicating that the exponential law must break down somewhere before the center of the line. This integrated optical depth is at least 280 kc/s, giving an average density of at least .5/cc. The value η = 13 kc/s

---

[28] Bolton, J. G.; van Damme, K. J.; Gardner, F. F.; and Robinson, B. J. Nature, 201, 279 (1964)

[29] Weaver, H. F. and Williams, D. R. W. Nature, 201, 279, (1962)

is a direct measure of the steepness of the sides of the line, and supplies a typical bandwidth, irrespective of the behavior of optical depth for $\tau > 3$. This value is more typical of single components in absorption than of an emission profile.

The phase effects near this line are very complicated and are illustrated in Figure 16c. Firstly, it is clear that the center of gravity of the source moves north-west on the positive frequency side, by a rather large amount, possibly 2'. This of necessity must refer to the large component, as this lies off the center core of the source. This movement is roughly perpendicular to the galactic plane. The effect at negative frequencies is not so clear. Each of the two weak lines appears to have a different phase shift associated with it, and in addition there is possible a resolution sensitive effect on the edge of the deep line. The only thing that one may deduce about the source from these phase shifts, is that while the absorption is relatively constant over a component of the order of 4' in diameter, it may vary quite markedly within the antenna beam, 36'.

Since there are seven kiloparsecs of clouds all lined up on the same frequency, one would expect that there should be quite a large number of clouds in the deep feature, enough so that it becomes difficult to see why it should

differ so much from the expected profile, if indeed the expected profile is made up of the emission of many clouds like those in the absorption profile. Since the width of this feature (to R = 1/2) is about 90 kc/s, and this is at least three times the usual width of a single cloud absorption feature, there must be at least three clouds in the feature. From the frequency data in Section 4.1, one finds that one would expect 17 clouds of optical depth greater than one half, or a total of twenty-nine clouds. This number is getting large enough that the difference in the widths of the absorption and emission features is becoming statistically significant. The width of the emission to half maximum points is 220 kc/s, two and a half times the width of the absorption feature.

The center frequency of the deep feature is about +1 kc/s. This is undoubtedly somewhat coincidental, as the local standard of rest is not known to such accuracy. However, the general principle that the great mass of hydrogen between here and the center displays no relative motion with respect to the local standard of rest should supply some constraints to the model of radial streaming of hydrogen in the galaxy. For instance, of the four models considered by Braes (1963), only the one involving only circular motion of the hydrogen predicts that this line should be centered at zero. Because of the uncertainty of

the number of clouds involved in this feature, it is impossible to set a limit to the distance that this center frequency might be displaced by the statistics of small numbers, but it is certainly less than 5 km/s, half the width of the feature, which would reject a radial velocity varying as $1/R^2$, and cast grave doubts on a model involving an outward motion of the local standard of rest with respect to the surrounding hydrogen which have been suggested by Kerr[30] to sort out the spiral structure of the galaxy.

The parameters of the weak features are listed below, including the position angle associated with the heaviest absorption as deduced from the phase data.

center frequency	τ_o	σ	$\int \tau \, d\nu$	PA
151.1 ± 2	0.26 ± 0.05	10.3 ± 3	6.7	
109.6 ± 2	0.14 ± 0.03	5.1 ± 2	1.8	
-68.3 ± 2	0.57 ± 0.05	11.4 ± 3	16	90
-104.0 ± 2	0.33 ± 0.04	15.8 ± 3	13	240

These features are probably simply clouds with high random velocities. At 100° K their center of mass is approaching at 7 km/s, and, if these are ten parsec clouds, they represent a total of about eight hundred solar masses. They probably do not represent an important part in the kinematics of the galaxy.

---

30 Kerr, F. J. MN, 123, 327, (1962)

3.5 Orion A

The profile of this source shows a marked change with baseline, indicating a change in optical depth across the source, even though the source is only half a kiloparsec distant, the closest source in the sample. The profiles observed with the various baselines are shown in Figure 18b. Figure 18a, the expected profile, is again taken from CRW. It is not clear that the difference between the profiles observed with the 200 foot north-south and 200 foot east-west baselines is significant, because a frequency shift of the steep side of the profile of only one kc/s would bring the two profiles within the allowable error. However, the difference between the 200 foot and 100 foot profiles is certainly real, because the bottom of the profile is very well observed with the integrators, and the observed difference is over three times the standard deviation of this point. There are also some profiles taken at large positive hour angles with a 200 foot east-west baseline which show intermediate cases. They also show that if the profile is divided into two components in the obvious way, the change is due mainly to a change in the deeper, narrower, one.

The 400 foot profile also differs significantly from the others, being much lower on the positive side of the profile.

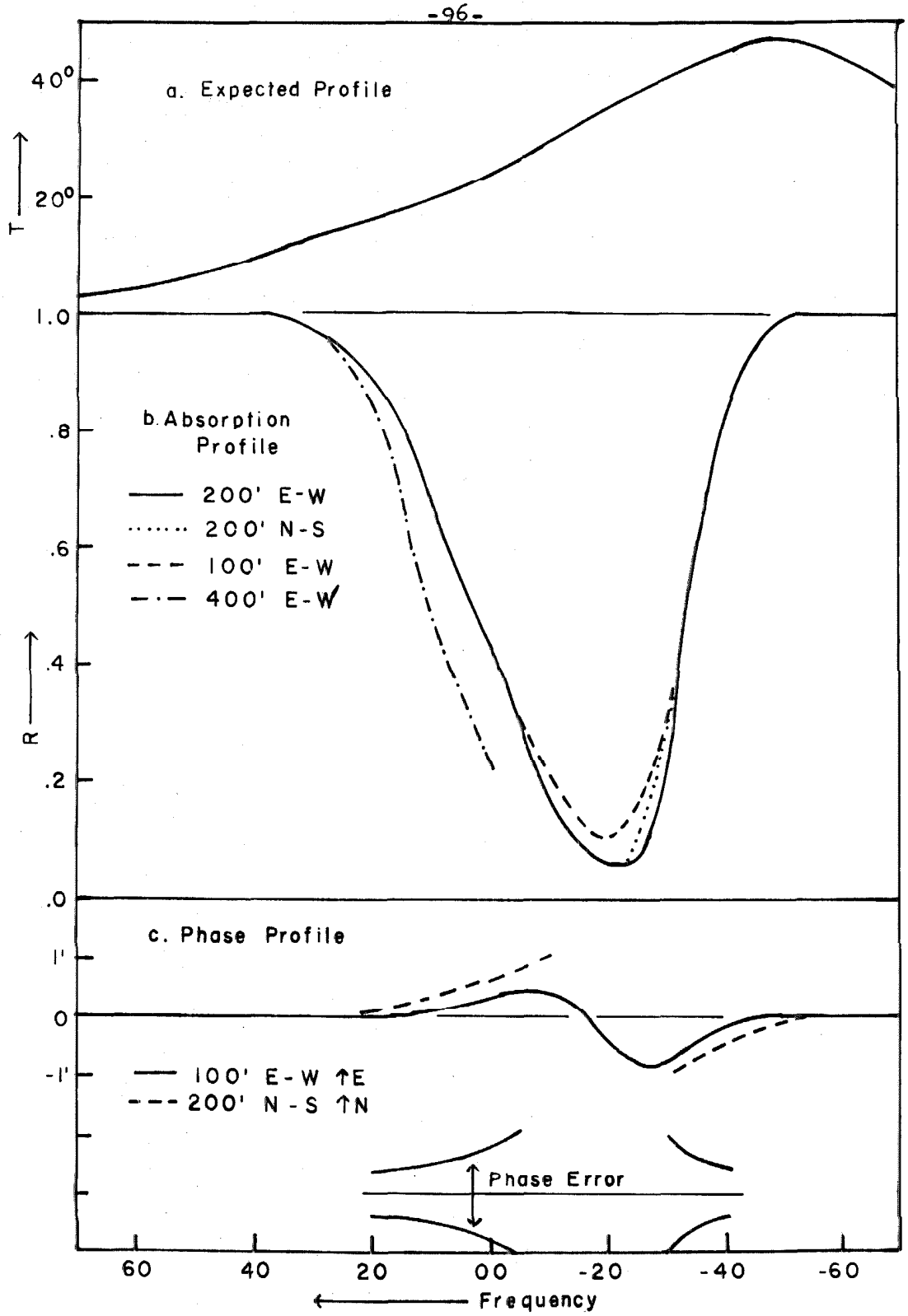

Figure 18. Orion A absorption Spectrum.

An appropriately weighted average of the 200 foot east-west and north-south baselines was given to the computer for least squares analysis into components. An initial guess of only two components was used, although at least one of the small quirks in the profile reported in CRW appears to be real, but only about equal to noise in size. The resulting fit was so good, about 1.8 times the theoretical error, that it was felt that the determination of a third component from this data could not be supported. The parameters of the two fitted Gaussians are as follows:

center frequency	τ_o	σ
-21.4 ± 0.6	2.01 ± 0.15	6.7 ± 0.45
-11.7 ± 0.9	1.19 ± 0.09	14.2 ± 0.5

The 100 foot east-west observations are adequately described by reducing the depth in the deeper feature from 2.0 to 1.2, suggesting that the cloud causing this feature covers a comparatively small area in the center of the source. The optical depth reported by CRW with a single dish and by Muller is much smaller yet, indicating that perhaps both clouds are centralized over the most intense part of the source. The observations are consistant with an absorbing disk 4' in diameter of optical depth greater than 2 centered on the source. The further deepening at 400 foot spacing could be due to the fact that the source brightness distri-

bution is split in two by the other absorbing cloud as well, and that its visibility function is thus descending faster than that of the unabsorbed source, rather than its optical depth actually being the value measured over the center of the source. The phase curves for the 100 foot east-west and the 200 foot north-south baselines are shown in Figure 18c. The variation of the phase is not significant in the three kc/s bandwidth for which equation (2), Section 2.2, applies, but it appears to reproduce from record to record. The 200 foot east-west phase curve appears to look about the same as the 100 foot baseline curve, except because the line is deeper, the extremes of the curve in the bottom of the line are not seen. There is a marked similarity between this curve and that for the deep line in Cas A, but in this case the feature can be divided into two components on the basis of differing dispersions and slightly different frequencies, so I associate each line with a different position. The maximum displacement appears to be as great as 1!3, which corresponds to about the same in displacement of the aforementioned 4' disk from the center of the source.

The integrated optical depths of the two components are 34 kc/s for the narrow component and 42 for the broad component. These correspond to 1.3×10^{21} and 1.6×10^{21} atoms/sq cm respectively, at a temperature of 100° K. A typical distance in the narrow line appears to be about 4',

which at the maximum distance of 500 parsecs, corresponds to only 0.6 parsec. The density of hydrogen with a typical distance of 0.6 parsec is 680 atoms/cc. Although the density is extremely high, the mass is rather small because of the very small volume of this cloud. The mass of the cloud is only about 2.6 solar masses. These numbers are rather extreme, but because of the change of the profile between 100 feet and 200 feet spacing, it would seem impossible to say that the typical distance in this cloud is greater than one parsec. If we take a one parsec cloud, the density would be 420 atoms/cc, and the mass would come up to seven solar masses.

These densities are extremely high for HI regions, but are rather less than some of the densities encountered in the Orion Nebula itself. It seems fairly likely that this cloud is associated in some way with the nebula, either being an ejectus of it, part of a primeval HI region which has not yet been ionized, or even a region in the process of condensing into a star. If it is the last, it must be doing so under the influence of an external force, as it is gravitationally unstable.

In order that the second component produce the observed phase change, which appears to be associated with it, this cloud, too, must be very little larger than the source. Its typical length must not be much greater than 10', or 1.5 pc. This gives a density of 350 atoms/cc and a mass of 20 $M_{\odot}$.

3.6 The Omega Nebula.

A composite profile for the source is shown in Figure 19b. It is the average of the 100 foot, 200 foot east-west and the 200 foot north-south scans, except in the region near the bottom of the line at about -98 kc/s, where the north-south profile appears to be somewhat less deep than the other profiles. In this region the composite profile follows the average of the east-west profiles. It is not clear that this deviation is significant. There is also a very slight suggestion that the 100 foot profile might be slightly deeper in the neighborhood of the -30 kc/s feature also, but this effect is comparable with noise. The phase profile is given in Figure 19b. It has been smoothed to 12 kc/s bandwidth to increase its significance. It indicates that the structure is probably rather complicated. There appears to be at least one more component to the profile than reported in CRW, as the feature at -30 kc/s appears double as was suggested there. For the present this has been interpreted as a narrow component superimposed on a broader one, as in Taurus A, rather than as two side by side components. The phase curve indicates that this is probably somewhat of a simplification, but the present data probably do not justify a more complicated model. The broad and narrow components give a somewhat better fit on the plus frequency side of the profile than two side by

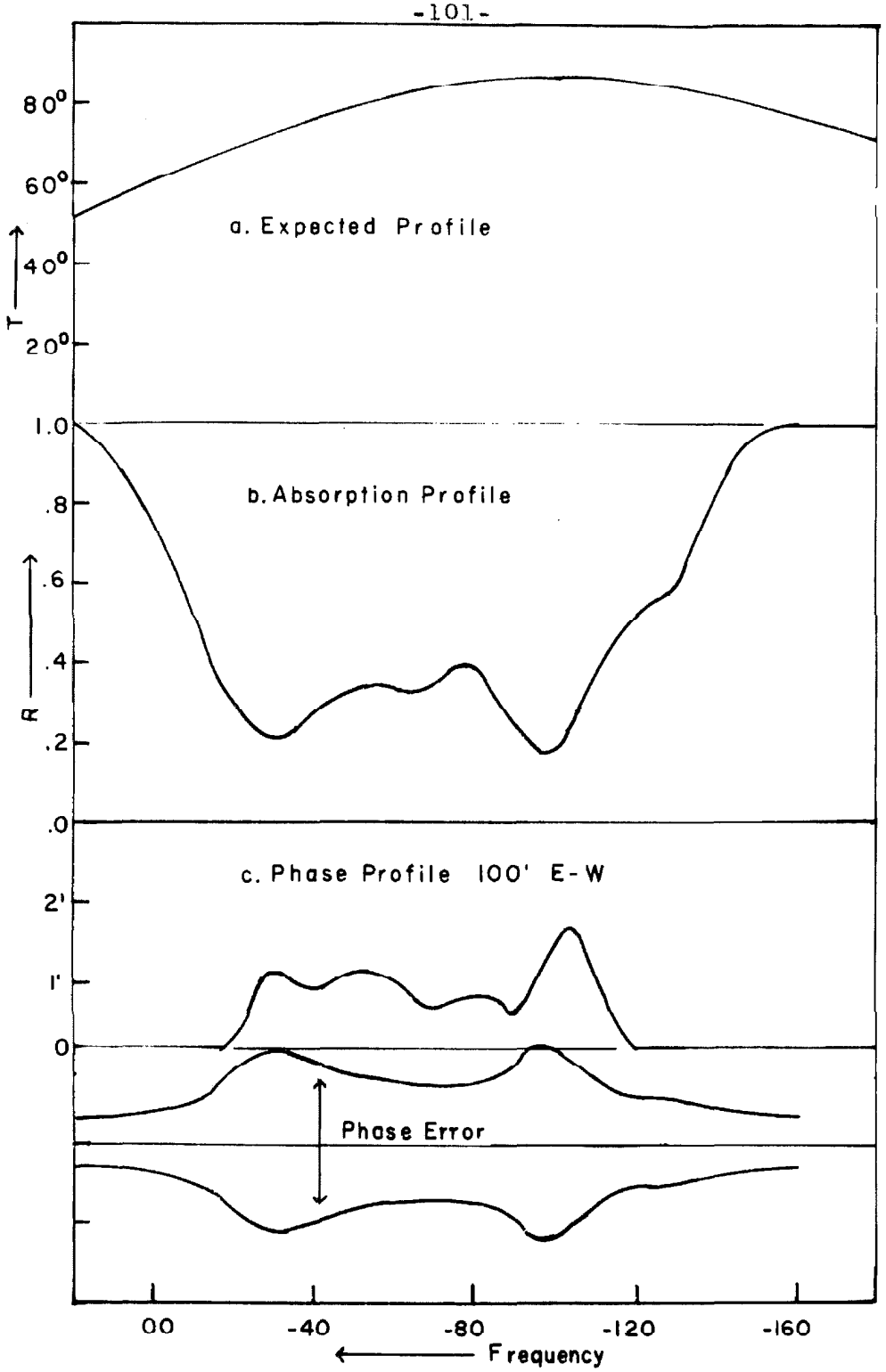

Figure 19. Omega Nebula Absorption Spectrum.

side components, but the true resolution is probably into three or more components. This profile agrees fairly well with the interferometer profile of CRW, but still differs greatly from the single dish profile of CRW. Because of this difference, another pencil beam investigation of this object would be highly desirable to check the observation.

The values of the parameters to the components fitted here are as follows:

f_o	τ_o	σ
-32.5 + 1.0	1.42 + 0.08	17.6 + 0.8
-29.9 + 1.6	0.15 + 0.07	4.2 + 2.2
-68.5 + 1.0	0.87 + 0.07	11.7 + 1.5
-98.2 + 0.7	1.61 + 0.08	10.5 + 1.0
-125.2 + 1.8	0.57 + 0.06	11.2 + 1.2

The north-south profile would be fit somewhat better if the optical depth of the component at -98 kc/s were decreased in optical depth from 1.61 to 1.14. If this is indeed real and a resolution effect, it implies that the size of the cloud is comparable with the size of the source, about 7', corresponding to 5 pc at the 2.5 kpc kinematical distance. Since the effect seems to depend more on the azimuth of the baseline rather than its length, the absorption might be regarded as a bar, with its long axis north-south. The phase measurements, though they are barely significant, indicate that most of the other components, with the possible ex-

ception of the ones at -32.5 kc/s and -125 kc/s, are only slightly larger than the source. If we take an angular diameter of 15' for each component which shows a phase effect, the following characteristics of the clouds result:

f	$\int \tau\, dv$	Dist. kpc	N_H 10^{20}/cc	L pc	n_H	$M/M_\odot$
-32.5	62	0.8	24	10	75	1300
-29.9	1.6	0.8	0.6	5	4	9
-68.5	25	1.7	10	10	31	530
-98.2	42	2.5	16	5	102	220
-125.2	16	3.1	6.2	10	20	340

The three densest of these clouds have escape velocities above the speed of sound, but still well below their internal turbulent velocities. If the profile is to be resolved into more components, the escape velocity of each goes down.

The dynamical distance of the most distant feature in the absorption profile is 3.1 kpc. If we take this to be the distance of the source, then the total integrated optical depth of 147 kc/s corresponds to a mean density of 0.6 atoms/cc, a value much in line with those obtained for other radio sources.

3.7 The Weaker Radio Sources.

A total of sixteen other radio sources have been examined for absorption with lesser attention. Some of these

were so large that their profiles have been taken from the single dish measurements reported in CRW rather than from new, interferometer measurements. For six of this sixteen it is possible to report only that they appear to be unabsorbed to a given limit. Some information about the radio sources and their observations is presented in Table VI. A brief comment about each is given below. The profiles are presented in Figures 20-23. An error, essentially the error in R at the line bottoms, is shown in a bar on the figure. The expected profiles are taken from interpolation in the intermediate latitude catalogue of van Woerden, Takakubo, and Braes (1962) if at intermediate latitudes, and from either Muller and Westerhout[31] or Kerr, Hindeman, and Gum[32] if near the plane. A list of components is found in Table VII. A brief comment about each is given below.

1) Fornax A is apparently unabsorbed in the frequency range searched. $R > 0.5$ from +120 kc/s to -20 kc/s.

2) 3C 123. This source has a simple absorption line as reported in CRW. A brief integration of forty minutes duration was taken at the apparent line bottom. The result was a non-significant detection of the source, with $R = 0.17$

---

31 Muller, C. A. and Westerhout, G BAN, 13, 151, (1957)

32 Kerr, F. J.; Hindman, J. V.; and Gum, C. S. Aust J Phys 12, 270, (1959)

Table VI Source Characteristics

Source	l^{II}	b^{II}	I/I_{Cyg}	Nature	Dist kpc	Size	Baseline	Visibility
Fornax A	185.9	-56.5	0.065	Galaxy	--	30'	100' E-W	.30
3C 123	170.6	-11.4	0.039	Galaxy	--	12"	200' N-S	1.00
Pictor A	251.0	-34.6	0.040	Galaxy	--	7!5	100' E-W	.70
Taurus A	184.5	- 5.8	0.59	SN	1.1	5'		
Orion A	209.1	-19.3	0.27	Em Neb	0.5	6!5		
CTB 31	167.9	- 1.1	0.10	Em Neb		15'	100' E-W	.81
Hydra A	242.9	25.1	0.036	Galaxy	--	5'	200' N-S	.90
M87	322.4	74.5	0.133	Galaxy	--	6!5	200' N-S	.60
Cen A	309.5	19.5	0.24	Galaxy	--	7'	283' NW-SE	.90
Her A	23.1	28.9	0.039	Galaxy	--	2!3	200' N-S	.90
NGC 6334	349.8	2.5	0.090	Em Neb		12'	(CRW)	
3C 353	21.2	19.6	0.039	Galaxy	--	5'	200' N-S	.90
W22	320.8	- 0.6	0.16	Em Neb	1	36'	(CRW)	
Sgr A	0	0	0.68	Gal Nuc	10	3!5		
M8	6.0	- 1.2	0.10	Em Neb	1.2	12'	100' E-W	.35
W37	17.0	0.7	0.056	Em Neb	1.3	12'	100' E-W	.39
M17	15.0	- 0.7	0.40	Em Neb		7'		
W43	30.7	0.8	0.082	Em Neb		15'	100' E-W	.31
W51	49.1	- 0.4	0.10			18'	(CRW)	
Cyg A	76.5	5.8	1.00	Galaxy	--	2'	200' N-S	1.00
Cas A	111.5	- 0.2	1.62		3.4	4!4		

± 0.10, resulting in an optical depth of $1.8^{+1.8}_{-0.5}$. The center frequency is -24 ± 5 kc/s, comparing well with the -22 quoted in CRW. The full width to half R points is 22 ± 8 kc/s, corresponding to a dispersion of 8 kc/s.

3) Pictor A. This source is unabsorbed. $R > 0.7$ from +200 to -200 kc/s.

4) CTB 31. A total of about two and a half hours of integration time allows only the setting of a lower limit to the optical depth in this profile, $R < 0.15$, $\tau > 2$. If one fits a Gaussian to the sides of the profile which are visible, then the slopes indicate that the maximum optical depth is about 3.6. A dispersion of 12.6 kc/s was derived in the same fashion. This is probably too far to reliably extrapolate with a Gaussian shape. The profile is definitely composed of two components in approximately the positions noted in CRW. The parameters of the source are quoted in Table VII. The total integrated optical depth is greater than 100 kc/s.

5) Hydra A. This source is unabsorbed. $R > 0.7$ from +200 to -200 kc/s.

6) M87. This source is unabsorbed. $R > 0.9$ from +250 to -200 kc/s.

7) Centaurus A. This source is unabsorbed. $R > 0.85$ from +80 to -140 kc/s.

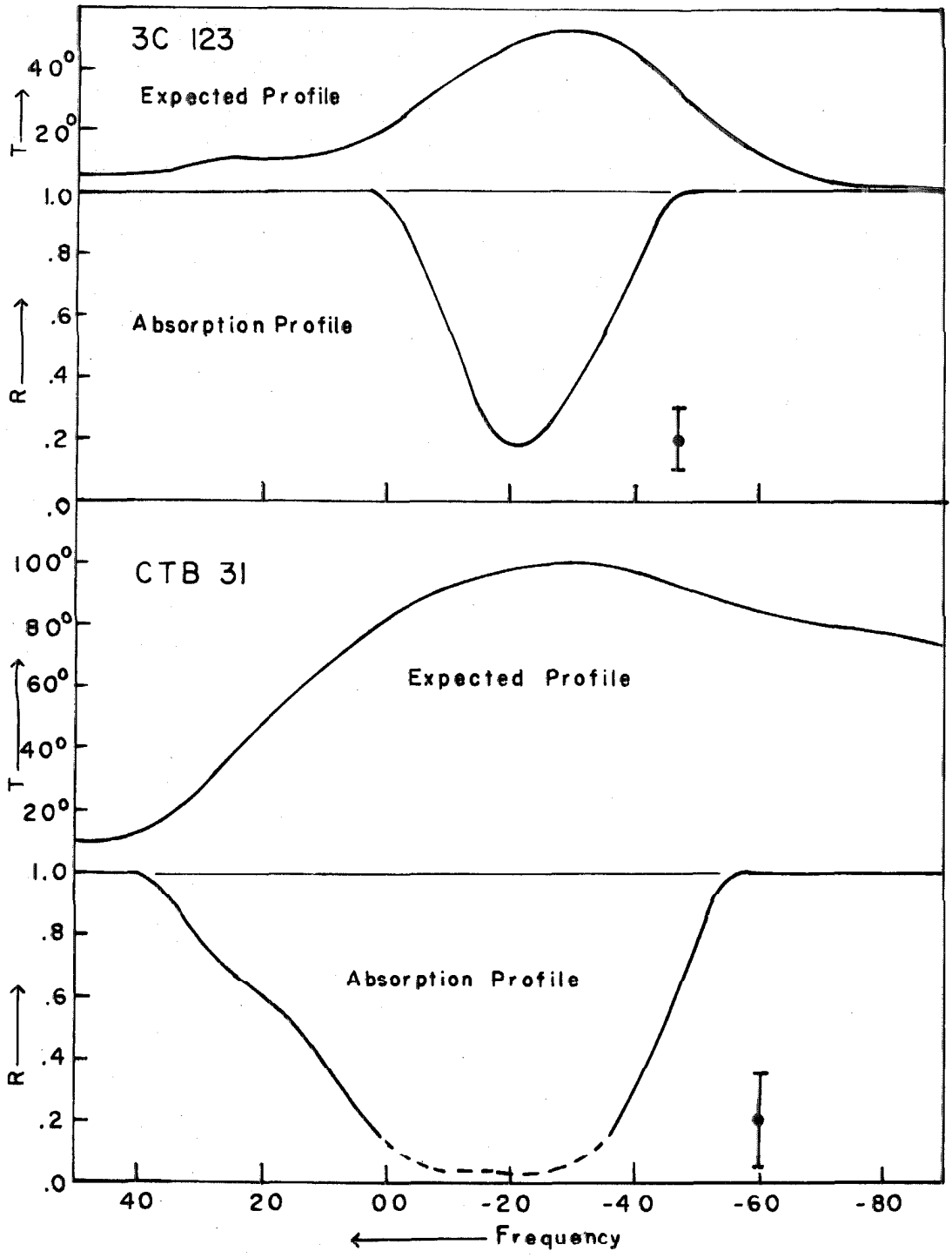

Figure 20. Absorption Spectra for 3C 123 and CTB 31.

8) Hercules A. This source is apparently unabsorbed. $R > 0.5$ from +100 to -200 kc/s.

9) NGC 6334. This source is so highly resolved with the interferometer that there is no longer sufficient signal to noise ratio to obtain useful information about the profile. It is possible to see that the source is absorbed in the appropriate region, and nothing more. The components listed in Table VII are taken from the single dish observations of CRW.

10) 3C 353. This source appears to have a single, simple line with an optical depth greater than 1. The parameters are listed in Table VII. The width is rather uncertain because the depth is unknown. It is unlikely to be much greater than the quoted figure.

11) W22. This source also is highly resolved, and the components in Table VII are taken from the single dish observations of CRW.

12) M8. The scatter in the data prevents one from seeing more than the general shape of the profile. The profile appears to resemble that of the Crab Nebula, with a broad component centered at about zero frequency and a deep and narrow one centered at about -30 kc/s. The parameters are given in Table VII.

13) W37. Again the signal to noise ratio is sufficiently bad that one can only say that the source is absorbed.

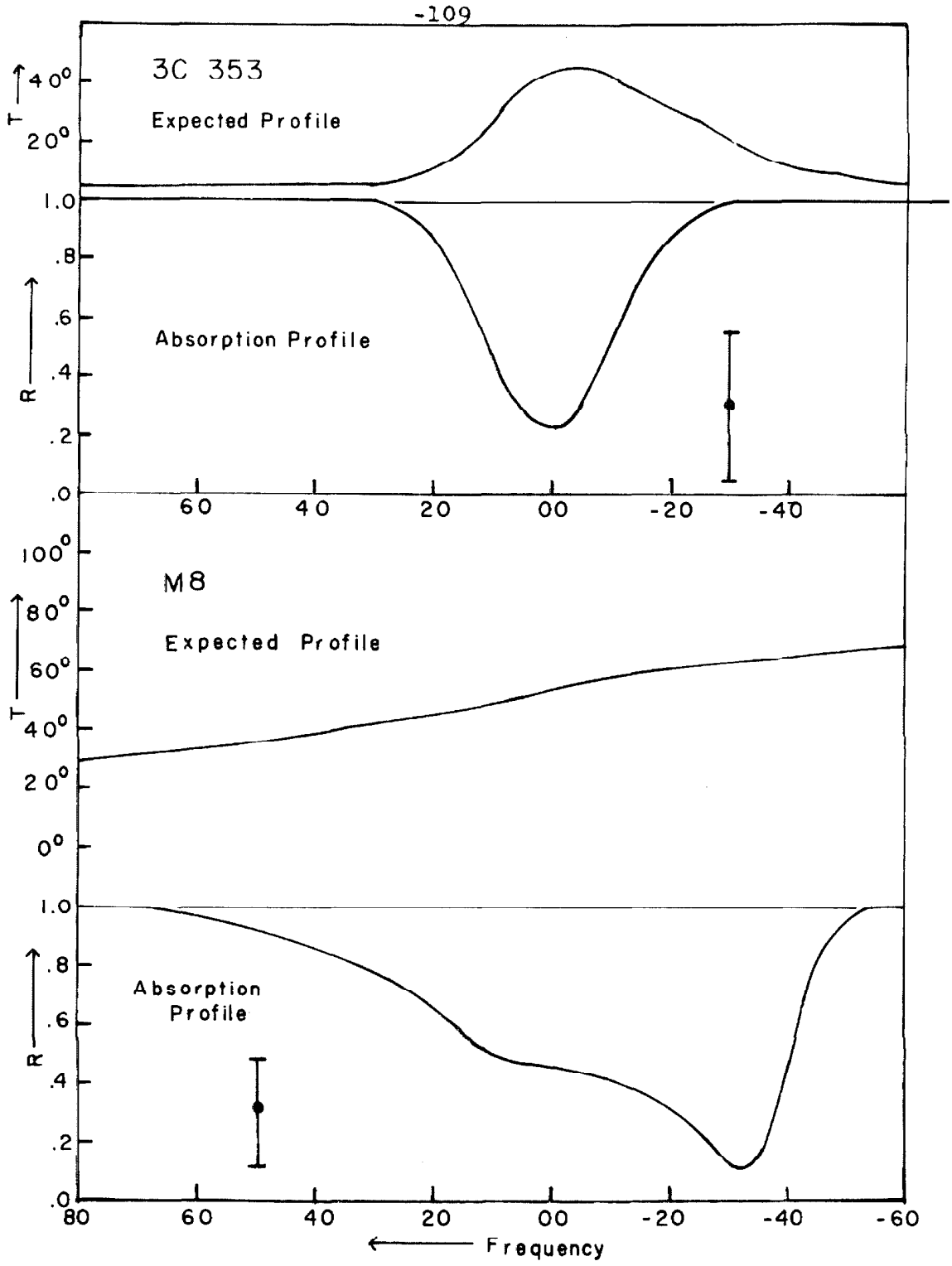

Figure 21. Absorption Spectra for 3C 353 and M8.

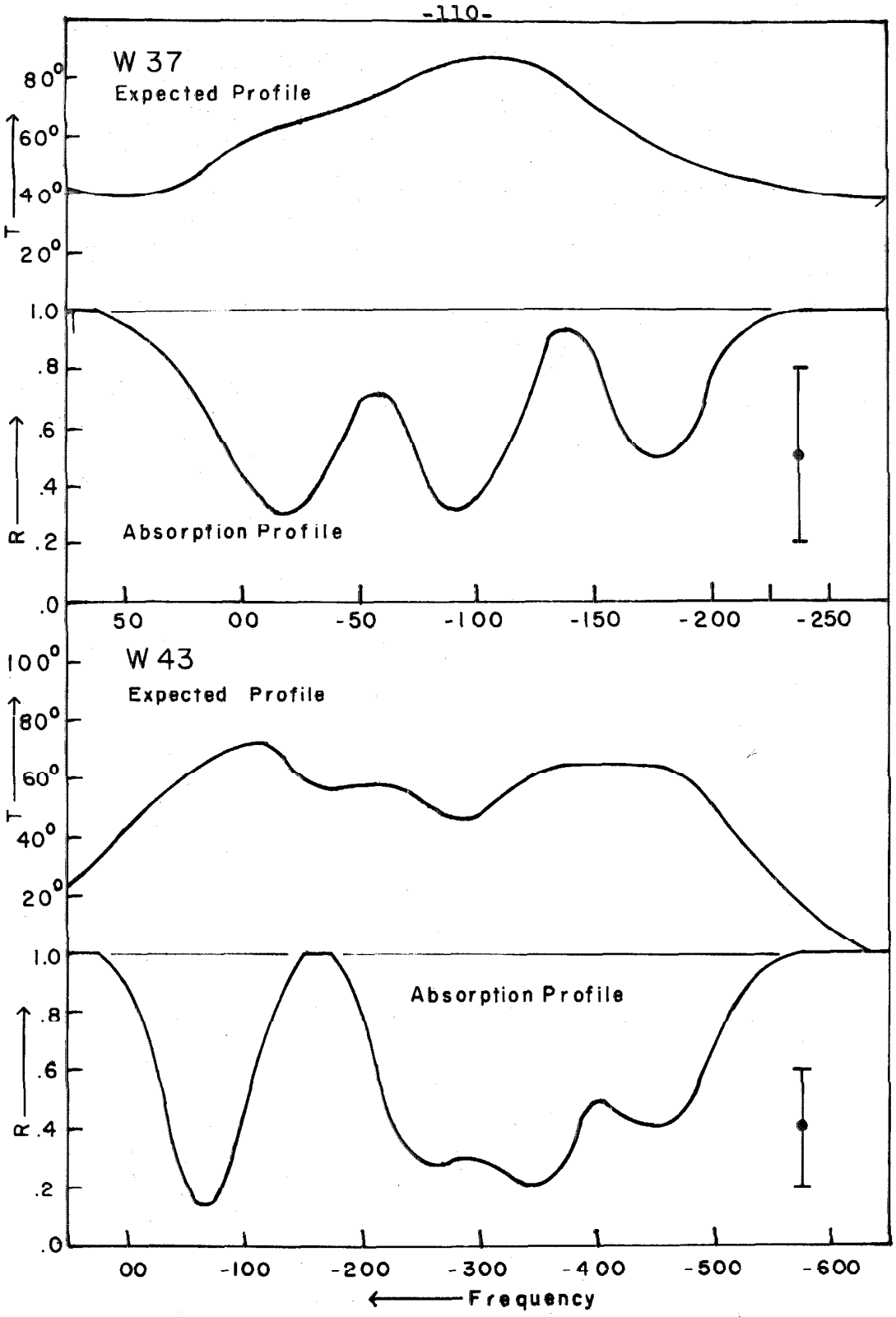

Figure 22. Absorption Spectra for W37 and W43.

The spectrum appears to have three components with quite high maxima between them.

14) W43. Again the signal to noise ratio has been reduced by resolution to such a level that one may only say when the source is absorbed and when it is not absorbed. However, it appears from these observations that the single dish observations of CRW erred in showing the region from -200 to -300 kc/s as free from absorption. On the basis of interferometer records of rather poor quality, a third component has been added to the profile, at -260 kc/s. The other three component parameters are taken from CRW. The peak between the two features at large negative frequencies shows up very well, perhaps better than shown in CRW.

15) W 51. This very large source is resolved beyond any hope of deciphering the interferometer records. The component parameters have been taken from CRW.

16) Cygnus A. This source is listed with the weak sources because its absorption is more readily accessible to a frequency switched receiver, and hence it was not thoroughly studied here. Since there are only a few scans of the profile, the signal to noise ratio is characteristic of the weak sources rather than that of the five strong sources. However, there appears to be a frequency splitting of the feature near zero velocity visible even with the poor accuracy available. The two components listed in Table VII

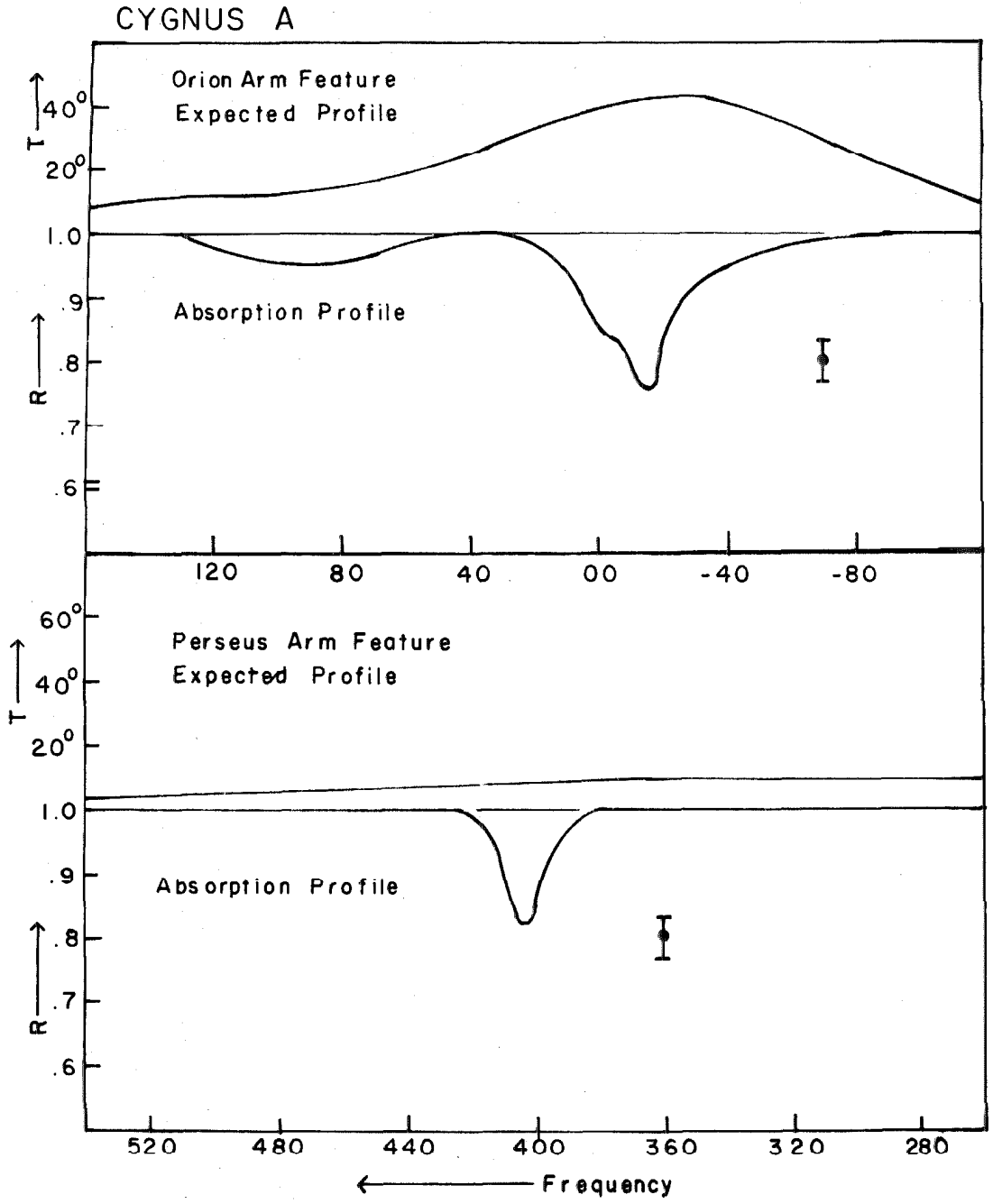

Figure 23. Absorption Spectrum for Cygnus A.

correspond to blends of those quoted by Shuter and Verschuur. They are listed below:

Shuter and Verschuur			Present Investigation		
f_o	τ_o	σ	f_o	τ_o	σ
-31.0	.14	4.1			
-20.0	.31	4.2	-17	.27	7.9
-12.0	.20	2.8			
-7.0	.11	3.4	- 1.5	.15	7.2
1.0	.16	4.7			

The measurements of Shuter and Verschuur are to be preferred in the case of this feature, because they had a frequency switched receiver, and because they spent a great deal more time observing this feature.

TABLE VII

Source	f_o	V	τ_o	σ	$\int \tau \, d\nu$	r	Class
Cas A	155 ±2 kc/s	-32.8	0.30±.10	5.9±1.3 kc/s	3.1	2.6 kpc	WD
	180 ±1.0	-38.0	2.4 ±.2	11.3±1.0	68	2.9	S
	177 ±2	-37.4	0.7 ±.3	3.6±1.0	6.3	2.9	WD
	198 ±4	-41.8	0.40±.15	8.5±3	8.5	3.2	E
	213 ±6	-45.0	0.35±.15	6.2±3	5.4	3.6	E
	227.5±0.7	-48.0	$6.7 \pm^{\infty}_{1.2}$	7.0±1.0	117	3.8	S
	-37.6±3	7.9	0.09±.02	9.1±3	2.0	---	WD
	-16.0±2.2	3.4	0.10±.02	6.3±2	1.6	---	WD
	1.9±2.2	-0.4	1.41±.3	5.8±0.7	20	0	WD
	7.1±1.2	-1.5	0.73±.4	3.7±1.2	6.8	0.1	WD
	22.8±1.5	-4.8	0.14±.02	8.0±1.3	2.8	0.4	WD
	54.5±4	-11.5	0.07±.02	12.9±4	2.3	1.0	WD
Tau A	-51.6±1.0	10.9	0.86±.08	6.0±0.3	12.9		S
	-50.5±0.8	10.7	0.58±.08	2.7±0.3	4.1		E
	-37.9±2.0	8.0	0.14±.03	3.7±1.4	1.2		E
	-18.7±1.1	3.9	0.82±.10	10.7±0.8	22		WD
	-10.7±1.1	2.3	0.12±.10	3.4±1.1	1.0		WD
	5.9±3.5	-1.2	0.07±.03	6.0±2.5	1.0		WD
Sgr A	254.8±1.0	-53.8	1.08±.06	13.7±0.7	37	7	S
	291.8±3	-61.6	0.10±.04	5.1±3	1.3		WD
	151.1±2.0	-31.9	0.26±.05	10.3±3	6.7		S
	109.6±2.0	-23.2	0.14±.03	5.1±2	1.8		S
	1.0±1.5	- 0.2	>3	<45	>230		S
	- 68.3±2.0	14.4	0.57±.05	11.4±3	16.3		S
	-104.0±2.0	22.0	0.33±.04	15.8±3	13.1		S

Table VII (continued)

Source	f_o	V	τ_o	σ	$\int \tau\, d\nu$	r	Class
Orion A	-21.4±0.6	4.5	2.01±.15	6.7±0.45	34	---	WD
	-11.7±0.9	2.5	1.19±.09	14.2±0.5	42	---	WD
Omega Neb	-32.5±1.0	6.9	1.42±.08	17.6±0.8	62	0.8	WD
	-29.9±1.6	6.3	0.15±.07	4.2±2.2	1.6	0.8	WD
	-68.5±1.0	14.5	0.87±.07	11.7±1.5	25	1.7	WD
	-98.2±0.7	20.7	1.61±.08	10.5±1.0	42	2.5	S
	-125.2±1.8	26.4	0.57±.06	11.2±1.2	16	3.1	WD
3C 123	-24 ±5	5.1	$1.8\ ^{+1.8}_{-0.5}$	8 ±3	36		S
CTB	-18 ±3	3.8	>2	12.6±3	>100		S
	20 ±5	-4.2	0.54±.2	4.3±1.4	5.8		WD
NGC 6334	-20 ±5	4.2	0.60±.35	22 ±3.5	33		WD
	27 ±5	-5.7	$1.5\ ^{+1.0}_{-0.6}$	6.9±1.1	26		S
3C 353	3 ±4	-0.6	>0.7	8.6±1.8	>15	0.6	S
W22	-54 ±10	11.4	>1.2	6.5±2.5	>20		S?
	-23 ±10	4.9	>1.4	5.4±2	>19		S?
	6 ±8	-1.3	>1.5	7.2±2.5	>27		S?
	60 ±8	-12.7	0.9±.3	7.6±2.5	17		S

Table VII (continued)

Source	f_o	V	τ_o	σ	$\int \tau\, dv$	r	Class
M8	0 ±20	0	$0.6^{+.6}_{-.3}$	29 ±7	44		WD
	-30 ±5	6.3	>1.2	6.5±2	>20		S
W37	-10 ±10	2.1	>1	7.2±3.5	>18	0.2	S
	-85 ±10	18.0	>1	7.2±3.5	>18	1.5	S
	-170 ±10	35.9	>0.5	5.4±3	> 7	3.4	S
W43	-60 ±7	12.7	>1.3	12.6±3.5	>41	0.9	S
	-260 ±30	54.9	>0.7	25 ±10	>44	4.0	S?
	-396 ±10	83.6	$0.65^{+.7}_{-.4}$	18.0±4.5	30	6.1	S
	-445 ±12	94.0	$0.56^{+.7}_{-.4}$	21.6±5.5	30	7.0	S
W51	-34 ±5	7.2	>1.5	<5.0	>20		S
	-60 ±4	12.7	$1.0^{+.8}_{-.4}$	10.0±2.8	29		WD
	-225 ±4	47.5	$0.8^{+.6}_{-.4}$	9.4±2.5	20		WD
	-260 ±4	54.9	$0.55^{+.5}_{-.3}$	9.8±2.5	15		WD
Cyg A	-17 ±3	3.6	0.27±.05	7.9±3	5.3	0.5, 4.2	S
	- 1.5±5	0.3	0.15±.05	7.2±3.5	2.7	0.0, 4.7	WD
	-50 ±15	10.5	0.04±.03?	10.8±3.5	1.1	2.3	WD
	90 ±10	-19.0	0.05±.03	17.3±3.5	2.2	6.6	S
	403 ±3	-85.1	0.17±.05	6.1±2.0	2.6	12.4	S

Table VIII. Line Bottoms

Source	f kc/s	R	-log R
Cas A	7.5	.155 ± .010	1.86
	177	.057 ± .008	2.86
	227.5	.0033± .0020	5.7
Tau A	-51.5	.24 ± .03	1.42
	-16	.43 ± .02	0.84
Sgr A	-102	.71 ± .04	0.34
	-67	.56 ± .04	0.58
	1	.028 ± .016	3.6
	109	.87 ± .03	0.14
	150	.77 ± .03	0.26
	255	.34 ± .03	1.08
Ori A *	-20	.040 ± .015	3.2
Omega Neb	-99	.175 ± .06	1.75
	-64	.33 ± .06	1.11
	-32	.21 ± .06	1.56

* 200 foot east-west spacing.

IV

THE STATISTICS OF THE CLOUDS

In this chapter I shall first present a brief discussion of the statistics of the components listed above, although the data is somewhat non-uniform because the chance of separating two close components depends strongly on the accuracy with which the profile is known, and therefore varies rapidly with the strength of the sources. I shall then present a few mathematical results and considerations for a possible explanation of the observations with a "raisin pudding" model of cold clouds in a hot medium.

The summary of all the data about the various components is presented in Table VII. In this table I have classified the components according to the difficulty of resolving them from their neighbors. Class S are the most easily separated components, those showing a separated peak in the absorption profile. Class WD, well defined, are those components which are marked in the profile with a strong inflection point, though they do not show a separate peak. Class E are those components which are carved from the excess left over when everything else has been subtracted. In the weak sources only class S components can be recognized.

In addition, in order to facilitate direct comparison with other observers, I present at this time a summary in Table VIII, which lists the peaks in absorption and the R-values for the profiles at these points for the strong sources.

Before starting the statistical discussion proper, there are two questions which should be brought up. These are the question whether clouds indeed sometimes show line broadening by microturbulence, or whether all line widths can be explained by thermal motions, and the question of whether the very close components are spacially separated or represent streams in a turbulent cloud.

Shuter and Verschuur succeed in resolving their profiles to the point that the broadening of their components is all attributable to thermal broadening. In this investigation, the greatest dispersions recorded which seem to be from unequivocably simple lines are about 10 kc/s, and all the lines which have a dispersion listed in Table VII greater than this have not been examined with sufficient sensitivity to say whether they are blends or not. This dispersion corresponds to a thermal broadening by hydrogen at a temperature of about 500° K, which is hot, but not excessively so. There appear to be somewhat more of these components than would be predicted on the theory of Kahn[33],

---

[33] Kahn, F. D. Gas Dynamics of Cosmic Clouds, p. 60, Interscience Pub. (1955)

but the present data are so incomplete that it is impossible to say definitely.

If the temperature of a cloud is independent of its mass, and all profile broadening is due to thermal motions, then $\sigma^2 \int \tau \, d\nu$ should be independent of σ, which it apparently is not. $\int \tau \, d\nu$ is roughly independent of σ, though with great scatter, which is possibly an indication that microturbulence is responsible for much of the line broadening.

The second question, whether the very close components are spatially separated or not, depends on the statistics of the cloud peculiar motions. If the cloud velocity dispersion is something like the 8 km/s deduced by Kwee, Muller, and Westerhout, then the coincidences of components of like optical depth in two features in the spectrum of Cas A and one in Taurus A are very improbably the result of chance stacking of components, and it is likely that the gas masses responsible for the two components are physically related. If, however, the cloud velocity dispersion is two or three times smaller than the emission dispersion, as suggested by the zero velocity feature in the spectrum of Sgr A, then these features become plausible coincidences, and may represent clouds which are more or less spatially separated.

4.1 Statistics of the Observed Components.

The most striking feature at once visible in the data

is the fact that the layer of clouds is very flat and dense. Of thirteen sources with b^{II} less than nineteen degrees, only one has absorption everywhere less than $\tau = 1/2$ (Cygnus A). Of the five sources with b^{II} greater than twenty degrees, none are detectably absorbed. For the three sources between nineteen and twenty degrees of latitude, two (3C 353, Orion A) are absorbed, and one (Centaurus A) is not.

It was reported in CRW that the law of number variation of τ_o was that the number of components with a given τ_o is proportional to $2^{-\tau_o}$. A histogram of the τ_o for each of the components in Table VII is plotted in Figure 24. (In this and the following histograms, the dotted lines refer to the five strong sources only--the full lines to all sources.) The slope appears slightly steeper than this law, and perhaps a more appropriate law would be $e^{-\tau_o}$, which is indicated on the graph. The point for the Perseus arm line in Cas A is anomalously deep. However, perhaps some of the other components would be moved out to that optical depth if an observation done with a more sensitive receiver succeeded in establishing the optical depths of some of the sources for which only a lower limit is known, or an observation with higher resolving power succeeded in locating local condensations of large optical depth.

It was suggested in CRW that the sun was possibly in a cloud, or sufficiently near to one that the cloud covered

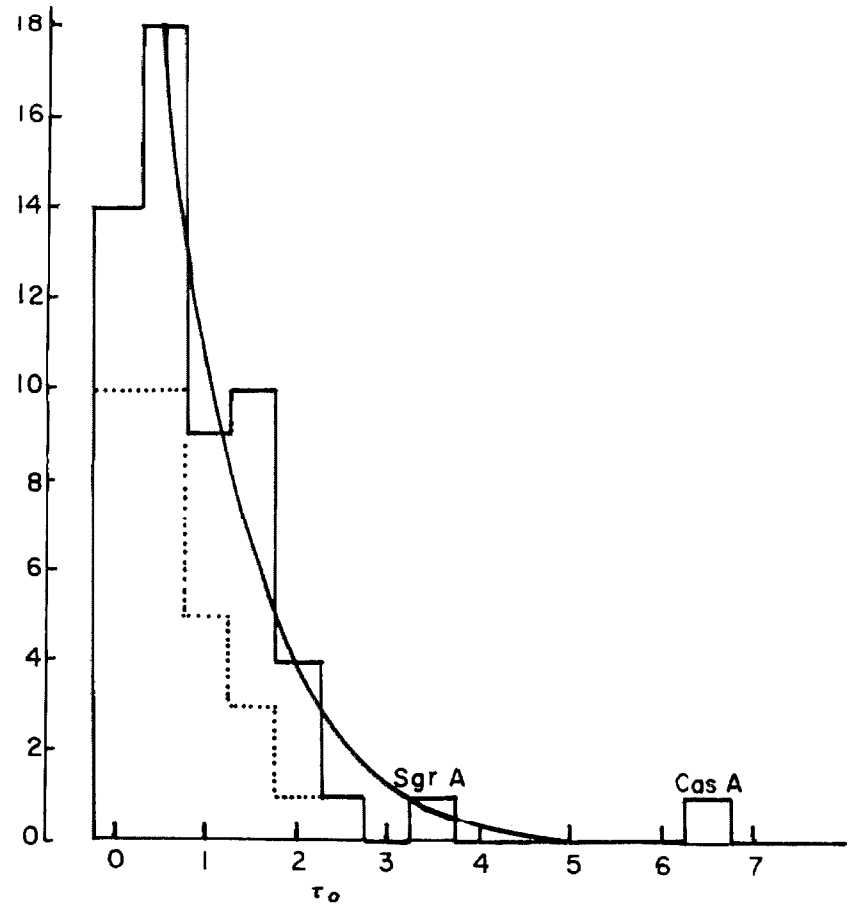

Figure 24. Histogram of τ_o.

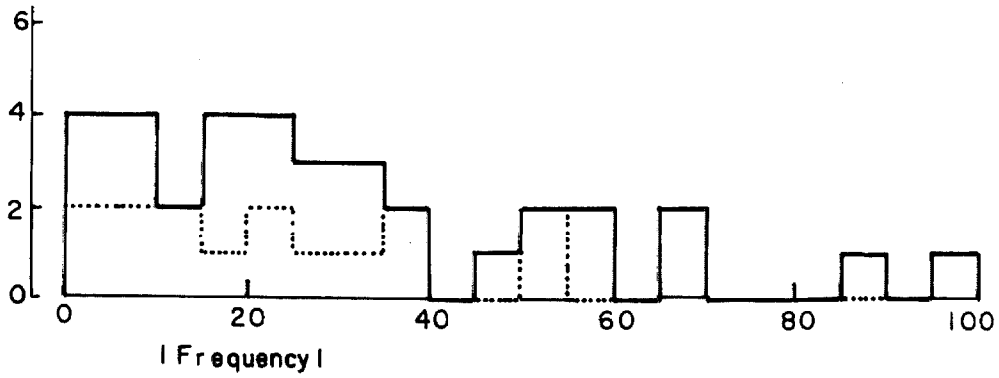

Figure 25. Histogram of central frequencies.

a large portion of the sky. If this were true, then one would expect an excess in the number of components with the velocity associated with the cloud, if it is near zero. A histogram of center frequencies is plotted in figure 25. It is seen that there is a gradual tapering off with a dispersion of perhaps 50 kc/s, which is to be associated with the local spiral arm, as the graph should consist of a central hump of the clouds in our spiral arm, and clouds from other spiral arms should be spread out over a much larger frequency range. There is no apparent excess of clouds at any frequency. Therefore, the existence of a cloud large enough in angular diameter to cover more than two or three of these sources is rather unlikely.

In order to estimate the efficiency of the splitting of the features into components, the frequency difference between neighboring components was taken, and a histogram of this quantity is shown in figure 26. This quantity should have a roughly Gaussian distribution, exactly Gaussian for a two component profile if the distribution of cloud velocities is Gaussian. The observed histogram rises to a peak, and then tapers off again. This is presumably due to the difficulty of separating components which arevery close together. The peak falls at 15 kc/s, so it was assumed that the errors in separation become reasonably small at separations larger than 17.5 kc/s. Fre-

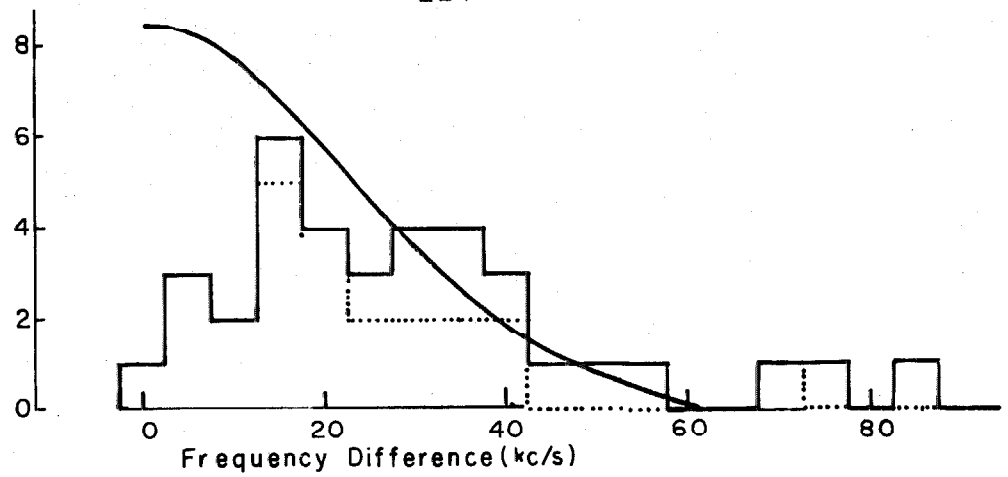

Figure 26. Histogram of frequency difference between adjacent components.

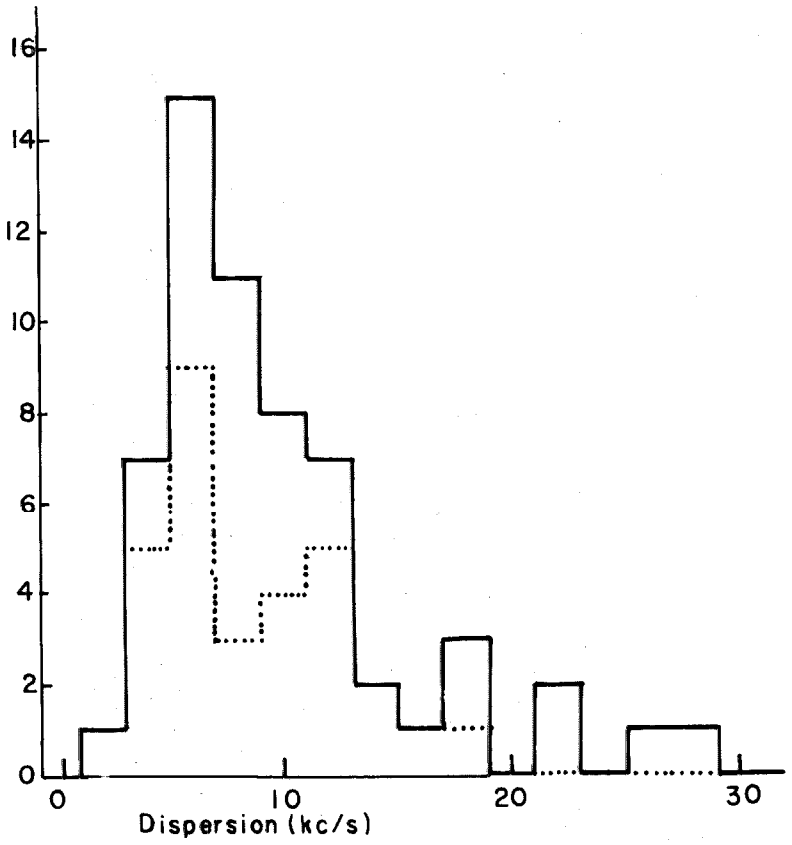

Figure 27. Histogram of dispersions.

quency differences greater than about 65 kc/s are probably chiefly due to differential galactic rotation. There are several points which fall off of figure 26 which are clearly due to components in different spiral arms. There is evidence neither for nor against Blaauw's substitution of an exponential law for a Gaussian one in this histogram, because many of these clouds are so distant that the effects of differential rotation are very important.

The histogram for $17.5 < f_1 - f_2 < 65$ was fitted with the tail of a Gaussian, which has a dispersion of about 22 kc/s and is also plotted on the diagram. The area in which this Gaussian lies above the histogram presumably indicates the incompleteness of the separation into components. Thus it is seen that at zero frequency separation, about two thirds of the features which are a superposition of two components have not been recognized as such. The area under the Gaussian is 48 sources, whereas 33 are counted in the histogram, so about 40% of the components listed here as single are actually double. Some of these will be unrecoverable with any reasonable signal to noise ratio, because of too close a match in both frequency and dispersion, or a weak line may be irretrievably lost near a strong line. The dispersion of this Gaussian is about $\sqrt{\frac{2}{N-1}}$ times the velocity dispersion of the clouds, if there are N clouds in a spiral arm. This indicates a velocity dispersion of

about 6 km/s if we set N = 4.

The histogram of component dispersions is shown in figure 27. The peak frequency seems to fall at a dispersion of 6 kc/s. Correction for the incompleteness mentioned above will cause this diagram to move somewhat to the left. Shuter and Verschuur, observing with a narrower bandwidth, and in general fitting the profiles with many more components than is done in the present investigation, found a median dispersion of only 3.5 kc/s. Both their and the present distributions are well to the left of the histogram of dispersions prepared by Takakubo and van Woerden for the Gaussian resolution of the profiles of the intermediate latitude catalogue, and so the problem pointed out by Shuter and Verschuur of this difference in emission and absorption profiles still remains with a rather more conservative choice of components in the absorption profiles.

Shuter and Verschuur used their resolution of profiles into Gaussian components to estimate the temperatures of the clouds on the assumption that the width of their components was due to the thermal doppler broadening of the hydrogen line. This proceedure may fall into error for two reasons, firstly because some of the dispersion is probably microturbulence, and secondly because the temperature depends on the square of the dispersion, and the dispersion depends on the number of components one tries

to fit a given profile with, which at the moment is a more or less subjective judgement. An illustration of this appears in the paper of Shuter and Verschuur, in which they resolve the Perseus arm feature of Cygnus A into four components of disperions from 2.2 to 4.7 kc/s, whereas they quote a least squares solution computed by Schwarz (Schwarz c) which has a quite acceptable error and employs only two components of dispersions 4.6 and 10.4 kc/s, rather significantly wider than the components produced by Shuter and Verschuur. The question of the dispersion of the components of a profile is at its most difficult when there is a small bump on the side of a deeper line, near the top of the profile. It is impossible to decide whether it is a narrow component localized near the point of its maximum effect on the profile, or the toe of a hidden, wider Guassian hidden below the main line, unless the signal to noise ratio is very good indeed. The small bumps and changes of slope do appear capable of giving fairly reliable temperatures, but one would like to see the process put on a more systematic and less subjective basis.

An estimate of the cloud density in space can be made from the number of components in front of source of known distance. We know distances in the following cases:

Cas A	3.4 kpc from optical data	5 clouds with $\tau > 1/2$
Tau A	1.1 kpc from optical data	3 clouds with $\tau > 1/2$
Orion A	0.5 kpc from optical data	2 clouds with $\tau > 1/2$
M17	3.1 kpc from kinematical distance of farthest cloud	4 clouds with $\tau > 1/2$

These average to 1.7 clouds/kpc. This is considerably greater than the 0.83 clouds/kpc reported in CRW, because the latter authors excluded the immediate neighborhood of the sun to make sure the same cloud was not counted twice. In so doing, they excluded a large part of the Orion arm of the galaxy, and thus weighted their density much more heavily with the interarm regions. They also blended several components which are resolved here.

This figure of 1.7 clouds per kiloparsec with $\tau > 1/2$ must be multiplied by a factor of 1.4 in order to correct for the incompleteness mentioned above, and, to derive the total line density of clouds, by about 1.65 to include the components with $\tau < 1/2$. The resulting figure is 4.1 clouds/kpc of all densities.

In the two sources in this spiral arm, Orion A and Taurus A, we have five clouds in 1.6 kpc, which, after correction for the clouds with $\tau < 1/2$ and for the incompleteness is 7.5 clouds/kpc, about twice the average from the other sources. This may be a reflection of the density contrast with the inter arm regions. This number of clouds is comparable with the eight to twelve clouds/kpc derived

by Blaauw.

4.2 The Hot Medium Model.

There are several pieces of evidence that there is a significant variation of spin temperature in space. These are collected here in order to have a general compilation of them in one place, although some of them have been mentioned elsewhere in this thesis.

The primary evidence is that the absorption profiles differ from the expected profiles. If spin temperatures are constant everywhere, the absorption must arise in exactly the same matter as the emission, and the absorption profiles must be at least statistically identical with the emission profiles.

The histogram of dispersions computed above, and that computed by Shuter and Verschuur, while they differ somewhat, are both very different from that obtained in an analysis of the emission profiles at intermediate latitudes by Takakubo and van Woerden, who concluded that overlapping and blending effects were not of excessive importance.

There are only a few clouds appearing in absorption in front of most sources, so the absorption profile may change greatly from one line of sight to another. If this property, rather than changing spin temperature, is invoked to explain the difference between the absorption and expected profiles, as was done by Hagen, Lilley, and McClain,

one encounters difficulties in explaining why the nearby emission in the plane is not breaking up into peaks as narrow as those in the absorption profiles. For instance, the clouds causing the deep Orion arm feature in Cas A fall very near to zero velocity. Even if they have a random velocity which cancels the differential galactic rotation, it is doubtful that they are more than half a kiloparsec away. There are certainly clouds in the Perseus arm feature which are more than five parsecs in diameter, in order to cover the source to a high average optical depth. At half a kiloparsec, one of these clouds would subtend at least half a degree, and thus should considerably influence the expected profile. This difficulty should be even more acute at longitudes near odd multiples of 45°, where the profiles are more spread out by differential rotation.

It is even more difficult to find a statistical reason for the difference between the expected and absorption profiles in the direction of the galactic center. Here there is a statistically significant number of clouds directly in front of the source, and there should be no purely statistical reason for the two profiles to be different.

There is some direct evidence that there are appreciable numbers of clouds with temperatures less than 125° K. Some line profiles may be interpreted as self absorption of the neutral hydrogen, implying a cool cloud in front of the

line radiation from hotter regions behind[34]. Also, the temperatures obtained by Shuter from widths of Gaussian components in absorption profiles are too low to account for the harmonic mean temperature obtained by Schmidt of 125° K.

All of these points tend to a conclusion that there may be significant contributions to the hydrogen emission from hydrogen which is not seen in absorption, because its temperature is too high. To make it completely invisible, it must be at a temperature in excess of 1000° K. If we now call to mind the fact that the clouds are gravitationally unstable, we see that we can attempt to give the clouds some stability through the pressure of a surrounding hot medium. Thus, although the above evidence is somewhat inconclusive, and certainly indicates no particular model of the interstellar medium, it indicates that it is perhaps worth investigating some models with an extreme range of temperatures. I propose to consider here a model with a hot medium surrounding much colder clouds.

Any reasonably exact model is extremely intractable mathematically, so a great many approximations have to be made to obtain useful equations. Expressions for $\overline{T_b}$ and $\overline{T_b^2}$,

---

[34] Heeschen, D. S. ApJ, 121, 569, (1955)
Davies, R. D. RMP, 30, 443, (1958)
Radhakrishnan, V. Pub ASP, 72, 296, (1960)

which is used to derive the temperature uncertainty by

$$(\Delta T)^2 = \overline{T^2} - \overline{T}^2 \quad ,$$

are derived in Appendix II under the following simplifying assumptions:

1) We consider a layer of thickness L in which the density of the medium and the probability density of cloud centers is independent of position.

2) If the temperature of the medium is T_1 and its density is n_m, then $\beta L n_m T_1$, where β is the absorption coefficient times temperature as used in equation (3) in Section 2.3.

3) The optical depth through a cloud is a constant τ_c if the distance from the center is less than a and the shift from the center frequency is less than σ, and zero otherwise.

4) All clouds have the same temperature T_c and density n_c.

5) The number of clouds with a given τ_c varies as $e^{-\tau_c}$.

A typical distance in this theory is b, a typical cloud radius divided by the ratio of cloud internal dispersion to the dispersion of cloud velocities, and by the fraction of space occupied by clouds, i. e. the distance one goes before hitting a cloud absorbing at a particular frequency. This typical distance is the reciprocal of the cloud density found in Section 4.1 multiplied by the ratio of cloud velocity dispersion to cloud internal dispersion. The expected

temperature plotted against the path length L simulates a T_f (1 - exp(-L/b)) curve, where

$$T_f = T_c + \beta n_m b$$

If we consider the clouds to be at a temperature of about 85° as quoted by Shuter and Verschuur from an earlier investigation by Shuter, then

$$\beta n_m b = 40°$$

According to van de Hulst, Muller, and Oort, the absorption coefficient is about 1/kpc. If we take b = 1 kpc,

$$n_m = 0.0049\ \Delta f$$

where Δf is the bandwidth of the emission in kc/s. Kwee, Muller, and Westerhout derive an average bandwidth of about 120 kc/s, which would give

$$n_m = 0.6 ,$$

about the same as derived in the usual fashion for a 125° medium. Thus, with this model about half of the interstellar matter is in cold clouds and half in the hot medium.

It is possible to estimate the temperature of the medium if one assumes that the clouds are made stable by pressure equilibrium with the surrounding medium. The values estimated here for nT inside the clouds tend to run to several thousand, so the medium may be at a temperature as high as ten thousand degrees. It is difficult to propose an energy source which will heat such a large mass to such a high temperature. The opacity of the medium would be in

the neighborhood of 0.01/kpc, and could be easily overlooked among the deep absorption features caused by the clouds.

The statistical uncertainty in the temperature resulting from a given path length starts at about 25° K for an optically thick layer, and gradually rises as the layer thickness is decreased to meet the expected brightness temperature at about 40°, and then descends again to zero with the brightness temperature.

The b suggested by the absorption coefficient of van de Hulst et al. is about one kiloparsec, whereas, if one takes the value of cloud density derived above, and multiplies by the ratio of cloud internal dispersion to cloud velocity dispersion, which is something like 6 kc/s/50kc/s, if the velocities have the dispersion indicated by the emission line work, then b would be 2 kpc. This discrepancy may be the result of the higher density within a spiral arm, which the measurement of van de Hulst et al. refers to, rather than the average density in the plane, which the 4 clouds per kiloparsec in Section 4.1 refers to. On the other hand, this may be an effect of a reduced dispersion of the cloud velocities below the 8 km/s average velocity quoted by Westerhout.

Whether this model is to be preferred to the model of all emitting clouds with no visible medium, it is certainly clear from this and previous investigations that the average

cloud has an optical thickness which is not small compared to one, and therefore that the mathematics from which hydrogen densities are computed must be revised in any case. One may not, for instance, say that mass is independent of spin temperature of regions of small surface brightness. The low brightness temperature may be due to actual low spin temperature or to a small portion of the beam occupied by a warmer cloud, rather than the thinness of the medium. The effect of such a change of model upon the masses and densities derived for the galactic hydrogen has yet to be completely investigated, especially for regions of small surface brightness.

APPENDIX I

TIME CONSTANT CORRECTIONS

In the out put of the receiver there was a time constant with equivalent circuit as follows:

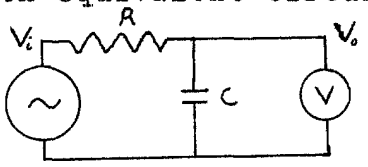

where the generator is a voltage generator and the voltmeter has infinite impedance.

The response at a given frequency ω is

$$V_o = \frac{V_i}{\sqrt{1+(\omega\tau)^2}}$$

where

$$\tau = RC$$

And the phase is retarded by ϕ

$$\tan\phi = \omega\tau$$

If two sine waves at frequency ω are run through slightly different time constants, τ_1 and τ_2, the relative phase at the output is changed by

$$\Delta\phi \approx (\tau_1 - \tau_2)\frac{d\phi}{d\tau} = \frac{(\tau_1-\tau_2)\omega}{1+(\omega\tau)^2}$$

If the input is a slowly modulated sine wave, the output will be approximately the same modulated sine wave, shifted in time by a small amount. To find this shift, we need the impulse solution to the time constant,

$$V_i = \delta(t)$$

$$V_o = \frac{1}{\tau} \begin{cases} 0 & t<0 \\ e^{-\frac{t}{\tau}} & \tau>0 \end{cases}$$

Consider the input

$$V_i(t) = \cos(\omega t+\phi) \begin{cases} 0 & -\infty<t<0 \\ t/b & 0<t<b \\ 1 & b<t<\infty \end{cases}$$

Then

$$V_o(t) = \frac{1}{\tau}\int_{-\infty}^{t} V_i(x)\, e^{\frac{x-t}{\tau}}\, dx$$

for $t<0$

$$V_o(t) = 0$$

for $0<t<b$

$$V_o(t) = \frac{1}{\tau b}\int_0^t x\cos(\omega t+\phi)\, e^{\frac{x-t}{\tau}}\, dx$$

$$= \frac{\tau}{b}\frac{1}{1+(\omega\tau)^2}\left[\cos(\omega t+\phi)+\omega\tau\sin(\omega t+\phi)\right]$$

$$-\frac{\tau}{b}\frac{1}{(1+(\omega\tau)^2)^2}\left[(1-(\omega\tau)^2)\cos(\omega t+\phi)+2\omega\tau\sin(\omega t+\phi)\right]$$

$$+\frac{\tau}{b}\frac{1}{(1+(\omega\tau)^2)^2}\left[(1-(\omega\tau)^2)\cos\phi+2\omega\tau\sin\phi\right]$$

for $b<t$

$$V_o(t) = V_o(b)\, e^{-\frac{t-b}{\tau}} + \frac{1}{\tau}\int_b^t \cos(\omega x+\phi)\, e^{\frac{x-t}{\tau}}\, dx$$

$$= e^{-\frac{t-b}{\tau}}\left[V_o(b)-\frac{1}{1+(\omega\tau)^2}\left(\cos(\omega b+\phi)+\omega\tau\sin(\omega b+\phi)\right)\right]$$

$$+\frac{1}{1+(\omega\tau)^2}\left[\cos(\omega t+\phi)+\omega\tau\sin(\omega t+\phi)\right]$$

If $\omega b \gg 1$, i. e. if there are several fringes on the slope, and $b \gg \tau$, then well away from the "corners" of the modulating function this is approximately

$t<0$

$V_o(t) = 0$

$0<t<b$

$$V_o(t) = A(t)\cos(\omega t+\phi+\theta(t))$$

where

$$A(t) = \frac{1}{1+(\omega\tau)^2}\left\{\left[\frac{t}{b} - \frac{\tau}{b}\,\frac{1-(\omega\tau)^2}{1+(\omega\tau)^2}\right]^2 + (\omega\tau)^2\left[\frac{t}{b} - \frac{\tau}{b}\,\frac{2}{1+(\omega\tau)^2}\right]^2\right\}^{\frac{1}{2}}$$

$$\approx \frac{1}{\sqrt{1+(\omega\tau)^2}} \quad \frac{t - \frac{\tau}{1+(\omega\tau)^2}}{b}$$

and

$$\tan\theta(t) = \frac{\omega\tau\left(\frac{t}{b} - \frac{2}{1+(\omega\tau)^2}\,\frac{\tau}{b}\right)}{\frac{t}{b} - \frac{1-(\omega\tau)^2}{1+(\omega\tau)^2}\,\frac{\tau}{b}} \approx \omega\tau\left(1 - \frac{\tau}{t}\right)$$

for $t > b$

$$V_o(t) \approx \frac{1}{\sqrt{1+(\omega\tau)^2}}\cos(\omega t + \phi + \theta)$$

$$\tan\theta = \omega\tau$$

The output modulation pattern is thus retarded by

$$\frac{\tau}{1+(\omega\tau)^2}$$

behind the input modulation pattern, and the phase is subject to strange changes within a few τ of the time the sine wave is turned on. The delay of the modulation pattern by

$$\frac{\tau}{1+(\omega\tau)^2}$$

instead of by τ as in a simple receiver is quite general and holds for all slow modulation patterns.

APPENDIX II

THE MATHEMATICS OF A HOT MEDIUM

First of all, let us consider spherical clouds. Let the probability of finding the center of a cloud with

$\tau_c <$ central optical depth $< \tau_c + d\tau_c$

$\sigma <$ frequency dispersion $< \sigma + d\sigma$

$T <$ temperature $< T + dT$

$f_o <$ central frequency $< f_o + df_o$

$a <$ radius $< a + da$

in volume dV be

$$\eta(\tau_c, \sigma, T, f_o, a, \vec{r})\, d\tau_c\, d\sigma\, dT\, df_o\, da\, dV$$

These clouds are immersed in a medium of density $n_1(\vec{r}, f)$, temperature T_1 and velocity dispersion σ_1.

For each cloud the optical depth at a distance r from the center to the line of sight is

$$\tau(f) = \tau_c\, e^{-\frac{(f-f_o)^2}{2\sigma^2}}\, g\left(\frac{r}{a}\right)$$

Consider a layer of thickness L in which η is independent of $\vec{r}$. Let the probability that the brightness temperature is less than T_b be $\Psi(T_b)$. The probability that no clouds cover the line of sight is (1-p),

$$1-p = \exp - \int_0^\infty \pi a^2 L \left(\int \eta(\tau_c, \sigma, T, f_o, a)\, d\tau_c d\sigma dT\, df_o \right) da$$

Neglecting the overlapping of the clouds, the probability

of m clouds in the beam is

$$(1-p)\,p^m$$

Let $P_m(T_b)$ be the probability that the brightness temperature is less than T_b given m clouds in the line of sight. Then

$$\Psi(T_b) = (1-p)P_0(T_b) + p(1-p)P_1(T_b) + \cdots + p^m(1-p)P_m(T_b) + \cdots$$

The exact solution would involve the many integrals inherent in the various P_m, or their equivalents.

$$P_0 = I(T - \beta L\, n_1(f))$$

where I is the Heavyside unit function

$$I(x) = \begin{cases} 0 & x < 0 \\ 1 & x > 0 \end{cases}$$

The other P_m are extremely complicated. In order to simplify these, we make the following assumptions:

1) Take cylindrical clouds so that $g(x) = 1$.

2) Replace $e^{-\frac{(f-f_0)^2}{2\sigma^2}}$ by $I(f-f_0+\sigma) - I(f-f_0-\sigma)$.

3) All clouds have the same temperature T_c.

4) All clouds have the same density. This implies that the integrated optical depth is proportional to the radius, so we can write

$$a = a_0 \frac{r_c \sigma}{r_0 \sigma_0}$$

5) The distribution of center frequencies is uniform on a range $\sigma_2 \gg \sigma$.

6) Consider frequencies near zero, so that the proportion of clouds on the line of sight which absorb radiation at the frequency under discussion is $\frac{\sigma}{\sigma_2}$.

Now, the probability of no clouds on the line of sight which absorb at a given frequency is

$$1-q = \exp - \int_0^\infty \int_0^\infty \frac{\pi a^2 L}{\sigma_1} \int_0^\infty \eta(\tau_c, \sigma)\, d\tau_c\, \delta(a - a_0 \frac{\tau_c \sigma}{\tau_0 \sigma_0})\, da\, d\sigma$$

$$\equiv e^{-nL}$$

which defines the cloud density $\underline{n}$.

With these simplifications,

$$P_1(T_b) = \frac{\int_0^{l_0} \int_{\tau_1}^{\tau_2} \int_0^\infty \eta(\tau_c, \sigma)\, d\sigma\, d\tau_c\, dl}{\int_0^\infty \int_0^\infty \eta(\tau_c, \sigma)\, d\sigma\, d\tau_c}$$

where

$$l_0 = \begin{cases} 1 & T_b > T_m \\ \frac{T_b - T_c}{T_m} & T_c < T_b < T_m \\ 0 & T_b < T_c,\ T_b < T_m \end{cases}$$

$$T_m = n_1 \beta L$$

$$\left.\begin{aligned} \tau_1 &= 0 \\ \tau_2 &= -\ln R \end{aligned}\right\} \quad T_c > (1-l) T_m$$

$$\left.\begin{aligned} \tau_1 &= -\ln R \\ \tau_2 &= \infty \end{aligned}\right\} \quad T_c < (1-l) T_m$$

and

$$R = \max\left(0, \min\left(1, \frac{T_b - l T_m - T_c}{T_m - l T_m - T_c}\right)\right)$$

If $\eta(\tau_c, \sigma) = f(\sigma) e^{-\tau_c}$

$$P_1(T_b) = \begin{cases} 1 & T_b > T_m + T_c \\ \dfrac{T_b - T_c}{T_m} + \left(\dfrac{T_b}{T_m} - 1\right) \ln\left(\dfrac{T_c}{T_b - T_m}\right) & T_m + T_c > T_b > T_c,\ T_b > T_m \\ \left(\dfrac{T_b}{T_m} - 1\right) \ln \dfrac{T_c}{T_m - T_c} & T_c > T_b > T_m \\ \dfrac{T_b - T_c}{T_m} - \left(\dfrac{T_b}{T_m} - 1\right) \ln \dfrac{T_m - T_b}{T_m - T_c} & T_m > T_b > T_c \\ 0 & T_b < T_m,\ T_b < T_c \end{cases}$$

If $p_1 = \dfrac{d P_1}{d T_b}$

$$T_m p_1(T_b) = \begin{cases} 0 & T_b > T_m + T_c \\ \ln \dfrac{T_c}{T_b - T_m} & T_m + T_c > T_b > T_c,\ T_b > T_m \\ \ln \dfrac{T_c}{T_c - T_m} & T_c > T_b > T_m \\ \ln \dfrac{T_m - T_c}{T_m - T_b} & T_m > T_b > T_c \\ 0 & T_b < T_m,\ T_b < T_c \end{cases}$$

Beyond the second cloud, it matters very little what happens, as it is improbable that much radiation from beyond the second cloud will reach the observer. Let us consider an infinitely thick layer of clouds and hot medium. It will have a brightness temperature

$$T_b \approx T_c + L_1 \beta n_1 + L_2 \beta n_1 e^{-\tau_{c1}}$$

where the first cloud is L_1 from the observer and the second is L_2 beyond that.

$$P_\infty = \frac{dP_\infty}{dT_b} = \begin{cases} 0 & T_b < T_c \\ \int_0^\infty \int_0^\infty e^{-\tau_{c1}} e^{-L_2 n} e^{-\left(\frac{T_b - T_c}{\beta n_1} - L_2 e^{-\tau_{c1}}\right) n} \, d\tau_{c1} \, dL_2 & T_b > T_c \end{cases}$$

$$= \begin{cases} 0 & T_b < T_c \\ \frac{\beta n_1}{n} \, e^{-\frac{T_b - T_c}{\beta n_1} n} & T_b > T_c \end{cases}$$

We now have

$$\Psi(T_b) \approx (1-q) I(T_b - T_m) + (1-q) q P_1(T_b) + q^2 I(T_b - T_c)\left(1 - e^{-\frac{T_b - T_c}{\beta n_1}}\right)$$

The mean temperature is

$$\overline{T_b} = \int_0^\infty T_b \frac{d\Psi}{dT_b} dT_b \approx (1-q) T_m + q(1-q) \frac{T_c + \frac{3}{2} T_m}{2} + q^2 \left(T_c + \frac{n_1 \beta}{n}\right)$$

And the mean square temperature $\overline{T_b^2}$ is given by

$$\overline{T_b^2} \approx (1-q) T_m^2 + q(1-q)\left(\frac{T_c^2}{3} + \frac{2}{3} T_c T_m + \frac{T_m^2}{9}\right) + q^2\left(2\left(\frac{n_1 \beta}{n}\right)^2 + 2 T_c \frac{n_1 \beta}{n} + T_c^2\right)$$

REFERENCES

Blaauw, A. BAN, 11, 459, (1952)

------ Interstellar Matter in Galaxies, (Ed. L. Woltjer) p. 48. Benjamin Press (1962)

Bolton, J. G.; van Damme, K. J.; Gardner, F. F.; and Robinson, B. J. Nature, 201, 279 (1964)

Bolton, J. G. and Westfold, K. C. Aust J Sci Res, 3, 19, (1950)

Braes, L. L. E. BAN, 17, 132, (1963)

Clark, B. G.; Radhakrishnan, V.; and Wilson, R. W. ApJ, 135, 151, (1962)

Davies, R. D. MN, 116, 443, (1956)

------ RMP, 30, 443, (1958)

Davies, R. D.; Shuter, W. L. H.; Slater, C. H.; Verschuur, G. L.; and Wild, P. A. T. MN, 126, 353, (1963)

Davies, R. D.; Verschuur, G. L.; and Wild, P. A. T. Nature, 196, 563, (1962)

Dieter, N. H. and Ewen, H. I. Nature, 201, 279, (1964)

Egorova, T. M. Soviet Astronomy--AJ (translation) 7, 190, (1963)

Field, G. B. Interstellar Matter in Galaxies (Ed. L. Woltjer) p. 183, Benjamin Press (1962)

Hagen, J. P. and McClain, E. F. ApJ, 120, 368, (1954)

Hagen, J. P.; Lilley, A. E.; and McClain, E. F. ApJ, 122, 361, (1955)

Heeschen, D. S. ApJ, 121, 569,(1955)

van de Hulst, H. C. RMP, 30, 913, (1958)

van de Hulst, H. C.; Muller, C. A.; and Oort, J. H. BAN, 12, 117, (1954)

Kahn, F. D. Gas Dynamics of Cosmic Clouds, p. 60, Interscience Pub. (1955)

Kerr, F. J. MN, 123, 327, (1962)

Kerr, F. J.; Hindman, J. V.; and Gum, C. S. Aust J Phys, 12, 12, 270, (1959)

Kwee, K. K.; Muller, C. A. and Westerhout, G. BAN, 12, 211, (1954)

Lequeux, J. Ann d'Ap, 25, 221, (1962)

MacRae, D. A. and Westerhout, G. Lund Observatory, (1956)

Moore, R. H. and Zeigler, R. K. Los Alamos Scientific Report LA 2367

Morris, D.; Clark, B. G.; and Wilson, R. W. ApJ, 138, 889, (1963)

Muller, C. A. ApJ, 125, 830, (1957)

------ Paris Symposium (Ed. R. Bracewell) S. U. Press, (1958)

Muller, C. A. and Westerhout, G. BAN, 13, 151, (1957)

Radhakrishnan, V. Pub ASP, 72, 296, (1960)

Read, R. B. ApJ, 138, 1, (1963)

Ryzhkova, N. F.; Egorova, T. M.; Gasachinski, I. V.; and Bystrova, N. V. Soviet Astronomy--AJ (translation) 7, 12, (1963)

Rougoor, G. W. and Oort, J. H. Paris Symposium (Ed. R. Bracewell) S. U. Press (1958)

------ Proc Nat Ac Sci, 46, 1, (1960)

Schmidt, M. BAN, 13, 15, (1956)

------ BAN, 13, 247, (1957)

Spitzer, L. and Savedoff, M. P. ApJ, 111, 593, (1950)

Weaver, H. F. and Williams, D. R. W. Nature, 201, 279, (1964)

Weinreb, S. ApJ, 136, 1149, (1962)

Weinreb, S.; Barrett, A. H.; Meeks, M. L.; and Henry, J. C. Nature, 200, 829, (1964)

van Woerden, H.; Takakubo, K. and Braes, L. L. E. BAN, 16, 321, (1962)